

ENHANCED OIL RECOVERY FROM PALM OIL MILL
EFFLUENT USING ULTRASONICATION TECHNIQUE
FOR BIODIESEL PRODUCTION WITH TWO-STEP
ESTERIFICATION AND TRANSESTERIFICATION
PROCESS

TANG YEE MUN

MASTER OF ENGINEERING SCIENCE

FACULTY OF ENGINEERING AND GREEN
TECHNOLOGY
UNIVERSITI TUNKU ABDUL RAHMAN
JULY 2023

**ENHANCED OIL RECOVERY FROM PALM OIL MILL EFFLUENT
USING ULTRASONICATION TECHNIQUE FOR BIODIESEL
PRODUCTION WITH TWO-STEP ESTERIFICATION AND
TRANSESTERIFICATION PROCESS**

By

TANG YEE MUN

A dissertation submitted to the Department of Environmental Engineering,
Faculty of Engineering and Green Technology,
Universiti Tunku Abdul Rahman,
in partial fulfillment of the requirements for the degree of
Master of Engineering Science
July 2023

ABSTRACT

ENHANCED OIL RECOVERY FROM PALM OIL MILL EFFLUENT USING ULTRASONICATION TECHNIQUE FOR BIODIESEL PRODUCTION WITH TWO-STEP ESTERIFICATION AND TRANSESTERIFICATION PROCESS

Tang Yee Mun

The presence of oil and grease in palm oil mill effluent (POME) showed the possibility to be recovered and valorized as a biodiesel feedstock. However, the complex and relatively resistant impurities in POME limit the full recovery of intracellular lipids. To address this challenge, low frequency ultrasonication was proposed as a pre-treatment to enhance the oil recovery yield by liberating the entrapped oil via the cell disruption technique. This study focused on optimizing the ultrasonication conditions to maximize the improvement of oil recovery yield using Response Surface Methodology (RSM). The optimum conditions of 30.074 % ultrasonication amplitude, 0.167 minutes ultrasonication duration, and 2 cm probe immersion depth resulted in an additional 42.50 % improvement in oil recovery yield over non-treated POME, which is in close agreement with the model's prediction. Particle size distribution and microscopy analyses on POME demonstrated that ultrasonication was able to induce structural disorganization in the sample. Furthermore, the quality of the oil recovered from POME was not compromised by the intervention of ultrasonication. The cost-benefit analysis also revealed that ultrasonication pre-treatment is feasible for improving oil recovery from POME. The study was extended to biodiesel

production using POME-recovered oil through two-step esterification and transesterification process. Since these reactions are mass-transfer-restricted processes, the ultrasonication technique was also investigated as a process intensifier to enhance the free fatty acid (FFA) conversion. The ultrasound-intensified techniques outperformed the conventional approach. A maximum FFA conversion of 93 % can be achieved after 1 hour of ultrasonication at 30 % amplitude, with a methanol-to-oil molar ratio of 8:1 and an H₂SO₄ loading of 0.75 wt%. The attributes of biodiesel produced from POME-recovered oil are comparable to those of palm-based biodiesel in Malaysia. It also satisfies international and local standards, demonstrating its potential as an alternative source for biodiesel production.

ACKNOWLEDGEMENTS

I would like to express my utmost gratitude to everyone who contributed to the successful completion of this research. As the most important individual, I would like to extend my heartfelt appreciation to my research supervisor, Dr. Wong Lai Peng, and co-supervisor, Dr. Tan Kok Tat, for their invaluable advice, guidance, and enormous patience throughout the development of the research.

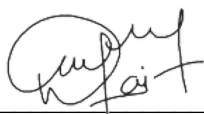
Next, I would like to express my deepest thanks to University Tunku Abdul Rahman (UTAR) for providing a scholarship and research fund (UTARRF) for this research (IPSR/RMC/UTARRF/2020-C1-W01). Special thanks to Tian Siang Oil Mill for granting permission for sample collection. I would also like to express my gratitude to the Department of Laboratory Management and Safety Administration, especially Puan Zila Binti Mohd Tahir, Ms. Ng Suk Ting, Mr. Yong Tzyy Jeng, and Puan Ropidah Hamimi Binti Mohd Zain, for their invaluable assistance in this study. Also, my heartfelt gratitude goes to Dr. Pang Yean Ling for permitting the use of her instrument.

Finally, I must express my profound gratitude to my family for their unwavering support and encouragement throughout my education. Not to forget all my friends who had helped me unconditionally throughout my research and thesis writing. This accomplishment would not have been possible without them. Thank you.

APPROVAL SHEET

This dissertation entitled “**ENHANCED OIL RECOVERY FROM PALM OIL MILL EFFLUENT USING ULTRASONICATION TECHNIQUE FOR BIODIESEL PRODUCTION WITH TWO-STEP ESTERIFICATION AND TRANSESTERIFICATION PROCESS**” was prepared by TANG YEE MUN and submitted as partial fulfillment of the requirements for the degree of Master of Engineering Science at Universiti Tunku Abdul Rahman.

Approved by:



(ChM. Dr. WONG LAI PENG)

Date: 21st July 2023

Assistant Professor/Supervisor

Department of Environmental Engineering

Faculty of Engineering and Green Technology

Universiti Tunku Abdul Rahman



(Dr. TAN KOK TAT)

Date: 21st July 2023

Assistant Professor/Co-supervisor

Department of Petrochemical Engineering

Faculty of Engineering and Green Technology

Universiti Tunku Abdul Rahman

FACULTY OF ENGINEERING AND GREEN TECHNOLOGY

UNIVERSITI TUNKU ABDUL RAHMAN

Date: 21st July 2023

SUBMISSION OF DISSERTATION

It is hereby certified that **TANG YEE MUN** (ID No: **21AGM01157**) has completed this dissertation entitled “ENHANCED OIL RECOVERY FROM PALM OIL MILL EFFLUENT USING ULTRASONICATION TECHNIQUE FOR BIODIESEL PRODUCTION WITH TWO-STEP ESTERIFICATION AND TRANSESTERIFICATION PROCESS” under the supervision of Dr. Wong Lai Peng (Supervisor) from the Department of Environmental Engineering, Faculty of Engineering and Green Technology, and Dr. Tan Kok Tat (Co-Supervisor) from the Department of Petrochemical Engineering, Faculty of Engineering and Green Technology.

I understand that University will upload softcopy of my dissertation in pdf format into UTAR Institutional Repository, which may be made accessible to UTAR community and public.

Yours truly,



(TANG YEE MUN)

DECLARATION

I hereby declare that the dissertation is based on my original work except for quotations and citations which have been duly acknowledged. I also declare that it has not been previously or concurrently submitted for any other degree at UTAR or other institutions.

Name Tang Yee Mun

Date 21st July 2023

TABLE OF CONTENTS

	Page
ABSTRACT	ii
ACKNOWLEDGEMENTS	iv
APPROVAL SHEET	v
SUBMISSION SHEET	vi
DECLARATION	vii
LIST OF TABLES	xi
LIST OF FIGURES	xiv
LIST OF ABBREVIATIONS	xviii
CHAPTER	
1.0 INTRODUCTION	1
1.1 Background of the Research	1
1.2 Problem Statement	2
1.3 Research Objectives	4
1.4 Scope of the Research	5
1.5 Importance of the Research	6
1.6 Organization of the Dissertation	7
1.7 Limitations of the Research	9
2.0 LITERATURE REVIEW	10
2.1 A Glance into the Palm Oil Industry	10
2.1.1 History and Development of Oil Palm	10
2.1.2 Palm Oil Milling Processes	13
2.2 Waste Generation in Palm Oil Mill	15
2.2.1 Palm Oil Mill Effluent (POME)	15
2.2.2 Presence of Oil and Grease (O&G) in POME	17
2.2.3 Effect of Residual Oil from Untreated POME	19
2.3 Oil Recovery and Removal Methods from POME	20
2.3.1 Physical Method	21
2.3.2 Chemical Method	22
2.3.3 Physicochemical Method	24
2.3.4 Comparison of Oil Management Strategies for POME	25
2.4 Ultrasonication Pre-Treatment	27
2.4.1 Cavitation Phenomenon	30
2.4.2 Factors Affecting the Efficiency of Ultrasonication	33
2.4.2.1 Types of Ultrasonic Processors	33
2.4.2.2 Ultrasonication Conditions: Ultrasonication Frequency	34
2.4.2.3 Ultrasonication Conditions:	

	Ultrasonication Power	35
	2.4.2.4 Ultrasonication Conditions:	
	Ultrasonication Duration	36
	2.4.2.5 Probe Position	37
	2.5 Biodiesel as a Sustainable Energy Source	38
	2.5.1 Transesterification	40
	2.5.2 Homogeneous Catalyst	42
	2.5.3 Two-Step Esterification and Transesterification	44
	2.5.4 Ultrasound-Assisted Biodiesel Production	48
	2.6 Quality of Crude Palm Oil (CPO)	50
	2.7 Quality of Biodiesel	53
3.0	RESEARCH METHODOLOGY	55
3.1	Overall Research Methodology	55
3.2	POME Sample Collection	58
3.3	POME Sample Characterization	59
	3.3.1 Methods for Determination of O&G	59
3.4	Ultrasonication Pre-Treatment Conditions for Oil Enhancement Process	60
	3.4.1 Preliminary Study using OFAT	62
	3.4.2 Optimization Study using RSM	64
3.5	Recovery of O&G from POME	69
3.6	Evaluation of Ultrasonication Pre-Treatment Impact on POME and Recovered Oil	71
	3.6.1 Impact of Ultrasonication Pre-Treatment on POME	72
	3.6.2 Impact of Ultrasonication Pre-Treatment on Recovered Oil	74
3.7	Cost-Benefit Analysis	77
	3.7.1 Cost Estimation	79
	3.7.2 Benefit Estimation	81
	3.7.3 Economic Evaluation of Investment Feasibility	81
3.8	Feasibility Study of Using Recovered Oil from POME as Biodiesel Feedstock	83
	3.8.1 Potential of Using Ultrasonication Technique as a Process Intensifier for FFA Conversion	85
	3.8.2 Ultrasonication Conditions for Esterification Process	87
	3.8.3 Biodiesel Analysis	88
4.0	RESULTS AND DISCUSSIONS	90
4.1	Raw POME Sample Characterization	90
4.2	Preliminary Study of Ultrasonication Conditions for Oil Enhancement Process using OFAT	92
	4.2.1 Influence of Ultrasonication Amplitude on Oil Content	92
	4.2.2 Influence of Ultrasonication Duration on Oil Content	95
	4.2.3 Influence of Probe Immersion Depth on	

	Oil Content	98
4.3	Optimization Study of Ultrasonication Conditions for Maximum Improvement of Oil Yield using RSM	100
4.3.1	Fit Summary, ANOVA, and Diagnostic Plots	103
4.3.2	3D Response Surface Plots	106
4.3.3	Optimization and Validation of Model	111
4.4	Evaluation of Ultrasonication Pre-Treatment Impact on POME and Recovered Oil	113
4.4.1	Impact of Ultrasonication Pre-Treatment on POME	113
4.4.2	Impact of Ultrasonication Pre-Treatment on Recovered Oil	118
4.5	Cost-Benefit Analysis on Enhancement of Oil Recovery using Ultrasonication Technique	125
4.5.1	Cost Estimation	125
4.5.2	Benefit Estimation	130
4.5.3	Economic Evaluation of Investment Feasibility	132
4.6	Feasibility Study of Using Recovered Oil from POME as Biodiesel Feedstock	134
4.6.1	Potential of Using Ultrasonication Technique as a Process Intensifier for FFA Conversion	134
4.6.2	Influence of Ultrasonication Amplitude on Acid Value and FFA Conversion	137
4.6.3	Influence of Ultrasonication Duration on Acid Value and FFA Conversion	139
4.6.4	Physicochemical Quality of Biodiesel	141
5.0	CONCLUSIONS AND RECOMMENDATIONS	146
5.1	Conclusions	146
5.1.1	General Conclusion	146
5.1.2	Conclusion for Objective 1	147
5.1.3	Conclusion for Objective 2	148
5.1.4	Conclusion for Objective 3	148
5.1.5	Conclusion for Objective 4	148
5.2	Recommendations	149
	REFERENCES	151
	APPENDICES	165
A	List of Chemicals and Instruments	165
B	Methods for Preserving Samples	167
C	Methods for Characterization of POME	168
D	Methods for Evaluating the Quality of Recovered Oil	175
E	Cost-Benefit Analysis	178
F	Preparation of Methanol-to-Oil Molar Ratio and Catalyst Loading for Biodiesel Production	181
G	Characterization Results of POME	183
H	Pearson Correlation Coefficient Analysis	184
I	Biodiesel Analysis	186

LIST OF TABLES

Table		Page
2.1	General Characteristics of Raw POME (Loh, et al., 2017; Kamyab e,t al., 2018; Mahmud, et al., 2021)	16
2.2	Regulatory Discharge Limits for POME (Department of Environment (DOE) Malaysia, 1977)	17
2.3	Classification of Oil Droplets (Al-Husaini and Sakthipandi, 2020)	18
2.4	Overview of Oil Management Strategies for POME	26
2.5	Improvement of Oil Yield from Various Feedstocks using Ultrasonication Pre-Treatment	28
2.6	Behavior of Acoustic Cavitation Bubbles: Stable and Transient	32
2.7	Routes for Biodiesel Synthesis (Zahan and Kano, 2018)	40
2.8	Types of Catalysts for Transesterification Reaction	42
2.9	Treatment of High FFA Feedstock through Sulfuric Acid-Catalyzed Esterification	46
2.10	Quality Specification for CPO in accordance with MS 814:2007	51
2.11	Classification of Palm Oil Quality based on DOBI	52
2.12	Fatty Acid Composition of CPO in accordance with MS 814:2007	52
2.13	Standard Specifications for Biodiesel Fuel and a Comparison of Physicochemical Properties of Palm-Based Biodiesel in Malaysia with respect to Diesel Fuel Standard	54
3.1	Methods for Characterization of POME	59
3.2	Range of Independent Variables for Optimization Study	67
3.3	Assumptions for Cost-Benefit Analysis	79

3.4	Computation for Profitability Analysis and Four Investment Criteria	82
3.5	Annotations for the Approaches and its Operating Temperature	85
3.6	Range of Independent Variables for Esterification Process	87
4.1	Characteristics of POME for Sample Collected for Six Months	90
4.2	Pearson Correlation Coefficient Analysis	92
4.3	CCD: Experimental Parameters and Responses	101
4.4	Fit Summary	103
4.5	Coefficient of Variables in the Regression Models and Their Significance	104
4.6	Verification of Forecasted Responses for Ultrasonication Pre-Treatment on POME	112
4.7	POME Particle Size Profiles of Different Ultrasonication Dosage	114
4.8	Solid Profiles of Non-Treated and Ultrasound-Treated POME	115
4.9	Absorption Frequency for the Respective Functional Group in ATR Test Results	119
4.10	Characteristics of Residual Oil Recovered from Non-Treated and Ultrasound-Treated POME	120
4.11	Purchase Cost of Equipment	125
4.12	Cost Estimation for Total Capital Investment	127
4.13	Cost Estimation for Operating Cost	129
4.14	Benefit Estimation from Product Sales Revenue	130
4.15	COD Removal Efficiency After Oil Recovery	131
4.16	Profitability Analysis	132
4.17	Net Present Value Calculation	133

4.18	Payback Period, Return on Investment, and Benefit-Cost Ratio	133
4.19	Fatty Acid Composition of POME-Methyl Ester	142
4.20	Comparison of Physicochemical Properties of POME Biodiesel with Standard Specifications	143
A.1	List of Chemicals Involved in the Research	165
A.2	List of Instruments Involved in the Research	166
B.1	Preservation Methods and the Maximum Holding Time for Each Parameters (United States Environmental Protection Agency, 1982)	167
E.1	Percentage for Estimating Capital Investment Items Based on Delivered-Equipment Cost (Peter, Timmerhaus and West, 2003)	180
G.1	Properties of POME for Sample Collected for Six Months	183
H.1	Characterization Data on O&G and BOD	184
I.1	Retention Time with Respective Analyte	190
I.2	Analytes in Biodiesel Produced from POME Recovered-Oil with its Respective Area	192

LIST OF FIGURES

Figures		Page
2.1	Cross-Sectional Part of an Oil Palm Fruit (Wondi, et al., 2020)	10
2.2	Global Palm Oil Production (Ritchie and Roser, 2021; Hassan, Mariati and Ng, 2021)	11
2.3	Forecasted CPO Production in Malaysia by MPOB (Nur Aisha, 2021)	12
2.4	Generation of POME in the Wet Palm Oil Milling Process	13
2.5	Distribution of Product and Waste from EFB (Kamyab, et al., 2018)	15
2.6	Mechanisms of liquid-liquid extraction (Suzuki, et al., 2020)	23
2.7	Mechanisms of Ultrasonic Irradiation	31
2.8	Types of Ultrasonic Processors: (A) Ultrasonic Bath and (B) Ultrasonic Probe	34
2.9	Estimated Cost for Biodiesel Production (Zulqarnain, et al., 2021)	39
2.10	Reaction Scheme of Transesterification (Luna, et al., 2016)	41
2.11	Reaction Scheme of Esterification of Fatty Acids (Tavizón-Pozos, et al., 2021)	45
3.1	PRISMA Flow Diagram for Systematic Review	56
3.2	Overall Flowchart	57
3.3	Raw POME Sampling Collection Point from Tian Siang	58
3.4	Ultrasonic Probe System	61
3.5	Schematic of the Experimental Setup with Varied Probe Immersion Depth	63
3.6	Process Flow of RSM	65

3.7	Experimental Cubic Space (BBD – White Points with Central Grey Point, FCCD – Black Points with Central Grey Point)	66
3.8	Process Flow of Oil Recovery from POME	69
3.9	Flow of Evaluation of Ultrasonication Pre-Treatment Impact	71
3.10	PSA (Malvern Mastersizer 2000)	72
3.11	FESEM (JEOL JSM6701F)	73
3.12	Binocular Microscope (Optika B-190)	74
3.13	FTIR-ATR (PerkinElmer Spectrum Two)	75
3.14	Oxygen Bomb Calorimeter (IKA Calorimeter System C200)	76
3.15	Process Flow of Cost-Benefit Analysis	77
3.16	Process Flow of Feasibility Study of Using Recovery Oil from POME for Biodiesel Production	84
3.17	GC-FID (Shimadzu, GC-2010 Plus)	88
3.18	Calibrated Pycnometer	89
3.19	Discovery Hybrid Rheometer (DHR-1)	89
4.1	Effect of Different Ultrasonication Amplitude on Oil Content from POME (Conditions: Ultrasonication Duration: 30 seconds and Probe Immersion Depth: 2 cm)	93
4.2	Effect of Different Ultrasonication Duration (Minutes) on Oil Content from POME (Conditions: Ultrasonication Amplitude: 30 % and Probe Immersion Depth: 2 cm)	95
4.3	Effect of Different Ultrasonication Duration (Seconds) on Oil Content from POME (Conditions: Ultrasonication Amplitude: 30 % and Probe Immersion Depth: 2 cm)	97
4.4	Effect of Different Probe Immersion Depth on Oil Content from POME (Conditions: Ultrasonication Amplitude: 30 % and Ultrasonication Duration: 30 seconds)	98

4.5	Effect of Different (A) Ultrasonication Amplitude, (B) Ultrasonication Duration, and (C) Probe Immersion Depth on the Improvement of Oil Yield from POME using RSM	102
4.6	Design-Expert Plots: (A) Predicted Versus Actual and (B) Residual Versus Run	105
4.7	3D Response Surface Plot for Interaction Between AB	107
4.8	3D Response Surface Plot for Interaction Between AC	108
4.9	3D Response Surface Plot for Interaction Between BC	109
4.10	Perturbation Plot for Improvement of Oil Yield	110
4.11	Particle Size Distribution of Non-Treated and Ultrasound-Treated POME	114
4.12	SEM Images of POME: (A) Non-Treated and (B) Ultrasound-Treated	116
4.13	Microscopic Observation of POME: (A) Non-Treated and (B) Ultrasound-Treated	117
4.14	ATR Spectrum of Recovered Oil from POME	118
4.15	Residual Oil Recovered from (A) Non-Treated and (B) Ultrasound-Treated POME at Room Temperature	122
4.16	Comparison of Three Different Approaches for the Reduction of High FFA Feedstock	135
4.17	Effect of Different Ultrasonication Amplitude on AV and FFA Conversion (Conditions: Ultrasonication Duration: 15 minutes, Methanol-to-Oil Molar Ratio: 8:1, and H ₂ SO ₄ Loading: 0.75 wt%)	137
4.18	Effect of Different Ultrasonication Duration on AV and FFA Conversion (Conditions: Ultrasonication Amplitude: 30 %, Methanol-to-Oil Molar Ratio: 8:1, and H ₂ SO ₄ Loading: 0.75 wt%)	139
C.1	Portable Multiparameter (Eutech CyberScan PCD 650)	168

C.2	DO Meter (Eutech DO 2700)	169
C.3	BOD Incubator (VELP, FOC 225E)	170
C.4	BOD Bottles with Stopper in BOD Incubator	170
C.5	Vial Thermo-Reactor (HANNA HI 839800) and Portable Colorimeter (HACH DR/890)	171
C.6	Universal Oven (Mettler Universal UF 110)	172
C.7	Vacuum Filtration Setup for SS Determination	173
C.8	Muffle Furnace (LabTech LEF-103S-1)	174
D.1	UV-Vis Spectrophotometer (Jasco V-730)	175
I.1	GC Result for Supelco 37 Component FAME Mix	188
I.2	Certificate of Analysis – Certified Reference Material	189
I.3	GC Result for Biodiesel Produced from POME-Recovered Oil	191
I.4	Results of Ester Content and Oxidation Stability	193

LIST OF ABBREVIATIONS

2FI	Two-factors interactions
3D	Three-dimensional
ANOVA	Analysis of variance
AOCS	American Oil Chemist's Society
AP	Adequate precision
APHA	American Public Health Association
ASTM	American Society for Testing and Materials
ATR	Attenuated total reflectance
AV	Acid value
BBD	Box-Behnken design
BCR	Benefit-cost ratio
CCD	Central composite design
CEPCI	Chemical Engineering Plant Cost Index
COD	Chemical oxygen demand
CPKO	Crude palm kernel oil
CPO	Crude palm oil
CT	Conventional esterification at 60°C
CWA	Clean Water Act
DAF	Dissolved air flotation
DOBI	Deterioration of bleachability index
DOE	Department of Environment
DTGS	Deuterated triglycine sulphate
EN	European Standard

EQA	Environmental Quality Act
FAME	Fatty acid methyl ester
FCCD	Face-centered central composite design
FCI	Fixed capital investment
FEGT	Faculty of Engineering and Green Technology
FESEM	Field emission scanning electron microscope
FFA	Free fatty acid
FFB	Fresh fruit bunch
FTIR	Fourier-transform infrared spectroscopy
GC-FID	Gas chromatography with flame ionization detector
GCV	Gross calorific value
GHC	Gross heat of combustion
GMP	Good Manufacturing Practices
H ⁺	Hydrogen atoms
H ₂	Molecular hydrogen
H ₂ O	Water
H ₂ O ₂	Hydrogen peroxide
H ₂ SO ₄	Sulfuric acid
HACCP	Hazard Analysis and Critical Control Point
HHV	Higher heating value
HR+	High range plus
IV	Iodine value
KOH	Potassium hydroxide
LiOH	Lithium hydroxide
LLE	Liquid-liquid extraction

M&I	Moisture and impurities
MBA	Malaysian Biodiesel Association
MCO	Movement Control Order
MPOB	Malaysian Palm Oil Board
MPOC	Malaysian Palm Oil Council
MS	Malaysian Standards
$\text{Na}_2\text{S}_2\text{O}_3$	Sodium thiosulphate
Na_2SO_4	Anhydrous sodium sulphate
NaOH	Sodium hydroxide
$\text{NH}_3\text{-N}$	Ammoniacal nitrogen
NPV	Net present value
O&G	Oil and greases
OER	Oil extraction rate
OFAT	One-factor-at-a-time
OH·	Hydroxide radicals
PbP	Payback period
PFC	Progressive freezing concentration
POME	Palm oil mill effluent
PSA	Particle size analyzer
PV	Peroxide value
R^2	Coefficient of determination
R^2_{adj}	Adjusted coefficient of determination
ROI	Return on investment
RSM	Response surface methodology
SEM	Scanning electron microscopy

SIRIM	Standard and Industrial Research Institute of Malaysia
SLE	Solid-liquid extraction
SS	Suspended solids
TCI	Total capital investment
TN	Total nitrogen
TS	Total solids
TVS	Total volatile solid
UBT	Ultrasonic bath-assisted reaction at 60°C
UBWT	Ultrasonic bath-assisted reaction at room temperature
UPWT	Ultrasonic probe-assisted reaction at room temperature
UV-Vis	Ultraviolet-visible

CHAPTER 1

INTRODUCTION

1.1 Background of the Research

As the world evolves towards energy sustainability, scholars and stakeholders are striving to reduce the consumption of fossil fuels, while transforming the processed-palm-oil waste into biofuel came on top of the plan. These days, the growth of palm oil enterprises is proliferating, particularly in Southeast Asia, due to the increased demand from the food and beverage, oleochemical, and biodiesel industries. Concurrent with this rising production, the massive volume of processed waste has become a worrying consequence. The waste generated throughout the palm oil milling process was substantially greater than the actual product produced, with nearly 3 tons of palm oil mill effluent (POME) were created for every ton of crude palm oil (CPO) extracted (Hosseini and Wahid, 2015). According to the source from Oil World, the global CPO production in 2021 was 78.5 million tons; based on the ratio, approximately 235.5 million tons of wastewater were generated.

POME is a high-strength acidic contaminant with a high concentration of solids and organic content that is detrimental to the environment if discharged indiscriminately. Despite enhanced extraction efficiency in palm oil mills, a considerable amount of oil and grease (O&G) was unavoidably discovered in

the effluent as oil losses (130 – 18,000 mg/L) (Kamyab, et al., 2018). The government-mandated maximum permitted discharge level for O&G is 50 mg/L (Department of Environment Malaysia, 1977). While palm oil millers have been focusing on adhering to the stringent discharge limits through biological treatment, they have frequently overlooked the importance of resource recovery.

Oil recovery from POME is one of the advanced waste management approaches. It not only enables the palm oil sector to utilize the recovered oil as a sustainable energy source, but it also considerably minimizes waste deposition and mitigates negative impacts. Although substantial research has been conducted on the oil recovery methods in POME, considerably less is known about the enhancement of oil recovery yield using ultrasonication. Hence, this research will provide a new focal point on waste valorization via enhanced oil recovery, thereby progressing the industry toward sustainable development.

1.2 Problem Statement

Ever since the global depletion of fossil fuel reserves and the rise in environmental pollution, massive efforts have been devoted to biodiesel research. The high expenses of edible feedstock and the food versus fuel issue, had sparked interest in searching for cheaper and non-edible alternatives for biodiesel production. Meanwhile, the continuous growth in palm oil production inevitably leads to vast quantities of underutilized oily wastewater that is detrimental to the environment. These issues can generally be addressed by valorizing POME through oil recovery.

The complex and relatively resistant impurities in POME limit the full recovery of intracellular O&G. This reduces the efficiency of oil recovery and contributes to resource wastefulness in the long term. Ultrasonication is an acoustic green technology capable of inducing physical and chemical effects on sonicated materials through the cavitation effect. Considering that oil is entrained in the POME particles, this research hypothesized that ultrasonication could ideally disrupt the complex particles and liberate the oil content.

Due to the limited research on ultrasound-enhanced oil recovery from POME, there is insufficient information on the process operating parameters and the quality of recovered oil. Feasibility studies for ultrasound enhancement are also rarely reported. Hence, this study comprised comprehensive research on optimal ultrasonication conditions, a quality assessment of recovered oil, and a cost-benefit analysis.

Residual oil recovered from POME possesses a high free fatty acid (FFA) content, which is incompatible with the conventional biodiesel production method using single-stage alkaline-catalyzed transesterification. As a result, an acid-esterification pre-treatment is required prior to the alkaline-catalyzed transesterification to convert the FFA to fatty acid methyl ester (FAME). Nonetheless, these reactions are mass-transfer-restricted processes due to the miscibility of the reactants. To circumvent this obstacle, ultrasonication was also investigated as a process intensifier to enhance FFA conversion.

1.3 Research Objectives

This research aims to investigate the potential of using ultrasound as a pre-treatment to improve oil recovery from POME for biodiesel production. The objectives of this research include the following:

- 1) To determine the optimum ultrasonication conditions for maximum improvement of oil recovery yield by using Response Surface Methodology (RSM).
- 2) To evaluate the impact of ultrasonication pre-treatment on POME and recovered oil.
- 3) To investigate the feasibility of utilizing ultrasonication as a pre-treatment to enhance the oil recovery from POME by conducting a cost-benefit analysis.
- 4) To synthesize and characterize biodiesel from POME-recovered oil through two-step esterification and transesterification process.

1.4 Scope of the Research

This research focused on optimizing the ultrasonication conditions (i.e., ultrasonication amplitude, ultrasonication duration, and probe immersion depth) to maximize the improvement of oil recovery yield using RSM. The data obtained were then analyzed via analysis of variance (ANOVA) to determine the model's applicability. The physical morphology of POME with and without ultrasonication pre-treatment was characterized using both non-imaging (particle size distribution) and imaging tools (microscopy analysis). On the other hand, the properties of residual oil recovered from POME with and without ultrasonication pre-treatment were evaluated using a series of oil quality indices. Additionally, a cost-benefit analysis was also incorporated into this study to determine its feasibility.

The scope of the study was extended to biodiesel production using the recovered oil from POME with two-step esterification and transesterification process. The incorporation of ultrasound as a process intensifier in the acid-esterification reaction was investigated. Ultrasonication amplitude and ultrasonication duration were studied in relation to acid value (AV) and FFA conversion. Lastly, the biodiesel produced from POME-recovered oil was assessed and compared to international and local standards to evaluate its potential as an alternative biodiesel feedstock.

1.5 Importance of the Research

Overall, this research will provide scientific evidence for the potential use of ultrasound to improve oil recovery from POME. Success in enhancing oil recovery not only would accelerate the palm oil industry's transition to cleaner production by minimizing waste generation, but also would reveal a new economic opportunity for palm oil millers. Furthermore, the efficacy of subsequent biological treatment would be improved due to enhanced organic matter solubilization by ultrasonication pre-treatment, signifying the plausibility of employing ultrasonication with the existing POME treatment system. Additionally, this study will present the potential of recovered oil from POME as a sustainable feedstock for biodiesel production, which provides industrial symbiosis possibilities and contributes to the circular economy. This research would also serve as an essential benchmark and reference for future scholars who venture into oil recovery enhancement using ultrasonication.

1.6 Organization of the Dissertation

Chapter 1 involves a brief introduction to the research. It highlights the potential of oil recovery from POME for higher value-added products. However, the complexity of POME composition limits the full recovery of oil. Ultrasonication, a green and sustainable technique, has been proposed to enhance oil recovery. The benefits gained from the research, as well as the limitations are also addressed in this chapter.

Chapter 2 presents an overview of the palm oil industry and its waste generation. A detailed literature review of various oil management strategies in POME, along with their advantages and disadvantages, was provided. Recent research on the incorporation of ultrasonication pre-treatment to improve oil yield was also summarized. Furthermore, the ultrasonic cavitation phenomena, as well as the parameters influencing ultrasonication efficiency, were enlightened. This chapter also discusses biodiesel production techniques as well as their quality specifications.

Chapter 3 includes an overall flowchart to describe the experimental methodology briefly. This chapter provides the detailed procedure of the POME characterization methods, ultrasonication experimental setup, and experiment conditions. It also outlines the analytical technique used to assess the ultrasonication pre-treatment impact on POME and recovered oil. In addition, the investment criteria to be evaluated in the cost-benefit analysis were

presented. This chapter also outlined the feasibility study of using recovered oil from POME as biodiesel feedstock.

Chapter 4 presents the results and discussions in detail. These include the parameters studies on ultrasound enhancement, evaluation of ultrasonication pre-treatment impact on POME and recovered oil, as well as cost-benefit analysis. Additionally, the reduction of high FFA feedstock through various approaches was demonstrated. The conformity of biodiesel products to quality standards was also evaluated in this chapter.

Chapter 5 summarizes the key findings obtained in this research study and the conclusions for each objective. In addition, this chapter also presents recommendations for future research directions.

1.7 Limitations of the Research

One of the limitations of the research is that the ultrasonic probe is susceptible to wear and tear even with regular usage. The ultrasonic probe is composed of titanium alloy. Erosion from probe tips would result in the loss of some metal particles, creating an uneven surface. As a result, the efficiency of ultrasonication might be affected. It is also possible that the metal fragments would be leached into the sample, affecting the quality of the product recovered. As a result of ultrasonic processing limitations for dependable operation, the ultrasonication amplitude range is fixed at 20 – 40 %.

This study's cost-benefit analysis is just a preliminary estimate, focused on the use of ultrasonication pre-treatment to improve oil recovery from POME. The operational costs associated with oil recovery and downstream processing are not taken into consideration. On top of that, the capital investment was computed as a percentage of delivered equipment cost, with the equipment cost scaled using the *six-tenths factor rule*.

Lab-scaled experimental work can only recover a limited amount of oil and biodiesel. This study examined only ultrasonic probe-assisted reaction operational parameters, such as ultrasonication amplitude and duration, as well as some essential biodiesel attributes, like density, ester content, oxidation stability, and viscosity.

CHAPTER 2

LITERATURE REVIEW

2.1 A Glance into the Palm Oil Industry

Oil palm fruit (*Elaeis guineensis*) commonly yields two distinct types of oil: crude palm oil (CPO), which is acquired from the fruit's mesocarp (flesh), and crude palm kernel oil (CPKO), which is acquired from the fruit's kernel (seed). Figure 2.1 illustrates the transverse section of an oil palm fruit.

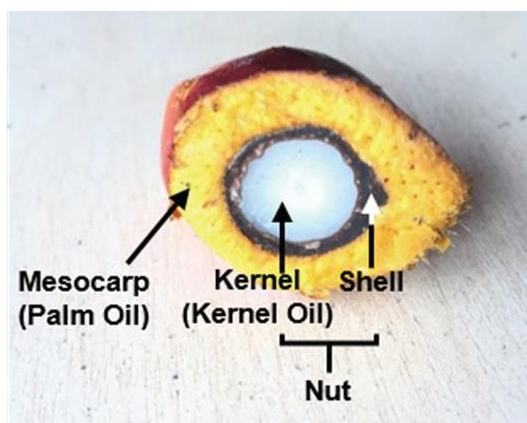


Figure 2.1: Cross-Sectional Part of an Oil Palm Fruit (Wondi, et al., 2020)

2.1.1 History and Development of Oil Palm

Commercial cultivation of oil palm trees in Malaysia began in 1917, and the industry has evolved significantly since the 1960s as a means of diversifying the country's economy away from its traditional reliance on rubber and tin. Over

the past 60 years, palm oil production has surged significantly due to expanding global population and driving demand from the food and beverage, oleochemical, and biodiesel industries. This assertion is supported by the graph in Figure 2.2, which displays the historical trajectory of worldwide palm oil production. In 2019, global palm oil production reached a new high of 76 million tons, which is 39 times the output from 1970. Malaysian Palm Oil Council (MPOC) forecasted that the global CPO production in 2020 would exceed that of in 2019. Unfortunately, the total palm oil output declined by 3.5 % instead, primarily due to the extended drought in Indonesia. This scenario was aggravated further by the COVID-19 outbreak and Movement Control Order (MCO) over the world, which caused labor scarcity, and, as a result, indirectly impeded palm oil production.

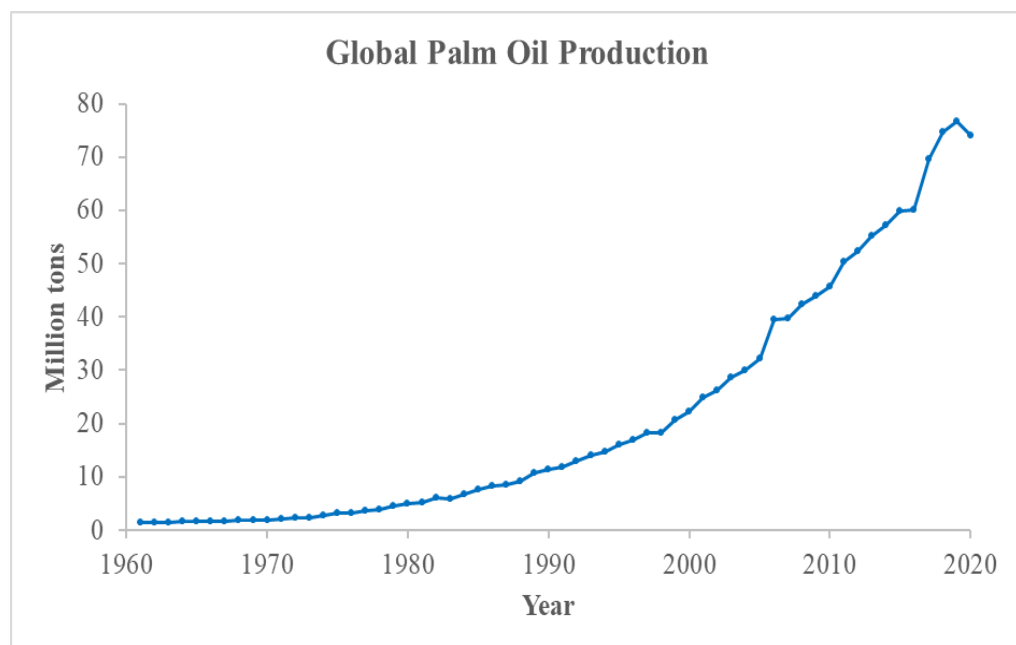


Figure 2.2: Global Palm Oil Production (Ritchie and Roser, 2021; Hassan, Mariati and Ng, 2021)

However, this is only a temporary setback as palm oil production in Malaysia is expected to rebound in 2021, owing to the maturation of oil palm fields replanted in 2018, resulting in higher yields. In addition, the recent adjustment in Indonesia’s export tax structure, which incentivizes palm oil exports, will most certainly shift the demand for CPO from Indonesia to Malaysia (Hassan, Mariati and Ng, 2021). Along with technological advancements in the palm oil sectors, the Malaysian Palm Oil Board (MPOB) anticipates that palm oil production in Malaysia will increase gradually and steadily over the next five to ten years, reaching 25 million tons by 2030, as indicated in Figure 2.3. Nonetheless, the continual expansion of palm oil production will undoubtedly lead to enormous amounts of waste.

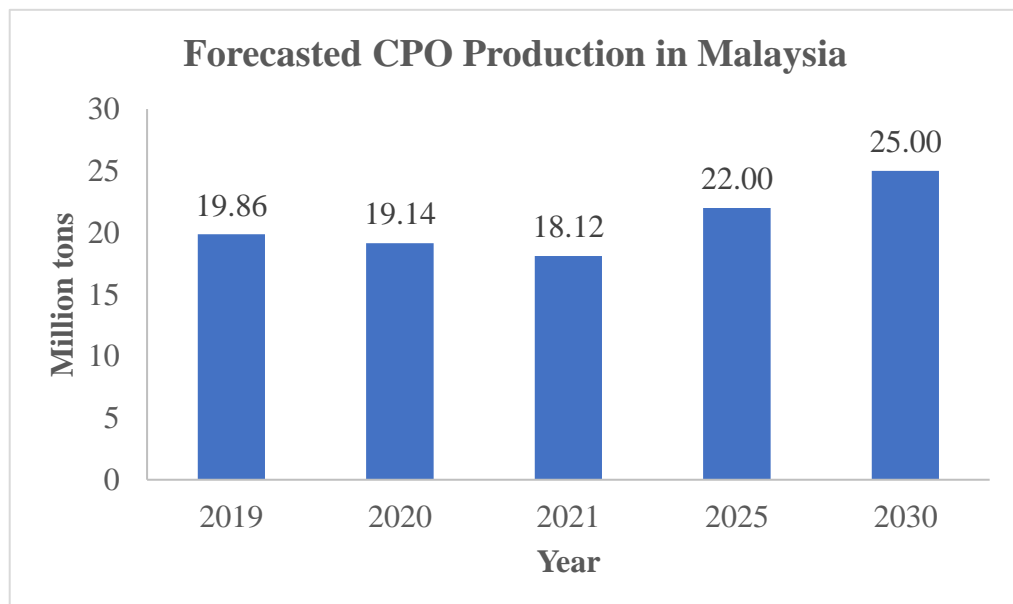


Figure 2.3: Forecasted CPO Production in Malaysia by MPOB (Nur Aisha, 2021)

2.1.2 Palm Oil Milling Processes

The wet milling technique, which employs steam and hot water, is the most prevalent method used in palm oil extraction. As a water-intensive process, a typical extraction operation of 1 ton of CPO would require 5 to 7.5 tons of water, with over half of it ending up as liquid waste (Mohammad, et al., 2021). Figure 2.4 illustrates the palm oil milling process flow along with POME generation.

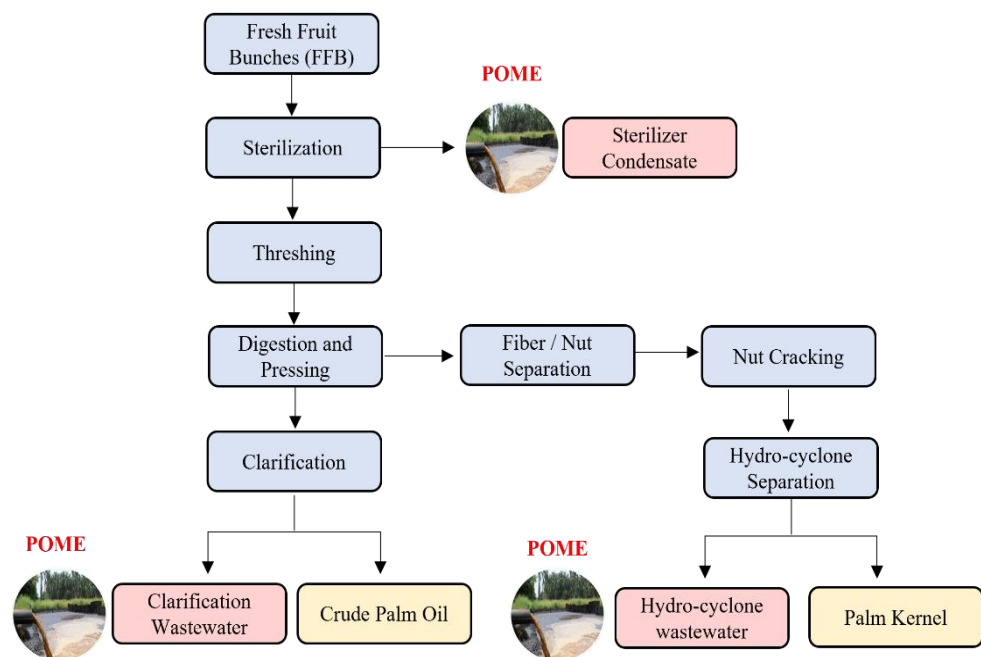


Figure 2.4: Generation of POME in the Wet Palm Oil Milling Process

Harvested fresh fruit bunches (FFBs) from the plantations are immediately transported to the mills for grading prior to processing. The wet milling process begins with sterilizing of high-quality FFBs using high-temperature pressurized steam. Sterilization of FFBs is performed primarily to deactivate the natural hydrolytic enzyme responsible for oil hydrolysis and to improve fruit pericarp detachment from the bunch. The sterilizer condensate

accounts for 36 % of the total POME, making it one of the significant contributors to POME accumulation. Majority of the oil loss in the condensate occurs due to a prolonged sterilizer cycle or overripe fruit.

The sterilized FFBs were fed into a rotating drum thresher for fruit stripping operation. Following that, the loose fruitlets were loaded into a steam-heated digester and mechanical screw press for CPO extraction. This procedure yields an oil-water mixture as well as pressed cake. The pressed liquor was then pumped into a clarifier tank to facilitate the oil separation process. The top layer of oil was skimmed, purified, and vacuum-dried for storage before being dispatched for export or refining. On the other hand, the bottom layer of underflow sludge was passed through a decanter for enhanced oil extraction efficiency or directly drained into sludge pits nearby. Over 60 % of the total amount of POME is accumulated through crude oil clarification. Majority of the oil loss in the crude oil clarification occurs due to hydraulic overloading.

In contrast, the pressed cake was transferred to the kernel recovery system, where a splitter machine would separate the nuts from the fibrous mesocarp before delivering them to a nut-cracking device. The resulting mash of shells and kernels was then segregated in a hydro-cyclone, which employs the centrifugal force created by water flow to separate the two components into their respective fractions based on their relative densities. The separated kernels were then kept in a kernel silo before being sent for CPKO extraction. The hydro-cyclone effluent is the third source of POME, accounting for 4 % of the total amount.

2.2 Waste Generation in Palm Oil Mill

The waste generated throughout the palm oil milling process was substantially more significant than the actual product yielded. As shown in Figure 2.5, the processing of 1,000 kg of FFB produces only 200 kg of palm oil, with the remainder being waste. These underutilized wastes can be classified into two distinct types: solid waste (44%) and liquid waste (56%), with POME being the most prominent oily pollutant in palm oil mills.

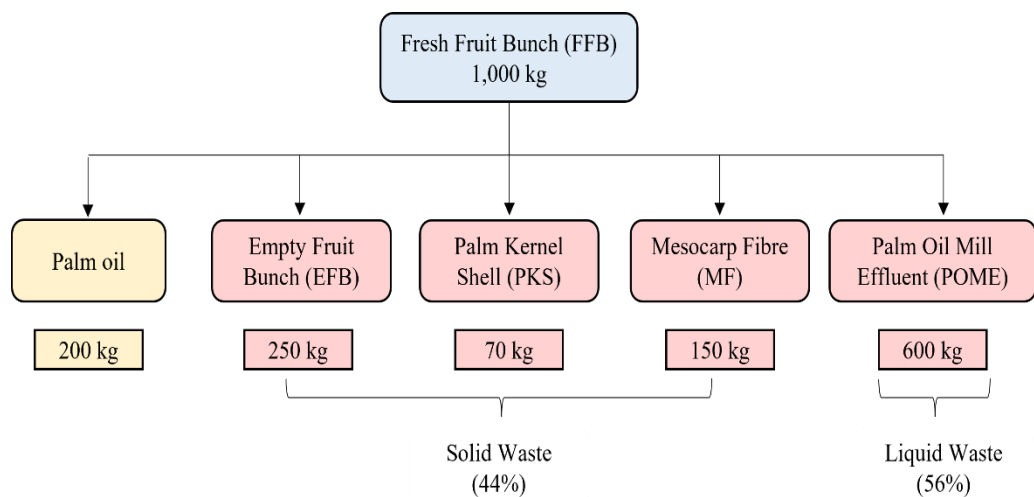


Figure 2.5: Distribution of Product and Waste from FFB (Kamyab, et al., 2018)

2.2.1 Palm Oil Mill Effluent (POME)

POME is a solid-liquid effluent composed primarily of fine cellulosic materials, water, and oil. Due to the heterogeneity of POME, no fixed values are provided for its attributes, as they fluctuate significantly in response to starting material qualities and processing variations. Table 2.1 summarizes the

general physicochemical properties of raw POME. Commonly, POME is a brownish, underutilized agro-industrial wastewater discharged at high temperatures and with a low pH value. Due to the elevation of solids, O&G, and organic contents, indiscriminate discharge of untreated POME on land and into waterway can be concomitantly sensitive to environmental issues. POME is also eutrophic and emits an unpleasant odor due to its rich mineral content.

Table 2.1: General Characteristics of Raw POME (Loh, et al., 2017; Kamyab, et al., 2018; Mahmud, et al., 2021)

Parameters	Concentration range
pH	3.3 – 5.7
Temperature	80 – 90 °C
Total solids (TS)	11,500 – 78,000 mg/L
Suspended solids (SS)	5,000 – 54,000 mg/L
Biochemical oxygen demand (BOD)	10,250 – 43,750 mg/L
Chemical oxygen demand (COD)	15,000 – 100,000 mg/L
Total nitrogen (TN)	180 – 1,400 mg/L
Ammoniacal nitrogen (NH ₃ -N)	4 – 80 mg/L
Oil and greases (O&G)	130 – 18,000 mg/L

To regulate and minimize the environmental pollution impact, Malaysia's government adopted the Environmental Quality Act (EQA) 1974 and established regulatory limits to the emission of POME. Table 2.2 shows the Environmental Quality (Prescribed Premises) (CPO) Regulations 1977 that govern the waste management practices in the palm oil sector.

Table 2.2: Regulatory Discharge Limits for POME (Department of Environment (DOE) Malaysia, 1977)

Parameters	Standard discharge limit
pH	5 – 9
Temperature	45 °C
Suspended solids (SS)	400 mg/L
Biochemical oxygen demand (BOD ₃)	100 mg/L
Total nitrogen (TN)	200 mg/L
Ammoniacal nitrogen (NH ₃ -N)	150 mg/L
Oil and greases (O&G)	50 mg/L

2.2.2 Presence of Oil and Grease (O&G) in POME

Section 304(a) of the Clean Water Act (CWA) classifies oil and grease (O&G) as conventional pollutants. Despite the improved milling process, the presence of residual oil in the waste stream is inevitable. The nature of residual oil in POME poses a challenge to efficient and effective treatment. Hence, understanding the behavior of oil droplets in POME is critical for determining appropriate sorts of oil recovery technologies.

In POME, oil droplets are present in two states: embedded in the solids and floating in the supernatant. Table 2.3 classifies the behavior of residual oil according to the droplet size.

Table 2.3: Classification of Oil Droplets (Al-Husaini and Sakthipandi, 2020)

Droplet size	Classification
< 5 μm	Soluble oil mixture
5 – 20 μm	Emulsified oil mixture
20 – 150 μm	Dispersed oil mixture
>150 μm	Free oil

Due to harsh mechanical processing, residual oil in POME is mostly in emulsified and dispersed form. In addition to that, the high concentration of natural surfactants present in POME also increases the oil's stability, making it more resistant to coalescence and more challenging to be separated by natural means. POME is highly complicated in nature due to the involvement of a diverse structure of cellulose, hemicellulose, and lignin (Hii, Yeap and Mashitah, 2012). The carbohydrate-rich particles in POME encapsulate bulk of the oil droplets due to their amphiphilic properties, with predominating lipophilic capabilities (Wan Sharifudin, et al., 2015). Oil in POME was either adhering to solid surfaces through surface adsorption or capillary adsorption in fibrous solids. In brief, the oil is believed to be primarily trapped in the suspended solids and inseparable mechanically from the multiphase system, contributing to the oil loss and poor recovery in the long term.

2.2.3 Effect of Residual Oil from Untreated POME

In recent years, biological treatment has been the most prevalent approach for the treatment of POME. Specially, this system comprises a succession of ponds that rely on microorganisms to decompose the organic components, mainly through the processes of hydrolysis and acidogenesis (Hassan, et al., 2005). Majority of the palm oil mills (85%) adopted solely ponding system due to their low-cost upfront capital, minimal technical skill requirements, and simple design. Despite POME's biodegradability ability, oil is notoriously difficult to be degraded biologically since not all microorganisms generate lipase enzymes that are capable of decomposing triglycerides.

Oil film deposition surrounding the microbes would interfere with the biological treatment by hindering the transmission of oxygen and soluble substrate for microbial degradation. This will ultimately result in a decrease in the efficacy of the wastewater treatment process and an increase in the operational treatment cost. Besides, the unrecovered O&G tends to accumulate on top of the water surface due to its poor solubility and low specific gravity. The formation of a widespread scum layer reduces the light penetration and photosynthesis rate when discharged to the water bodies, adversely affecting aquatic life due to the depletion of oxygen.

In 2021, 78.5 million tons of palm oil were produced globally while generating 236 million tons of POME. Not only did the process generate a considerable volume of effluent, but a rough speculation also indicates that the POME discharged contains approximately 1.18 million tons of residual oil that

is possible to recover. The action to ignore the recoverable residual oil from POME has not only damaged the environment, but it has also resulted in financial losses.

2.3 Oil Recovery and Removal Methods from POME

Although biological treatment shows a certain level of efficiency in treating POME, it frequently disregards the resource recovery from POME. Resource recovery is one of the most desirable environmental options for handling oily sludge. It not only enables the palm oil industry to reprocess and reformulate the recovered oil for energy recovery, but it also significantly reduces the volume of waste and alleviates the negative impact.

Oil recovery is somewhat identical to oil extraction, with the key distinction being that when a virgin source is employed, it is commonly referred to as 'extraction'. 'Oil recovery', on the other hand, is a term usually used to describe oil extraction from waste or subsequent oil extraction. Mechanisms employed in the study of oil extraction from virgin sources have also been applied in the oil recovery process. As oil recovery from POME has received less attention from the industry, this section intends to concisely review the oil management techniques that have been explored from POME on a laboratory scale to acquire insight for better effluent management. Various oil recovery and removal methods, including physical, chemical, as well as physicochemical, have been investigated as one of the waste management approaches for POME.

2.3.1 Physical Method

Oil recovery from POME could be accomplished by using trapping and skimming techniques. This entails the collection of all liquid effluent from the processing stages in a container and allowing it to stand for days until the oil components float to the surface and are skimmed off due to density differences. Commonly, this phenomenon is known as gravity separation. Laohaprapanon, Prasertsan and Kittikun (2005) compared gravity settling and centrifugation to physically separate oil from POME. It was discovered that centrifugation at 7,000 rpm for 15 minutes yielded comparable oil recovery to gravity settling at 55 °C for one day. On the other hand, Faisal, et al. (2016) proposed the incorporation of dissolved air flotation (DAF) into the oil skimming process to improve the efficiency of oil recovery for gravity separation. When pressurized air is supplied at the bottom of an open container, the resulting air bubbles will adhere to the microscopic oil droplets, causing them to float to the surface and be recovered by the skimming equipment. With an airflow rate of 11 L/min and a treatment time of 5 days, 52.6 % of the O&G in POME could be removed, representing a 39.9 % improvement over conventional separation.

Conventionally, physical separation is the most common and simplest method to adopt. Despite its relatively simple design and low operating expenses, it is inefficient as it necessitates a huge setup area and is only able to recover 35 – 55 % oil layer on the surface (Loh, et al., 2013; Wang, et al., 2015). In contrast, the oil encapsulated within the remnant source cannot be freed and

will be discharged as sludge. Consequently, the oil from the wastewater is not effectively recovered, necessitating a better recovery method.

2.3.2 Chemical Method

Solid-liquid extraction (SLE), commonly known as Soxhlet extraction, developed by Franz Von Soxhlet in the mid-18th century, has been used to separate various volatile compounds from solid samples. The process begins with the addition of extraction solvent into the boiling flask. As the flask is steadily heated, the solvent vaporizes as it reaches the boiling point. Through the side arm and condenser, the vaporized solvent condenses and drains into the Soxhlet extractor. The analyte of interest (oil) is extracted when the warm solvent contacts the oil source (POME). When the extractor is full, the analyte-containing solvent floods back into the flask. Repetition of cycles will result in complete extraction. Suwanno, et al. (2017) employed a laboratory-scale Soxhlet technique to recover residual oil from POME. They discovered that 80 % of the oil was recovered after 1 hour of reaction at 100°C with a sample-to-solvent ratio of 1:6.

Soxhlet extraction is a less commonly used method for oil recovery from POME on an industrial scale due to several limitations. One of the major drawbacks is that this technique is only applicable to solid samples. With the overwhelming presence of liquid phase in POME, a pre-treatment by drying is required prior to oil recovery. This will undoubtedly result in extended treatment time and higher production costs. Additionally, prolonged high-

temperature exposure may also result in lipid peroxidation and deterioration of recovered products (López-Bascón and Luque de Castro, 2020).

On the other hand, liquid-liquid extraction (LLE), often termed as chemical extraction or solvent extraction, is currently widely employed in the food, pharmaceutical, and petrochemical sectors for the extraction process. Analytes are isolated based on their relative solubility in two immiscible solutions. LLE differs from Soxhlet extraction in that it does not entail any heating. Figure 2.6 depicts the mechanisms of LLE, which consists of three fundamental steps: interaction, separation, and recovery of solvent.

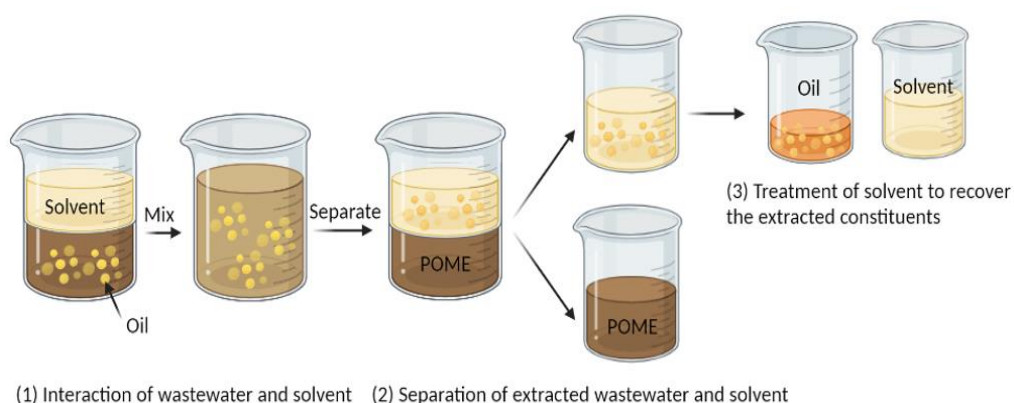


Figure 2.6: Mechanisms of liquid-liquid extraction (Suzuki, et al., 2020)

In POME, residual oil can be chemically recovered using non-polar solvents like n-hexane, n-heptane, pentane, petroleum ether, and benzene. Among various solvents, n-hexane is the most popular choice due to its superior oil extraction performance. Ahmad, et al. (2003) evaluated the impact of various parameters on POME oil yield, including solvent type, sample-to-solvent ratio, and reaction time. The highest oil yield obtained from POME is 5,400 mg/L under the conditions of a POME-to-hexane ratio of 1:0.6 for 20 minutes. The resemblance between LLE and oil content analysis allows for the assumption

that the recovered oil represents the total oil content, thereby demonstrating the high recoverability efficiency. Additionally, there are ongoing efforts being undertaken to commercialize solvent extraction as a viable method for POME oil recovery, affirming its industrial-scale practicability. One notable example is Mecpro Heavy Engineering Limited (2022), a reputable company specializing in process engineering for the palm oil industry, which has recently developed an innovative solvent extraction system known as the Mecpro Multi extraction system. The simultaneous recovery of both floating and emulsified oil from POME as well as wet mesocarp fibre is a key feature of MECPRO's process technology (Application no. 1709/DEL/2015A). The extraction process can be further improved by reducing the size of substrates, which increases their surface area and facilitates better solvent-substrate contact.

2.3.3 Physicochemical Method

Progressive freezing concentration (PFC) is a process of concentrating a solution that entails freezing or solidifying one liquid component to form a pure solid, and then separating the solidified fragment from the mother liquor. Mohamed Anuar, Amran and Ruslan (2020) discovered that the PFC technique could recover 67.9 % of O&G from POME after 1 hour at a coolant temperature of 6 °C. One of the main advantages of PFC is that it is a green technology that operates at low process temperature, which can help maintain thermally sensitive elements of the solution. However, the productivity of PFC is relatively poor, and the energy requirements for the process can be high, making it less economically viable in warm climates.

Adsorption is one of the most popular techniques adopted for oil separation from oily wastewater. Adsorption is a surface-related phenomenon in which the sorbate molecules adhere to the sorbent without penetrating it. Adsorbent materials can be either synthetic or natural. Several sorbents have been reported for the adsorption of oil from POME; including synthetic rubber powder (Ahmad, et al., 2005), chitosan (Ahmad, Sumathi and Hameed, 2005), palm shell activated carbon magnetic composite (Ngarmkam, Sirisathikul and Phalakornkule, 2011), modified oil palm leaf (Jahi, et al., 2015), esterified sago bark fiber waste (Wahi, et al., 2017), as well as polypropylene micro/nanofiber (PP-MNF) (Semilin, et al., 2021). The efficiency of the oil-water adsorption process is determined by the properties of sorbent, the most important of which are the hydrophobic and oleophilic properties. Physical pressing, chemical extraction, or supercritical carbon dioxide techniques can be used to recover the adsorbed oil from the sorbent. Adsorption is widely utilized for its benefits, such as high efficiency, ease of operation, and environmental friendliness. However, the concern over the reusability of adsorbent and post-adsorption treatment to recover the adsorbed oil is a huge disincentive to this technology as it will certainly increase the expenditure.

2.3.4 Comparison of Oil Management Strategies for POME

Table 2.4 provides an overview of various oil management strategies for POME, along with their advantages and disadvantages. Among those, chemical extraction would be the preferred option due to its high recoverability efficiency and industrial-scale practicability

Table 2.4: Overview of Oil Management Strategies for POME

Method	Advantages	Disadvantages
Physical separation	Simple design and low cost	Removes only free oil and requires a huge setup area
Soxhlet extraction	High oil yield	Adverse thermal effects
Chemical extraction	High efficiency and industrial practicability	Requires size reduction
Progressive freezing concentration	Maintain thermally sensitive elements	Low productivity
Adsorption	Ease of operation	Concern over reusability and post-adsorption

Whilst extensive research has been conducted on oil recovery methods, much less is known about the enhancement of oil recovery yield. The literature data in Section 2.2.2 have demonstrated the problems related to the availability of intracellular lipids. The prime drawback is the oil-bearing cell, where the complex and relatively resistant cell wall limits the full recovery of oil. Thus, a sustainable and cost-effective pre-treatment is required to disrupt the cellulosic components.

2.4 Ultrasonication Pre-Treatment

Ultrasound is a cyclic sound wave with a frequency greater than 20 kHz. Ultrasonication technique is often regarded as a ‘green technology’, as evidenced by its numerous advantages such as high efficiency, low equipment requirement, short operation duration (seconds to minutes), and ability to operate under atmospheric pressure and ambient temperature. Most notably, ultrasonication does not require any chemical enhancers to increase yield, which exhibits the benefit of being non-hazardous to the environment and contributes to waste reduction.

In recent years, ultrasound technology has acquired greater application in almost all disciplines, including the fields of medical and therapy, food and beverage, material cleaning, nanotechnology, industrial welding, and environmental applications (Mohammed and Alhajhoj, 2020). Hamidi, et al. (2021) presented a review on ultrasonic wave applications for improved oil recovery in petroleum reservoirs. Additionally, ultrasound technology has gained popularity for improving the extraction of intracellular components from various sources (Wen, et al., 2018). The mechano-acoustic (physical) and sonochemistry (chemical) effects of ultrasonic irradiation have garnered the attention of researchers. Ultrasonication can be applied either as a pre-treatment or simultaneously with extraction. Pre-treatment with ultrasound is becoming increasingly popular due to its reduced time and power requirements (Panadare, Gondaliya and Rathod, 2020). Table 2.5 summarizes the research on ultrasonication pre-treatment for enhanced oil yield.

Table 2.5: Improvement of Oil Yield from Various Feedstocks using Ultrasonication Pre-Treatment

Materials	Ultrasonic parameters	Key findings	References
Custard apple seed slurry	Probe, 20 kHz, 150 seconds, 30 W	Oil yield improved by 9.98 %. Ultrasonication pre-treatment requires lesser time and applied power than conventional and ultrasound-assisted extraction.	(Panadare, Gondaliya and Rathod, 2020)
Pomegranate seed slurry	Probe, 20 kHz, 10 minutes, 52 W	Oil yield improved by 18.4 %. Ultrasonication pre-treatment shortens the extraction time.	(Goula, et al., 2018)
Crude oil tank sludge in an oil refinery plant	Probe, 20 kHz, 60 seconds, 33 W	A combination of ultrasound and freeze/thaw provides satisfactory oil recovery results.	(Zhang, et al., 2012)
Oil shale	Probe, 15 minutes, 125 W	Ultrasonication pre-treatment enhances the effectiveness of conventional flotation.	(Altun, Hwang and Hicyilmaz, 2018)

Table 2.5 (Continued): Improvement of Oil Yield from Various Feedstocks using Ultrasonication Pre-Treatment

Materials	Ultrasonic parameters	Key findings	References
Intact hemp (<i>Cannabis sativa L.</i>) seed	Probe, 20 kHz, 10 minutes, 52 W	Ultrasonication pre-treatment improves oil yield by 3.3 % without any solvent assistance. However, it was observed that the degradation of antioxidant compounds occurred.	(Da Porto, Natolino and Decorti, 2015)
Paraffin oil and brine mixture	Bath, 40 kHz, 90 minutes, 500 W	Ultrasonication pre-treatment improves oil recovery up to 11 % and 12 % for water and surfactant flooding, respectively.	(Agi, et al., 2019)
<i>Moringa oleifera</i> lam. seed slurry	Bath, 40 kHz, 60 minutes, 50 W	Oil yield improved by 1.24 %. The recovered oil from ultrasound-treated sample has a lower peroxide value.	(Kayanan and Sagum, 2021)

The application of ultrasonic irradiation as a pre-treatment for the resistant lignocellulosic sample prior to obtaining the product of interest can contribute positively to the improvements in yields. As an innovative approach, ultrasonic irradiation induces vibration that could accelerate the release of intracellular materials by mechanically disrupting the cell wall barrier and lignin-carbohydrate complexes, hence, enhancing the extraction yield. Considering that the oil is entrained in the POME particles, ultrasonication pre-treatment can ideally disrupt the complex particles and liberate the oil content to enhance oil recovery.

2.4.1 Cavitation Phenomenon

Ultrasound is generated by two techniques: (1) magneto-strictive, which converts electrical energy to mechanical energy using magnetic coil, and (2) piezoelectric, which converts electrical energy to high-frequency mechanical energy using piezoelectric crystals. When ultrasound waves propagate through the sample, it generates a series of alternating cycles known as compression and rarefaction, which impose positive pressure by pushing the molecules together and negative pressure by pulling them apart. As a result of the instantaneous and enormous pressure difference, microbubbles occur in the rarefaction zones. These microbubbles expand in successive cycles by absorbing the ultrasonic energy and collapse violently upon reaching an unstable diameter. This phenomenon is known as ‘acoustic cavitation’ and is represented in Figure 2.7.

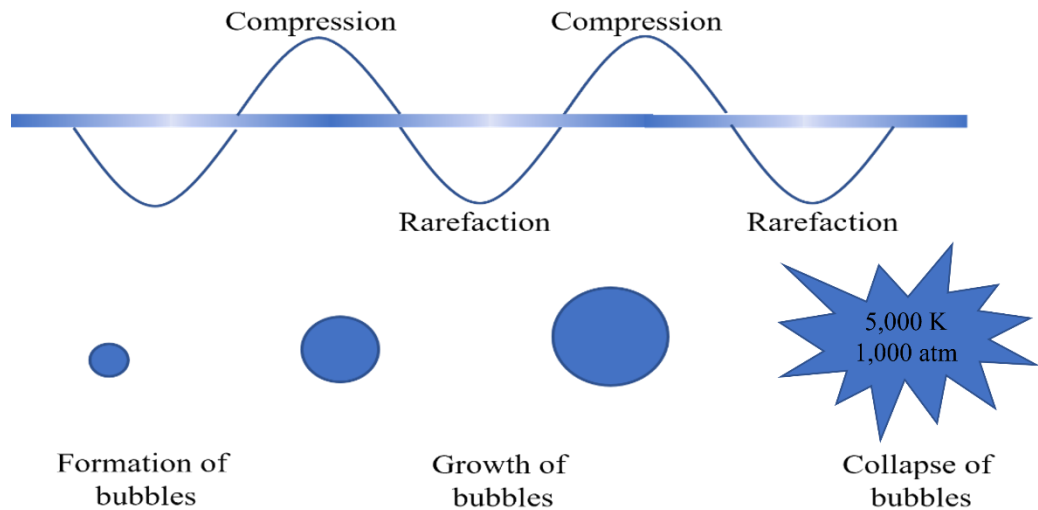


Figure 2.7: Mechanisms of Ultrasonic Irradiation

Cavitation can be classified into four principal types based on its generation mode: hydrodynamic, acoustic, particle, and light (Wu, et al., 2018). Among those, only hydrodynamic and acoustic cavitation can induce physical or chemical changes in a system (Rokhina, Lens and Virkutyte, 2009). The detonation of the cavitation bubbles induces shock waves, which in turn create intense localized heating (5,000 K), high pressure (1,000 atm), and a high heating and cooling rate (10^9 K/sec) at the liquid-gas interface turbulence (Suslick, 1998). All these effects take place on a microsecond timescale.

When ultrasound is used to irradiate liquids containing solids, such extreme conditions create other physical and mechanical effects, namely macroturbulence and hydromechanical shear forces created by a liquid jet stream travelling at a speed of 400 km/h. These effects can cause a reduction in particle size, breakdown of cell wall, and exudation of cellular content, all of which contribute to an increase in yield.

In addition, ultrasonication has been associated with sonochemistry reactions. The heat generated by the cavity implosion dissociates the water (H_2O) molecules into highly reactive hydroxide radicals ($\text{OH}\cdot$) and hydrogen (H^+) atoms. These radicals recombine during the rapid cooling phase to form hydrogen peroxide (H_2O_2) and molecular hydrogen (H_2). These reactive oxygen species will oxidize and degrade the solutes. Overall, ultrasonic irradiation is an emerging technology with a combination of physical (pyrolysis and shearing) and chemical effects (radical reaction).

Acoustic cavitation bubbles have two distinct behaviors: stable (non-inertial) and transient (inertial). Since stable cavitation can result in transient cavitation or vice versa, cavitation is not strictly classified. The line of difference between stable and transient microbubbles is displayed in Table 2.6.

Table 2.6: Behavior of Acoustic Cavitation Bubbles: Stable and Transient

Stable (non-inertial) cavitation	Transient (inertial) cavitation
Long lifespan and consistent shapes	Disintegrate in a few to hundreds of acoustic cycles and unstable shapes
Occurs at low ultrasonic intensities ($1 - 3 \text{ W/cm}^2$)	Occurs when ultrasonic intensities exceed 10 W/cm^2
Do not lead to cell degradation	Cause noticeable degradation

2.4.2 Factors Affecting the Efficiency of Ultrasonication

Numerous studies have been conducted to explore the impact of ultrasonic parameters and optimize them for maximum output while minimizing expenses and power usage. This section concentrates on several parameters that have gained the most attention in the literature.

2.4.2.1 Types of Ultrasonic Processors

As indicated in Figure 2.8, ultrasound can be brought about by employing either an ultrasonic bath (indirect) or an ultrasonic probe (direct). Cavitation occurs in an uncontrollable manner in ultrasonic bath devices, isolating the sample from the energy source. As a result of the reduced intensity, some authors suggest that the ultrasonication bath's application effects are more related to heat rather than cavitation (Patricio, et al., 2006). On the other hand, the ultrasonication zone in an ultrasonic probe device is directly at the end of a small tip and in direct contact with the sample. Therefore, the ultrasonication effects in probe devices are more intense and concentrated.

Among these two ultrasonication approaches, probe systems are typically favored over bath systems in the application for efficient intracellular extraction of biomolecules. Han, et al. (2018) investigated the various types of ultrasonic processors used in the extraction of phenolic compounds and discovered that the extraction yield attained using an ultrasonic probe was twice that of the ultrasonic bath approach.

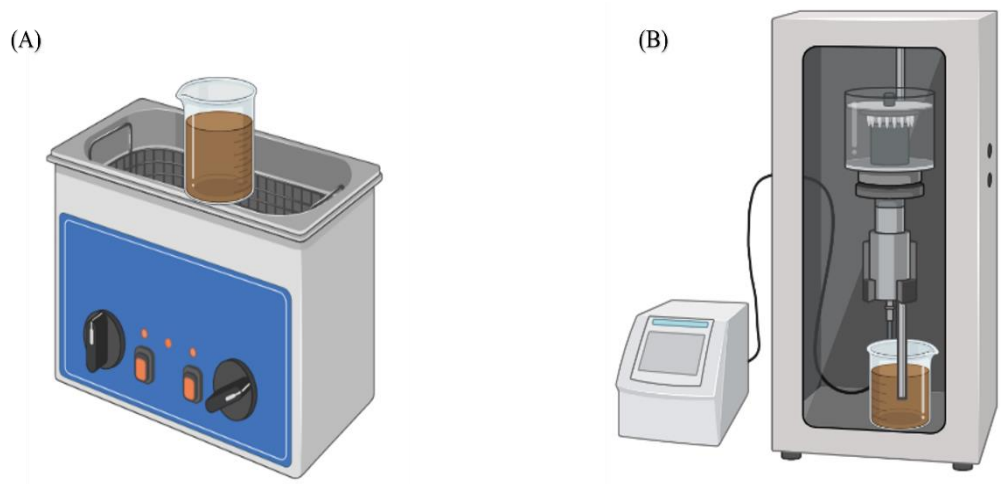


Figure 2.8: Types of Ultrasonic Processors: (A) Ultrasonic Bath and (B) Ultrasonic Probe

2.4.2.2 Ultrasonication Conditions: Ultrasonication Frequency

Given that ultrasound is a mechanical wave, frequency is one of the main elements influencing the cavitation effect. It is commonly expressed in the units of hertz (Hz) as the number of acoustic cycles per unit of time. In general, ultrasound applications can be distinguished into two groups: high-frequency ultrasound (2 – 20 MHz) and low-frequency ultrasound (20 – 100 kHz) (Altaf, et al., 2018). Non-destructive applications like medical imaging and chemical analyses rely primarily on high-frequency ultrasound. In contrast, low-frequency ultrasound is typically employed to alter the chemical or physical properties of materials (Gallo, Ferrara and Naviglio, 2018).

The frequency of ultrasonic waves is inversely proportional to the rarefaction phase's duration and the cavitation bubbles' size (Brotchie, Grieser and Ashokkumar, 2009). The growth of cavitation bubbles is less likely to be

triggered in high-frequency ultrasound because of the suppression of the compression-rarefaction cycle. Since cavitation is the critical process that releases the intracellular materials to the aqueous phase, which enhances the extraction yield, low-frequency ultrasound is preferred. At lower ultrasonication frequencies (< 100 kHz), mechanical effects and physical degradation are more prominent, whereas at higher ultrasonication frequencies (200 – 1,000 kHz), chemical effects are more prominent. There have been several investigations on the recovery of intracellular bioactive compounds by altering the frequencies (Kumar, Srivastav and Sharanagat, 2021). Vast majority of the studies engage at constant low frequencies (20 – 120 kHz), with 20 kHz being the most common.

2.4.2.3 Ultrasonication Conditions: Ultrasonication Power

There is a direct correlation between ultrasonication power and cavitation intensity. The ultrasonication amplitude has been commonly used to express the power delivered during ultrasonication, with values ranging from 0 % to 100 %, where 100 % represents the device's power rating. Amplitude is crucial in intensification as it reflects the distance of the ultrasound wave can longitudinally fluctuate. Increasing the ultrasonication amplitude enhances the cavitation intensity within the liquid. This can be explained by the fact that the quantity of cavitation bubbles is directly proportional to the power (Shojaeiarani, Bajwa and Holt, 2020).

However, the higher amplitude does not necessarily improve the process efficiency and cavitation effect. When extremely high ultrasonic amplitudes are applied, a high concentration of cavitation bubbles is formed, resulting in an extensive inter-bubble collision, deformation, and non-spherical collapse, which may not provide beneficial results (Kumar, Srivastav, and Sharanagat, 2021). Furthermore, the cavitation bubble layer accumulated around the probe impedes the energy transmission into the medium, lowering the ultrasonic efficiency. This is known as the decoupling or cushion effect. Additionally, transducers may experience premature failure due to extreme cavitation at the liquid-transducer interface. To avoid the undesirable effects, it is crucial to optimize the ultrasonication power.

2.4.2.4 Ultrasonication Conditions: Ultrasonication Duration

The standard hypothesis has been empirically proven by data from real-world experiments, which show that a higher yield can be attained by prolonging the reaction for a more extended period. However, the effect of increasing the ultrasonication duration is very much alike the effect of increasing the ultrasonication power. An increase in ultrasonication duration initially results in a higher yield, but this effect is just transitory, as further increment in time results in a decreasing yield.

Upon the initial increase in ultrasonication duration, the cavitation effect of the ultrasound stimulated the fragmentation and pore development of the tissue matrix from which the intracellular solute can be easily extracted, hence

increasing the yield. Due to the thermo-sensitivity and molecular alterations, ultrasonication was not suggested for a prolonged reaction time as it could lead to the degradation of the product of interest and the induction of undesired reactions. Aside from that, some data imply that ultrasonication could be set for less than a minute for energy cost optimization (Liu, et al., 2022).

2.4.2.5 Probe Position

In recent studies, the position of the ultrasonic probe has been investigated in relation to the ultrasound irradiation efficiency. Reportedly, geometric factors such as probe immersion depth can significantly affect the cavitation phenomena. According to Cao, et al. (2021), the maximum sound pressure occurs when the probe is positioned in proximity to the vessel bottom. This is because of the significant impedance differential that exists between the solution and the beaker wall. In addition to that, Fukunaga, et al. (2019) studied the ultrasonic fragmentation rate of micro-size particles under different horn positions. Attenuation may arise due to reflection, refraction, diffraction, or scattering of waves, and this is an issue that must be addressed. Hence, an optimum probe position is desirable to achieve maximum ultrasonication efficiency.

2.5 Biodiesel as a Sustainable Energy Source

The imminent depletion of fossil fuel reserves, combined with environmental concerns, has fueled the desire to achieve energy independence by encouraging the development of sustainable and ecologically friendly biofuels. Biodiesel, a renewable liquid fuel, has been advocated as a potential energy source in the future. It outperforms petroleum-based fuels in several aspects, including being biodegradable, non-toxic, and emitting fewer harmful pollutants. In addition to that, due to its similar qualities to diesel fuel, it can be utilized in existing diesel engines without requiring major modifications (Ogunkunle and Ahmed, 2019).

Figure 2.9 depicts the estimated expenditures for biodiesel production. The oil feedstock cost plays the most crucial factor in the commercial viability of biodiesel, accounting for 75 % of the overall cost of the process. Biodiesel can be synthesized from several sources of renewable lipids, including edible and non-edible oil, waste oil, animal fats, and microalgae. Commonly, edible oil is the leading resource for the manufacturing of biodiesel. Nevertheless, the utilization of edible oil invariably sparks controversy and establishes a conflict between the availability of food and fuel. To alleviate the problem, cheaper and non-edible feedstock like waste oil has received an upsurge in interest to be employed for biodiesel synthesis.

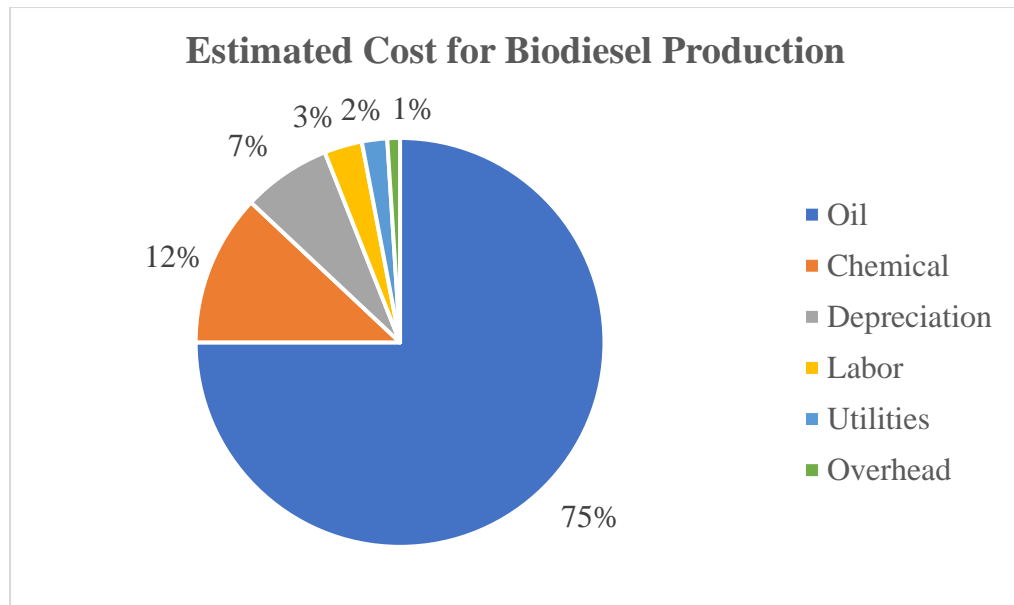


Figure 2.9: Estimated Cost for Biodiesel Production (Zulqarnain, et al., 2021)

The production of biodiesel can be accomplished in several routes, which are outlined in Table 2.7. Direct usage and blending of raw oil are among the earliest approaches, in which vegetable oil is used directly or in combination with petroleum fuel to power the engine. Microemulsion, on the other hand, is a colloidal equilibrium dispersion that arises spontaneously from the combination of two immiscible liquids. Thermal cracking is another approach that uses high temperatures to convert triglycerides into biofuel. In recent years, transesterification has been actively investigated as the most popular method of converting triglycerides into biodiesel. Of these methods, transesterification is the most prominent method for producing biodiesel due to its low production cost and high yield (Salaheldeen, et al., 2021).

Table 2.7: Routes for Biodiesel Synthesis (Zahan and Kano, 2018)

Methods	Main Process	Advantages	Disadvantages
Blending	Blend with petrol-fuel	Non-chemical process	High viscosity and problem in engine
Microemulsion	Solubilized in solvent and surfactant	Hybrid fuel	High viscosity and low stability
Thermal cracking	Conversion by means of heat	Effective and simple	High temperature and expensive
Transesterification	Reacted with alcohol and catalyst	High conversion	Required separation

2.5.1 Transesterification

Crude oil typically possesses a high viscosity, making it unsuitable for continuous running fuel. As a result, transesterification is performed to lower the viscosity by treating it with excess alcohol, coupled with a catalyst. Methanol is typically the most preferred alcohol used in biodiesel production due to its widespread accessibility, low cost, and improved reactivity (Ishak and Kamari, 2019). As illustrated in Figure 2.10, the transesterification pathway possesses a series of successive reversible reactions. Firstly, the triglyceride molecules react with alcohol to form diglyceride, which is then converted to monoglyceride and finally to glycerol, yielding one ester molecule per step.

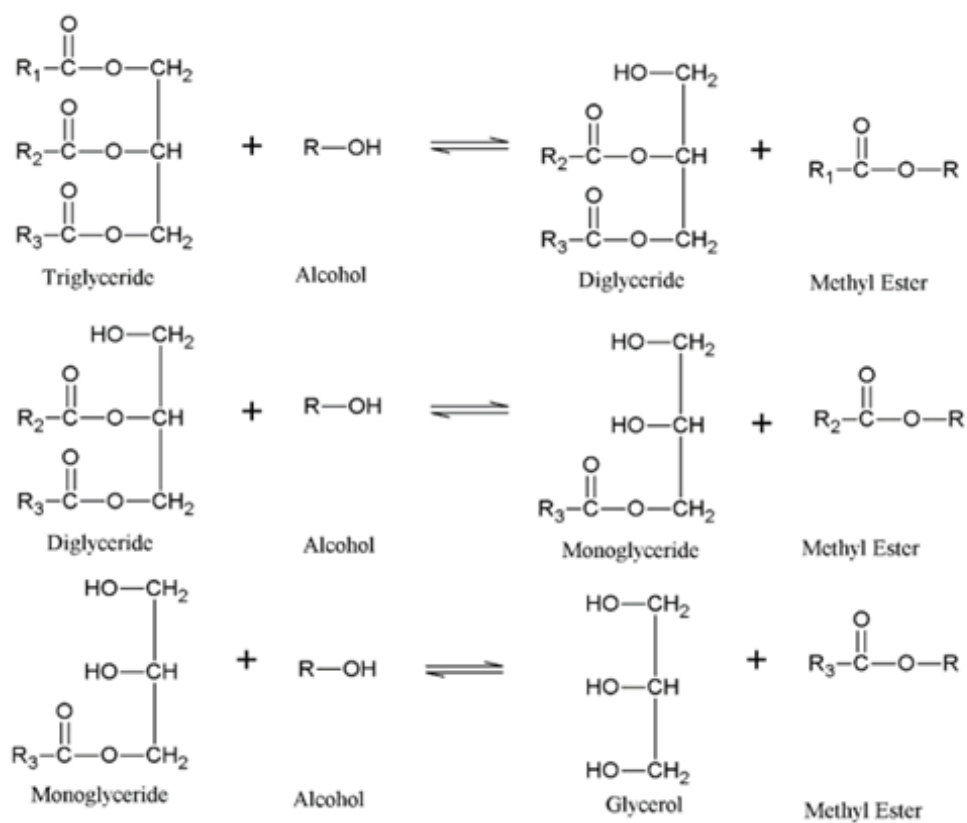


Figure 2.10: Reaction Scheme of Transesterification (Luna, et al., 2016)

The transesterification reaction is typically catalyzed, and numerous types of catalysts are available, including homogeneous, heterogeneous, and biocatalyst. Table 2.8 outlines the benefits and drawbacks associated with the various types of catalysts. Among these, the homogeneous catalyst is the most advantageous and applicable for industrial-scale biodiesel production.

Table 2.8: Types of Catalysts for Transesterification Reaction

Catalyst	Advantages	Disadvantages
Homogeneous	High efficiency, low cost and industrial applicable	Requires extensive separation
Heterogenous	Triphasic system which simplifies separation	Limitation of active sites and long reaction time
Biocatalyst	Environmentally friendly	High preparation cost, reusability issue, and low stability

2.5.2 Homogeneous Catalyst

The homogeneous catalyst can be categorized into two distinct groups: alkali and acid. Homogeneous alkali catalysts, such as alkali metal-based alkoxides and hydroxides, are the most common type of catalysts employed in the commercial sector as they can catalyze the reaction faster than acid catalysts. Furthermore, they are extensively employed not just because of their inexpensive cost, but also because of their ability to promote high yield in a minimal time under mild operating conditions. Cercado, Ballesteros and Capareda (2018) compared several types of homogeneous alkali catalysts for microalgae transesterification and discovered that sodium hydroxide (NaOH) and potassium hydroxide (KOH) performed better than lithium hydroxide (LiOH). KOH is favored over NaOH because it has a reduced propensity for soap formation, which subsequently reduces ester losses. In addition, unlike the murky gel glycerol created by NaOH, the glycerol formed by KOH is in liquid

form, and it is easier to separate from the methyl ester (Thaiyasuit, Pianthong and Worapun, 2012).

Despite their high catalytic reactivity and accessibility, their limitation is that the feedstock with a high FFA level and water content is not recommended. This is because water hydrolyses the triglycerides, resulting in increased FFAs and subsequent soap formation, both of which reduce the output. To enhance conversion, the feedstock utilized in alkaline-catalyzed transesterification should contain an FFA value of less than 2 wt%, corresponding to an AV of 4 mg KOH/g oil (Tan, et al., 2019). If this value is surpassed, saponification will occur, causing excess soap to gel. This will, in turn, increase the viscosity of the mixture and interfere with the product separation. An excessive amount of soap will not only impair yield, but will also partially consume the catalyst, leading to increased expenditures.

Homogeneous acid catalyst, on the other hand, is superior to alkali catalyst for feedstock containing a high FFA content as it can catalyze both transesterification and esterification reactions simultaneously by functioning as both a solvent and an esterification reagent. Besides, the benefits of using a homogeneous acid catalyst include increased resilience to moisture and the absence of soap production (Singh and Kumar, 2018). Due to its high acid strength, sulfuric acid (H_2SO_4) is one of the widely used acid catalysts because it tends to release more H^+ ions to protonate the fatty acids' carboxylic moiety.

However, the use of homogeneous acid as the only catalyst has been discouraged due to its comparatively poor catalytic activity, lengthy reaction time (> 48 hours), high temperature (70 – 200 °C) and pressure (6 – 10 bar) requirements (Parkar, Choudhary and Vijayanand, 2012). Although increasing the acid loading (5 wt%) and alcohol-to-oil molar ratio (20:1 – 45:1) can improve the reaction kinetics, it is unfavorable in commercial applications due to increased operating costs and reactor corrosion.

2.5.3 Two-Step Esterification and Transesterification

Low-cost raw materials, such as unrefined plant oil or waste vegetable oil, are more advantageous as they can offset the high manufacturing cost and food conflict associated with the use of expensive refined oil feedstock. Nevertheless, they possess a high FFA content and are incompatible with single-stage base-catalyzed transesterification. As a result, a pre-treatment is required prior to the base-catalyzed transesterification to convert the FFA to FAME, and this two-step process was advocated as a more efficient approach. The feedstock with a high FFA content will be first pre-treated with acid catalyst (1st step: FFA esterification) to lower the FFA level to less than 2 % by weight, followed by alcoholysis with alkali catalyst (2nd step: triglycerides transesterification) to produce biodiesel (Thoai, et al., 2019). By doing so, the undesirable saponification reaction can be avoided while boosting the FFA conversion. Figure 2.11 illustrates the esterification reaction between FFA (a carboxylic acid) and alcohol to produce ester compounds.

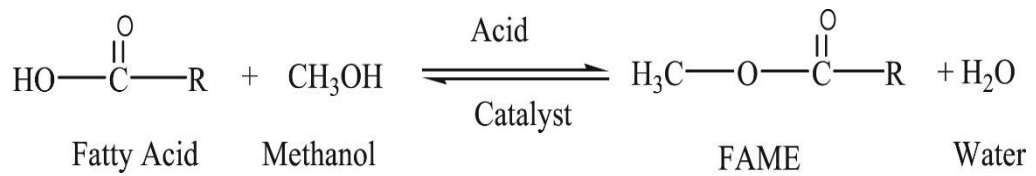


Figure 2.11: Reaction Scheme of Esterification of Fatty Acids (Tavizón-Pozos, et al., 2021)

Table 2.9 summarizes the recent publications related to the treatment of various high FFA feedstocks through sulfuric acid-catalyzed esterification. Most of the sulfuric acid-catalyzed esterification showed promising results with FFA conversion above 80 %, proving that they have a large potential to be further developed and utilized in the industrial scaled production. Four main parameters affect the conversion of FFA: catalyst loading, alcohol-to-oil molar ratio, reaction time, and operating temperature. In most sulfuric acid-catalyzed esterification reactions, the required catalyst loading amount was less than 5 wt%. According to the stoichiometric equation for esterification reaction (Figure 2.11), one mole of alcohol is required to react with one mole of fatty acids to produce one mole of alkyl ester, as a product, and one mole of water, as a co-product. However, esterification is also a reversible reaction. Hence, a high alcohol-to-oil molar ratio of about 6:1 to 16:1 is suggested for an effective reaction. The optimum reaction time for esterification ranged from 1 to 6 hours, varied with other operating conditions and types of catalyst utilized. Most investigations were conducted at temperatures below the boiling point of methanol (about 60 °C) to avoid unintended loss.

Table 2.9: Treatment of High FFA Feedstock through Sulfuric Acid-Catalyzed Esterification

Feedstock	Reaction conditions				Initial FFA to Final FFA (%)	Conversion (%)	References
	Catalyst	Alcohol to oil	Time	Temperature			
	loading (wt%)	molar ratio	(min)	(°C)			
Coconut fatty acid distillate	2.5	10:1	90	60	24.5 to 1.9	92.24	(Rajesh, et al., 2021)
Grease trap waste	3	6:1	180	75	36.4 to 0.84	97.69	(Tran, McMurchie and Ngothai, 2018)
Kapok Randu (<i>Ceiba pentandra</i>) seed oil	0.5	12:1	120	60	8.89 to 0.43	95.14	(Kusumaningtyas, Akbar and Widjanarko, 2019)
Rubber seed oil	1.38	16:1	120	50	23.2 to 0.16	99.3	(Chuah, et al., 2016)

Table 2.9 (Continued): Treatment of High FFA Feedstock through Sulfuric Acid-Catalyzed Esterification

Feedstock	Reaction conditions				Initial FFA to Final FFA (%)	Conversion (%)	References
	Catalyst loading (wt%)	Alcohol to oil molar ratio	Time (min)	Temperature (°C)			
Waste cooking oil	0.2	2.5:1	360	60	2.75 to 0.31	88.80	(Sahar, et al., 2018)
Waste fish oil	1.5	15:1	160	60	21 to 1.5	92.60	(Kara, et al., 2018)
Waste vegetable oils	0.41	10:1	60	60	13 to 0.53	95.92	(Photaworn, Tongurai and Kungsanunt, 2017)
Sludge palm oil	0.75	8:1	60	60	23.2 to < 2	94.00	(Hayyan, et al., 2011)

2.5.4 Ultrasound-Assisted Biodiesel Production

The most common problem encountered in biodiesel production is the immiscibility of oil and alcohol, which leads to a slow interphase mass transfer rate. There is also a noticeable issue with the current heating system for biodiesel reactions in terms of both technical circumstances and production costs. One of the primary advantages of conventional systems is their ease of installation and operation. However, only surface-level heat transfer occurs. As a result, heating became less effective, and energy consumption was higher.

Alternatively, ultrasonication appeared to be a promising auxiliary tool in accelerating biodiesel production. Low-frequency ultrasound has been widely demonstrated to be a highly effective technique for emulsifying immiscible liquids by inducing cavitation bubbles near the phase boundary. Cavitation bubbles that collapse asymmetrically generate microturbulence, which disrupts the phase boundary and induces emulsification. The mass transfer and interfacial area between the two phases increase as the emulsion forms, accelerating the reaction kinetics. Aside from providing intensive mixing, the uniform heating supplied by the localized temperature increase due to the cavitation effect reduces the energy consumption for external heating. Boffito, et al. (2014) proved the ability of ultrasound to raise the temperature intrinsically. The temperature of the sample was increased by 23°C within seconds of commencing ultrasonication, which was significantly quicker than the conventional heating. Furthermore, highly reactive species generated during

the dissociation of solvent vapor trapped in the cavitation can also aid in expediting the reaction.

Hsiao, et al. (2021) employed an ultrasound-assisted approach to produce biodiesel from spent cooking oil in a two-step esterification and transesterification process. After a total 80 minutes of ultrasonication at 600 W, the FFA effectively decreased from 2.18 % to 0.84 %, yielding an ester content of 97.05 %. It was discovered that ultrasound saved 42.9 % of the time compared to the conventional method, which took 140 minutes. Trinh, Yusup and Uemura (2018) investigated the acid esterification pre-treatment of high FFA rubber seed oil using direct ultrasonic irradiation. After 30 minutes of treatment with ultrasonic irradiation at 250 W, the highest FFA conversion of 98 % was achieved. In contrast with mechanical stirring under the same conditions, only 75 % of the FFA conversion was accomplished, indicating that ultrasound-assisted reaction intensified the FFA conversion. Sungnat and Wongwuttanasatian (2018), on the other hand, utilized indirect ultrasonic irradiation to perform acid-esterification on CPO. The FFA was reduced from 11.3 % to 0.63 % after 70 minutes of treatment at 200 W. However, there has been relatively little literature published on the comparison between direct and indirect ultrasonic irradiation on FFA conversion.

Several factors, including power applied and reaction time, influence the FFA conversion or biodiesel output in ultrasound-assisted reactions. Tan, et al. (2019) reviewed the factors affecting the efficiency of ultrasound-assisted transesterification, and the findings are summarized as follows. When compared

to mechanical stirring, it was discovered that the ultrasonication technique achieved 20 – 25 % and 16.67 – 25 % reductions in the catalyst loading and alcohol-to-oil molar ratio, respectively. With the assistance of ultrasound, the reaction time could also be lowered by at least 25 % and up to 95.8 %. It was also claimed that ultrasonication used 30 – 50 % the energy of mechanical agitation. Consequently, the integration of ultrasonication technique in biodiesel synthesis can minimize operating costs and energy consumption by eliminating the need for external heating and agitation due to the formation of hot spots and micro-jets.

2.6 Quality of Crude Palm Oil (CPO)

CPO is mainly composed of triacylglycerols, diacylglycerols, and monoacylglycerols, with a small fraction of unsaponifiable matter that includes impurities, FFA, moisture, and minor constituents of non-oil fatty matter. Carotenoids, phosphatides, squalene, sterols, tocopherols, and tocotrienols are among the minor components found in CPO (Goh, Choo and Ong, 1985).

Palm oil quality is regulated by both the government and the private sector. This is accomplished through the implementation of systematic assurance systems in line with international standards, such as Good Manufacturing Practices (GMP) and Hazard Analysis and Critical Control Point (HACCP) (Nizam and Mahmud, 2021). Table 2.10 outlines the quality requirements for CPO in accordance with Malaysian Standards (MS 814:2007). The adoption of Malaysian Standards (MS) is entirely optional, except for

circumstances in which the regulatory authorities make its application obligatory with the implementation of legislation or local by-laws.

Table 2.10: Quality Specifications for CPO in accordance with MS 814:2007

Characteristics	CPO	
	Special quality (SQ) grade	Standard quality (STD) grade
DOBI	Min 2.8	Min 2.3
M&I	Max 0.25 %	Max 0.25 %
FFA	Max 2.5 %	Max 5 %
PV	Max 1.0 meq/kg	Max 2.0 meq/kg

Evaluation of the quality of CPO is performed using metrics such as deterioration of bleachability index (DOBI), moisture and impurities (M&I), free fatty acid (FFA), and peroxide value (PV). DOBI value represents the sample's rate of oxidation as well as the ease of bleaching throughout the refining process. Table 2.11 categorizes the palm oil quality based on DOBI. M&I is another key parameter in determining the quality of CPO because it affects the oil's shelf life indirectly. Hydrolytic rancidity caused by the formation of FFA contributes to objectionable odor, poor stability, and processing difficulties. PV is a biomarker of the early stages of rancidity that occur under mild conditions, and a value less than 2.0 meq/kg indicated that the oil was fresh. Residual oil that compliances the quality specification for CPO can be employed for any edible purpose (Sulin and Mokhtar, 2019)

Table 2.11: Classification of Palm Oil Quality based on DOBI

DOBI value	Difficulties in refining	Grade
1.68 – 2.30	Hardest	Poor
2.31 – 2.92	Hard	Fair
2.93 – 3.24	Easy	Good
> 3.24	Easiest	Excellent

Table 2.12 summarizes the typical fatty acid composition of CPO in compliance with MS 814:2007. Due to its well-balanced fatty acid composition, CPO exhibits a semi-solid nature at ambient temperature.

Table 2.12: Fatty Acid Composition of CPO in accordance with MS 814:2007

Fatty acid composition (wt%)	Observed range
C12:0	0.0 – 0.5
C14:0	0.9 – 1.5
C16:0	39.2 – 45.8
C16:1	0.0 – 0.4
C18:0	3.7 – 5.1
C18:1	37.4 – 44.1
C18:2	8.7 – 12.5
C18:3	0.0 – 0.6
C20:0	0.0 – 0.5

2.7 Quality of Biodiesel

The establishment of biodiesel standards is a crucial step towards market entry and commercialization since it governs the quality and provides assurance to the end users. The international specifications for biodiesel quality monitoring are European Standard (EN 14214) and American Standard (ASTM D6751). The Standard and Industrial Research Institute of Malaysia (SIRIM) is responsible for establishing the quality standards for palm-based biodiesel in Malaysia. The Malaysian Standard (MS 2008:2008) was established in 2008, and it is primarily based on EN 14214, with minor adjustments suggested by the Technical Committee on Petroleum Fuels. Table 2.13 summarizes the standard specifications for biodiesel fuel and compares the physicochemical properties of palm-based biodiesel produced in Malaysia with respect to diesel fuel standards. In general, the palm-based biodiesel manufactured by the Malaysian Biodiesel Association (MBA) meets both the international and the local criteria, with properties comparable to diesel fuel.

Table 2.13: Standard Specifications for Biodiesel Fuel and a Comparison of Physiochemical Properties of Palm-Based Biodiesel in Malaysia with respect to Diesel Fuel Standard

Properties	MS 2008:2008	EN 14214	ASTM D6751	Malaysian CPO methyl ester	EN 590 (Diesel fuel)
Density at 15 °C	860 – 890 kg/m ³	860 – 890 kg/m ³	-	870 – 880 kg/m ³	820 – 845 kg/m ³
Ester content	Min 96.5 %	Min 96.5 %	-	> 98.5 %	-
Iodine value	Max 110	Max 120	-	52	-
Linolenic acid methyl esters	Max 12 wt%	Max 12 wt%	-	< 0.5 wt%	-
Oxidation stability at 110 °C	Min 6.0 hours	Min 6.0 hours	Min 3.0 hours	> 6 hours	-
Polyunsaturated methyl esters	Max 1 wt%	Max 1 wt%	-	< 0.1 wt%	-
Total acid value	Max 0.5 mg KOH/g	Max 0.5 mg KOH/g	Max 0.5 mg/KOH	< 0.5 mg KOH/g	-
Viscosity at 40 °C	3.5 – 5.0 mm ² /s	3.5 – 5.0 mm ² /s	1.9 – 6.0 mm ² /s	4.4 mm ² /s	2.0 – 4.5 mm ² /s

CHAPTER 3

RESEARCH METHODOLOGY

3.1 Overall Research Methodology

This research focused mainly on enhancing oil recovery from POME, as the oil encapsulated in the lignocellulosic particles of POME cannot be fully recovered. Various oil recovery methods have been investigated; however, the use of ultrasonication as a pre-treatment to improve the oil content from POME has yet to be studied.

A systematic review was conducted to identify studies related to ultrasound-enhanced oil recovery from POME, as illustrated by the PRISMA flow diagram in Figure 3.1. The electronic databases employed in the search strategy were Scopus, ScienceDirect, Google Scholar, and IEEE Xplore, with no publication date restriction. A comprehensive set of search terms centered on (1) *palm oil mill effluent* and (2) *ultrasonication*, including the international spelling variations as well as thesaurus. Of the 28 full texts reviewed on June 2021, searches returned no papers on the improvement of oil recovery from POME using ultrasonication. Since improving oil recovery from POME exhibits multiple benefits, it is crucial to investigate the potential of employing ultrasonication as a pre-treatment technique to boost oil recovery yield.

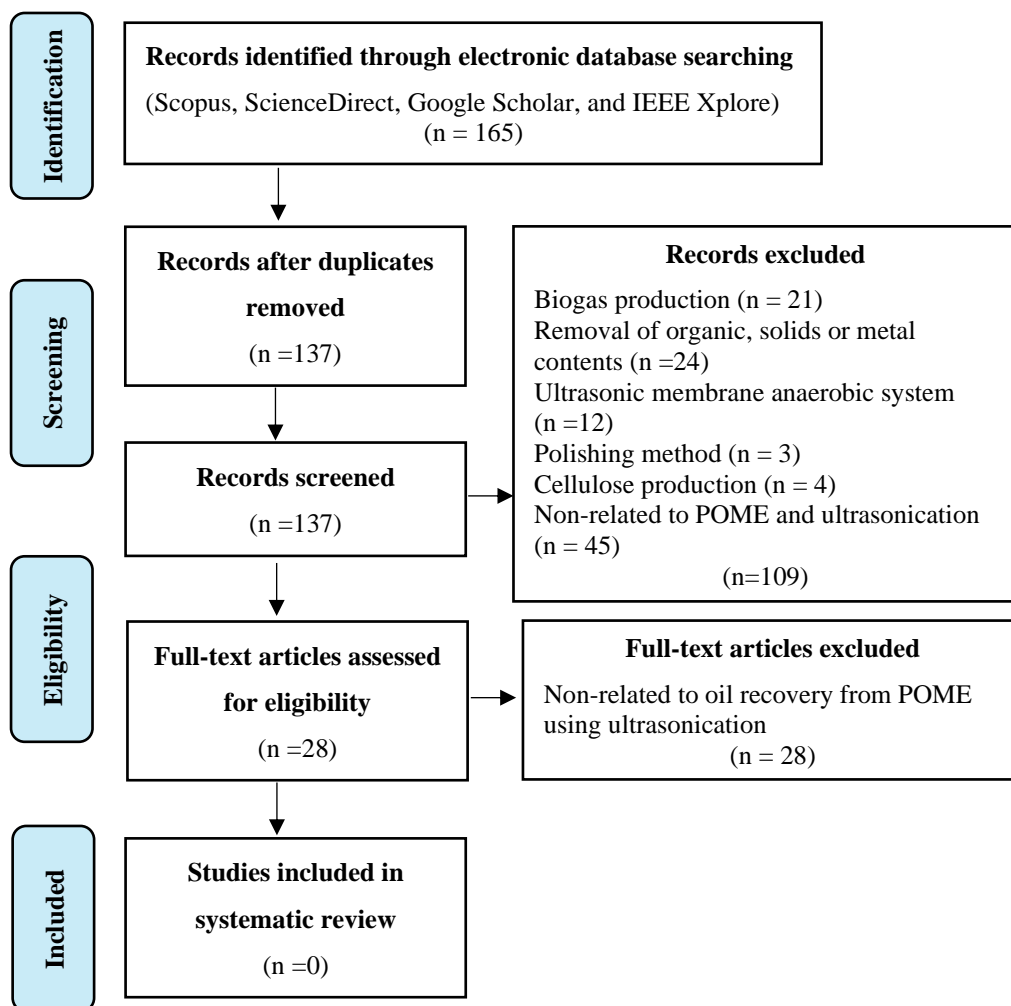


Figure 3.1: PRISMA Flow Diagram for Systematic Review

This research was performed using a quantitative approach, with an emphasis on data collection and statistical analysis. Figure 3.2 shows the overall research flowchart. Basically, this study is divided into two main stages: (1) enhancement of oil recovery from POME using ultrasonication technique and (2) biodiesel production using the recovered oil from POME. Appendix A contains a list of the chemicals and instruments required for this study.

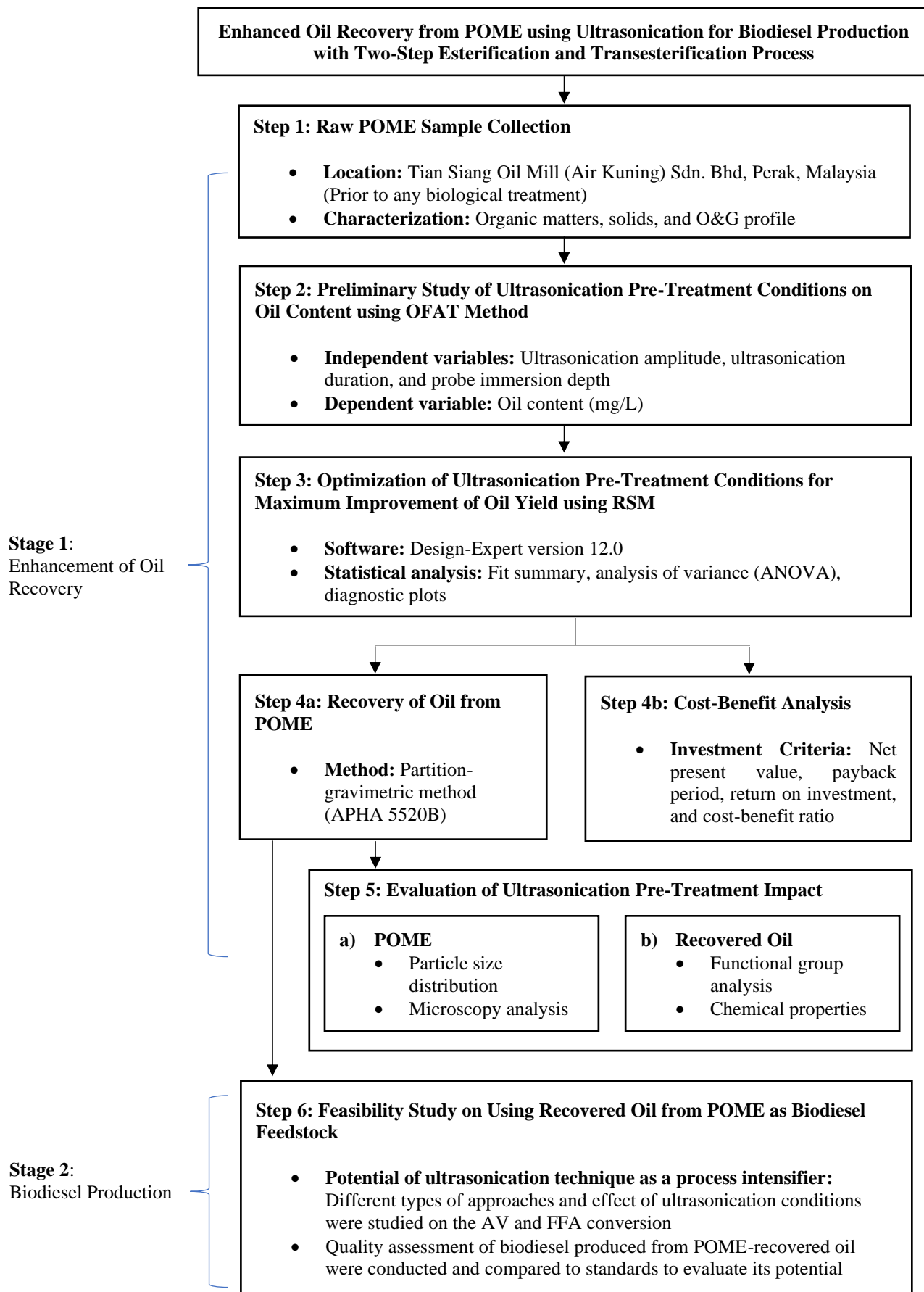


Figure 3.2: Overall Flowchart

3.2 POME Sample Collection

Tian Siang Oil Mill (Air Kuning) Sdn. Bhd., which is situated in the district of Batang Padang, Perak, Malaysia, was chosen as the site for sample collection. The mill was commissioned in the year of 2000, with a daily FFB process throughput of 80 MT/hr, expandable to 120 MT/hr. The mill operates on an ad hoc basis, depending on the demand and pricing. In addition to its palm oil milling operations, this mill also features a biogas anaerobic digestion facility. Tian Siang Oil Mill was 24.2 km apart from UTAR Kampar campus, and each journey took around two hours, including sample collection time. The raw POME sample was collected after the CPO processing from decanter and before any biological treatment process (Figure 3.3) and immediately transported to the FEGT environmental laboratory for analysis. To reduce the probability of chemical reaction occurrence and sample biodegradation, the samples were preserved and stored in accordance with the manner described in Appendix B by the United States Environmental Protection Agency (1982).

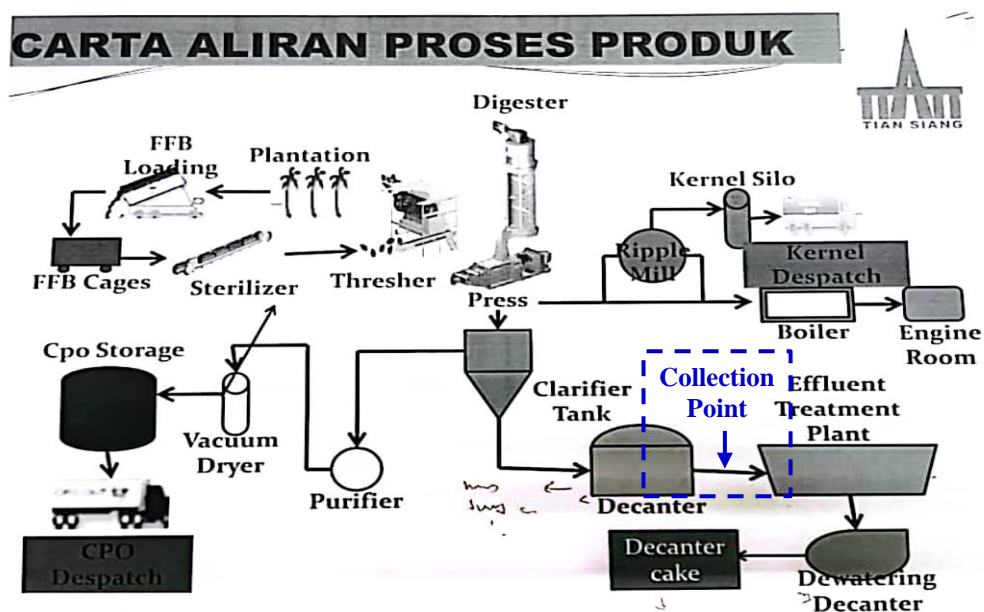


Figure 3.3: Raw POME Sampling Collection Point from Tian Siang

3.3 POME Sample Characterization

For each batch of samples collected, the characteristics of the POME sample were determined in triplicate in compliance with the American Public Health Association (APHA) Standard Methods (2017). This information is beneficial in providing an overview of its pollution potential. Table 3.1 and Appendix C outline the methods and provide an in-depth explanation of the parameter testing procedures.

Table 3.1: Methods for Characterization of POME

Parameter	Method
pH	APHA 4500 H ⁺
Biochemical Oxygen Demand (BOD)	APHA 5210 B
Chemical Oxygen Demand (COD)	APHA 5220 B
Total Solid (TS)	APHA 2540 B
Suspended Solid (SS)	APHA 2540 D
Total Volatile Solid (TVS)	APHA 2540 E

3.3.1 Methods for Determination of O&G

According to APHA Standard Methods, there are several ways to determine O&G, including the partition-gravimetric method (5520 B), partition-infrared method (5520 C) and Soxhlet method (5520 D). With POME moisture content predominantly at around 95 – 97 %, the overwhelming presence of the liquid phase rendered the Soxhlet method (5520 D) to be ineffective, as it is the

method of choice when the sample is solid. In addition to the drawbacks outlined in Section 2.3.2, the Soxhlet method would not be considered since it is time-consuming and energy intensive. The partition-infrared approach (5520 C), on the other hand, is intended for samples with low levels of O&G (< 10 mg/L). This is inappropriate for POME, which has an O&G concentration ranging from 130 to 18,000 mg/L. The partition-gravimetric method (5520 B), which employs the LLE technique, is appropriate for sludges with the behavior and consistency of aqueous liquids. In short, the partition-gravimetric approach (5520 B), further explained in Section 3.5, is the preferred method for determining O&G in POME. The general equation for the determination of O&G in POME is:

$$\text{Oil content (mg/L)} = \frac{(\text{Mass of residual oil,g}) \times 1000}{\text{Sample volume,L}} \quad (3.1)$$

3.4 Ultrasonication Pre-Treatment Conditions for Oil Enhancement Process

Ultrasonication is a straightforward physical pre-treatment that can be directly applied on POME to improve the oil recovery yield by disrupting the cell that encapsulates the lipids. In the present study, hydrodynamic mechanical shear forces induced by the cavitation effect of ultrasound are responsible for structural modification rather than the complete degradation of effluent.

An ultrasonic probe system consists of four fundamental components: a generator, a transducer, a booster, and a probe. The generator transforms the

grid's alternating current (AC) line voltage into high-frequency electrical energy, which the transducer converts into high-frequency mechanical vibration in the form of piezoelectric crystal oscillations. These mechanical vibrations are then conveyed to a booster, which is a mechanical amplifier capable of adjusting the amplitude of the vibrations. Lastly, ultrasonic waves are delivered into the sample via the probe.

As shown in Figure 3.4, an ultrasonic processor model *Q500* from *Qsonica* (*Newton, Connecticut*), equipped with a threaded-end type probe and a 1.3 cm diameter interchangeable titanium alloy tip, was utilized for the pre-treatment of 200 mL POME. This equipment operates at a frequency of 20 kHz and has a maximum power input and amplitude of 500 W and 120 μm , respectively. The batch ultrasonication chamber was a 250 mL borosilicate glass beaker with dimensions of 9.5 cm in height and 7.5 cm in diameter, respectively. The ultrasonic probe system was placed inside a sound-proof enclosure with interior walls coated with water-resistance acoustic foam.

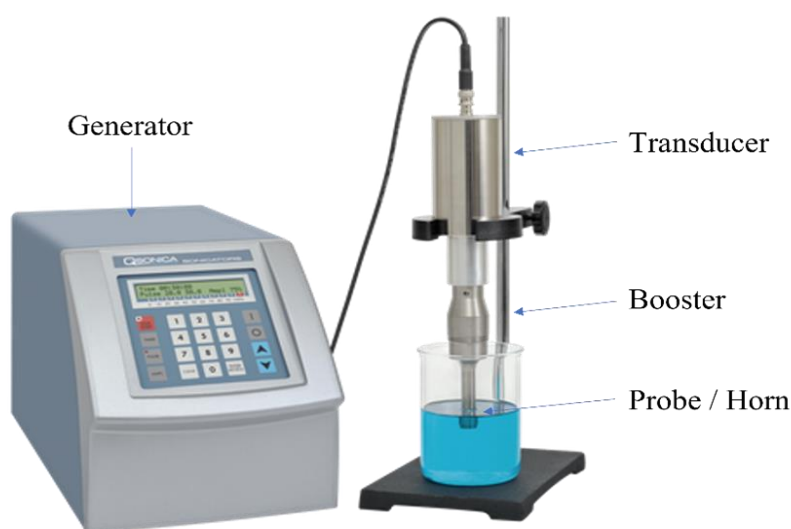


Figure 3.4: Ultrasonic Probe System

3.4.1 Preliminary Study using OFAT

Prior to the RSM optimization study, a preliminary study using a one-factor-at-a-time (OFAT) approach was adopted to evaluate the influence of each factor on the oil content (Equation 3.1) and identify the operating ranges for subsequent statistical design. The experiment was carried out in duplicate, and the mean value was expressed in the result. As discussed in Section 2.4.2, ultrasonication's effectiveness depends on several ultrasound parameters, such as ultrasonication power, duration, and probe position. It is vital to select the appropriate operating parameters to avoid unnecessary energy consumption, sample deterioration, and risk of equipment failure.

The ultrasonic processor is configured with adjustable amplitude and duration. Ultrasonication amplitude, which represents the ultrasonication intensity, is employed to indicate the power of the ultrasonic processor. Due to the limited amplitude control of the *Q500* ultrasonic processor (minimum workable amplitude is 20 %) and with the aim to avoid high energy consumption and risk of equipment failure, an ultrasonication amplitude ranging from 20 – 40 % was investigated on the oil content. Other parameters, such as ultrasonication duration of 30 seconds and probe immersion depth of 2 cm, were kept constant during the experiment.

The effect of ultrasonication duration on the oil content was studied from 1 – 30 minutes based on the typical range from the literature review (Table 2.5). Based on the result (Section 4.2.2), extended exposure to ultrasonication does not result in the enhancement of oil content; rather, it has an opposite effect.

Since this would contradict the research goal of enhancing oil recovery, the effect of ultrasonication duration in terms of seconds (15 – 60 seconds) was investigated, while other parameters, such as ultrasonication amplitude of 30 % and probe immersion depth of 2 cm, were maintained during the experiment.

As shown in Figure 3.5, the probe immersion depth, d , is defined as the distance between the probe tip and the liquid surface. To explore the effect of probe immersion depth in the reaction chamber on oil content, the probe position was varied from 1 – 5 cm using an adjustable support laboratory jack, while other factors, such as ultrasonication amplitude of 30 % and ultrasonication duration of 30 seconds, were maintained.

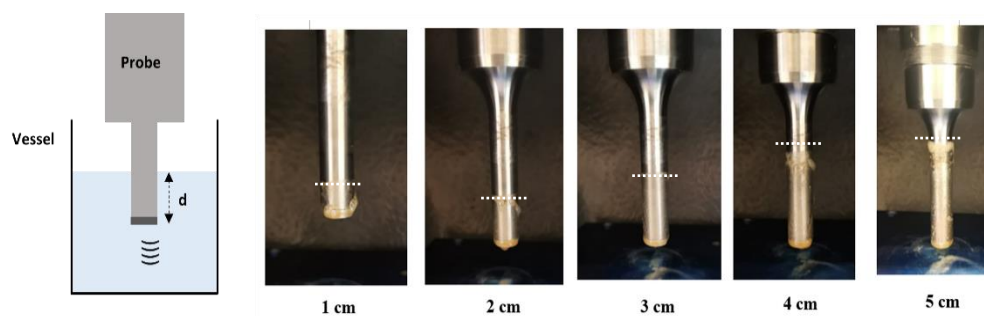


Figure 3.5: Schematic of the Experimental Setup with Varied Probe Immersion Depth

3.4.2 Optimization Study using RSM

The OFAT method employed in classical optimization studies is time-consuming and does not demonstrate the interaction effect between several factors. To address this constraint, RSM, a combination of statistical and mathematical approaches that incorporates the interaction effect between numerous elements, is utilized. Rather than investigating all conceivable combinations, the aggregate mix proportion can be determined with a minimum number of experiments. Figure 3.6 depicts a flow diagram of the RSM process, which comprises four fundamental steps.

The process begins with the selection of the appropriate type of experimental design model. RSM is commonly applied in conjunction with the Box-Behnken design (BBD) or central composite design (CCD). The primary distinction between BBD and CCD is the location of the experimental points within the experimental cubic space, as shown in Figure 3.7. BBD does not include the experimental cubic space's vertices, whereas CCD examines the borderline regions. As a result, BBD has fewer design points than CCD. CCD was selected as it reflects most continuous response surfaces over a relatively broad factor domain. According to past research, the most utilized type of CCD is either face-centered or rotatable. In this research, face-centered is preferable as rotatable has extended the design region beyond the defined variable bound and consists of non-allowable operating conditions.

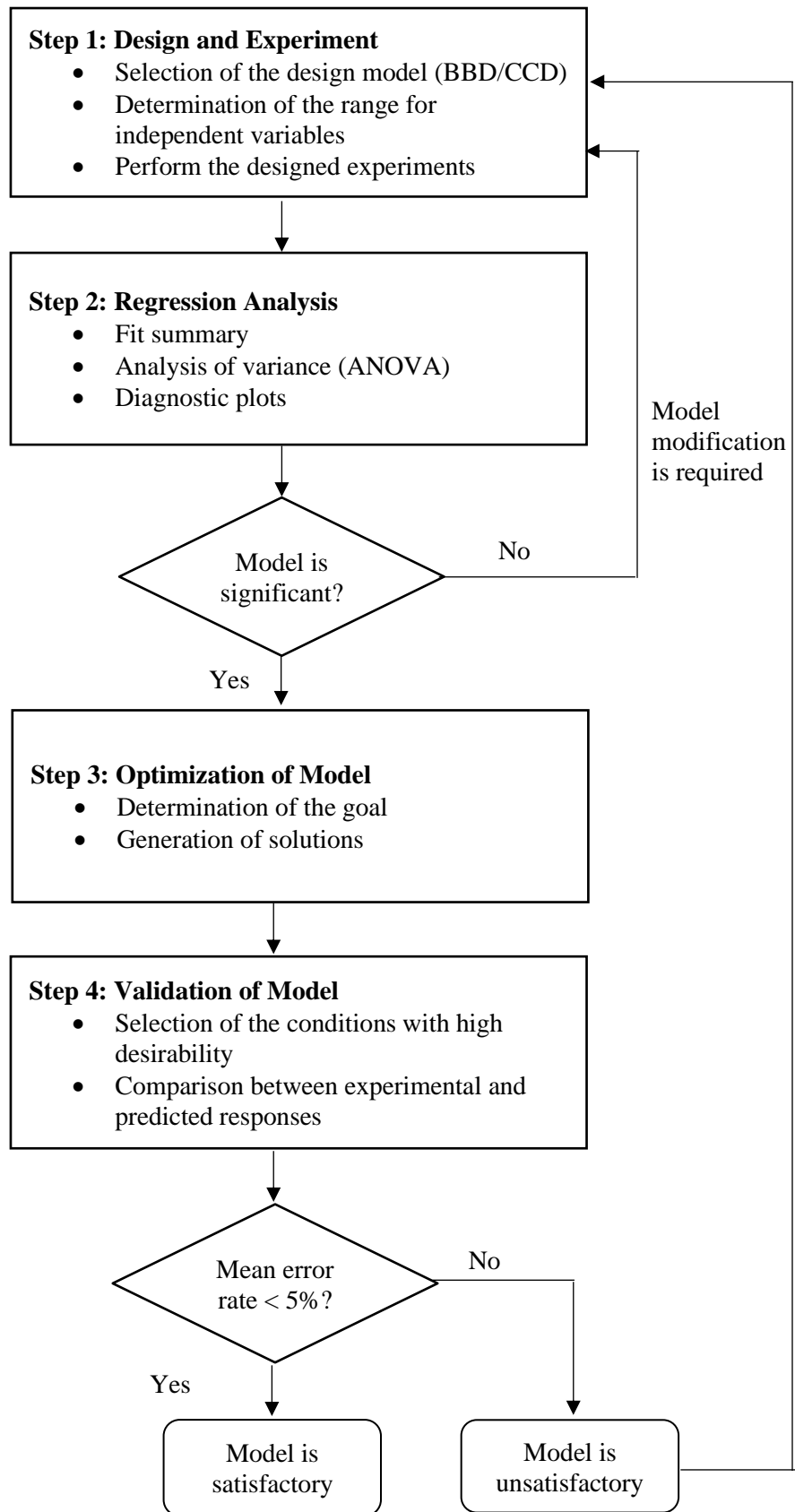


Figure 3.6: Process Flow of RSM

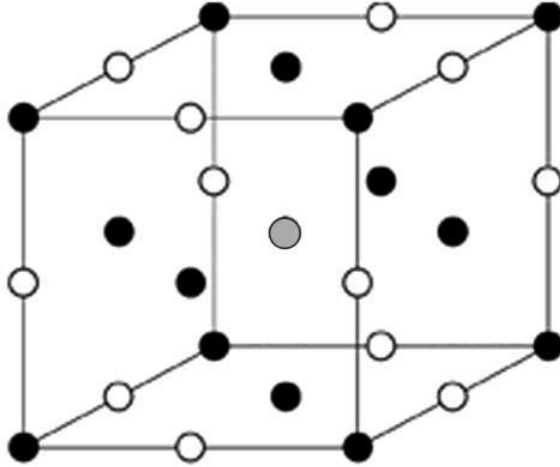


Figure 3.7: Experimental Cubic Space (BBD – White Points with Central Grey Point, FCCD – Black Points with Central Grey Point)

The range of independent variables for optimization was selected based on the results from preliminary study using OFAT (Section 4.2) and is summarized in Table 3.2. As the oil content will vary depending on various factors (Section 4.1), thus, the improvement of oil yield, as computed by Equation 3.2, was selected as the dependent variable, which is the response of the experiment. $O\&G_i$ is the oil content of the sample without ultrasonication pre-treatment, whereas $O\&G_f$ is the oil content of the sample with ultrasonication pre-treatment. The samples utilized throughout the optimization study are consistent; hence, the initial O&G concentration was the same (1,550 mg/L).

$$\text{Improvement of Oil Yield (\%)} = \left(\frac{O\&G_f - O\&G_i}{O\&G_i} \right) \times 100\% \quad (3.2)$$

Table 3.2: Range of Independent Variables for Optimization Study

Independent variables (Factors)	Dependent variable (Response)
A: Ultrasonication amplitude (20 – 40 %)	Y: Improvement of oil yield (%)
B: Ultrasonication duration (10 seconds – 4 minutes)	
C: Probe immersion depth (2 – 4 cm)	

A three-factor face-centered central composite design (FCCD) was applied using *Design-Expert version 12.0 (Stat-Ease Inc, Minneapolis, USA)* software to assess the combined impacts of three independent components and optimize the ultrasound pre-treatment conditions. The design comprises 2^n factorial runs with $2n$ axial runs and $2n$ replications of the center point, where n is the number of factors being investigated (for this case, $n = 3$). CCD generated a total of 20 designated experimental runs.

Next, the obtained experimental data were tabulated and analyzed statistically. The model's adequacy was assessed by the fit summary statistics test. Four sequential models are involved: linear, two-factor interactions (2FI), quadratic, and cubic. These tests select the highest-order non-aliased polynomial model. The coefficient of determination (R^2) serves as a quality indicator for the fitted polynomial model, and the Fisher's test (F-test) was utilized to validate the statistical significance. ANOVA was used to determine the significance of individual, quadratic, and interaction terms. The significance of model terms was evaluated using probability (p-value) with a 95% confidence level. The diagnostic plots assist in determining the model's

satisfactoriness by examining the pattern of all data points. The model's significance is indicated by the normal distribution of residuals and the absence of any outliers in the tested datasets. Insignificant models necessitate adjustments, such as model reduction and response transformation.

Design-Expert software is also capable of generating three-dimensional (3D) response surfaces, which display a more precise relationship between the variables and response. The polynomial equation derived from the regression analysis can be used to forecast the optimal conditions. The optimal ultrasonication conditions for the response were determined via numerical optimization. In this study, the factors were assigned to be in the range, whereas the response was aimed to be maximized. The RSM seeks a combination of factors that meets the conditions specified in each response and factor, and the anticipated conditions were validated through three replicate trials of high desirability. A mean error rate of less than 5 % was used as a benchmark to indicate the model's satisfactoriness for forecasting performance.

3.5 Recovery of O&G from POME

Figure 3.8 depicts the overall flow of oil recovery from POME. POME with and without ultrasonication pre-treatment was subjected to oil recovery in accordance with APHA 5520 B. This is a process of extracting constituents from a liquid solution by contacting them with another liquid in which the constituents are more soluble.

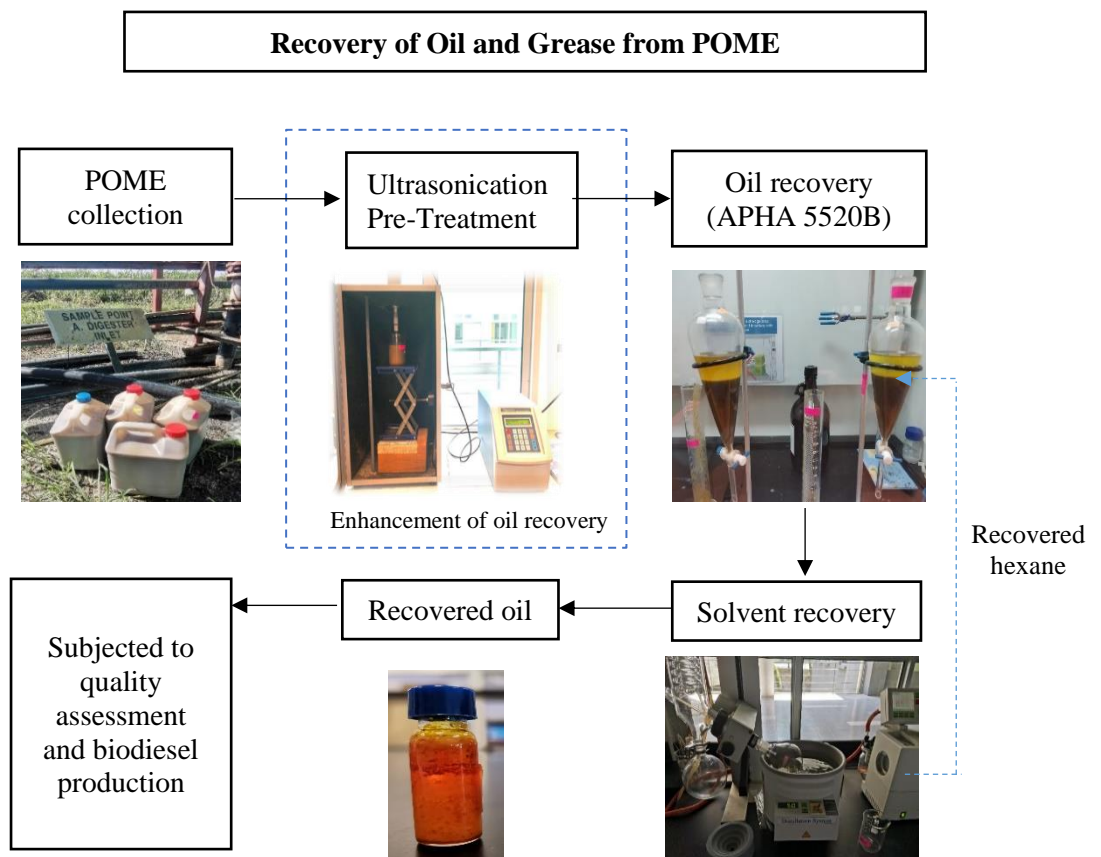


Figure 3.8: Process Flow of Oil Recovery from POME

A predetermined amount of POME sample was combined with hexane as the extraction solvent. The mixture was gently swirled to ensure thorough mixing before allowing the layers to separate in a separatory funnel. The bottom aqueous layer was discharged into an empty flask. In case of an emulsion greater than 5 mL exists, the top solvent layer was discharged into a centrifuge tube and centrifuged for 5 minutes at 2,400 rpm. Afterwards, the solvent layer was transferred into a clean evaporating flask through a funnel containing filter paper with anhydrous sodium sulphate Na_2SO_4 , which absorbs water. The extraction process was repeated twice after recombining the emulsion with the preceding aqueous layer. After three times of extractions, hexane was recovered by distilling off at its boiling point (70°C) using a rotary evaporator (Figure 3.8, solvent recovery). The recovered oil was dried in an oven at 105°C to remove any remaining solvent and moisture. This recovered oil can be further subjected to quality assessment (Section 3.6.2) and biodiesel production (Section 3.8).

3.6 Evaluation of Ultrasonication Pre-Treatment Impact on POME and Recovered Oil

This study postulated that ultrasonication pre-treatment could disrupt the complex particles in POME and liberate the oil content for enhancement of oil recovery. Also, it is hypothesized that this relatively mild pre-treatment will not adversely affect the quality of the oil. Thus, the impact of ultrasonication pre-treatment on POME and recovered oil was assessed, as shown in Figure 3.9.

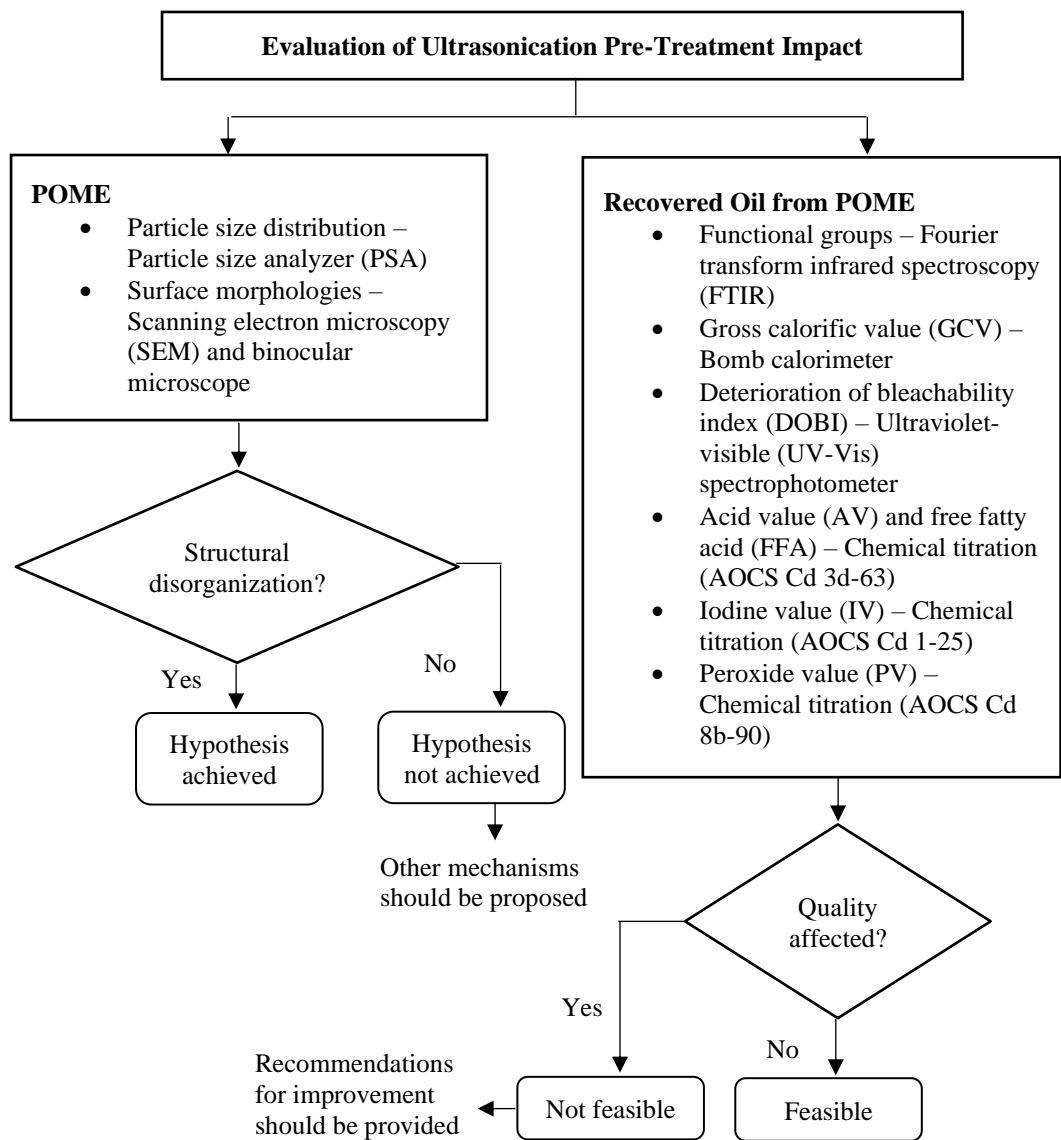


Figure 3.9: Flow of Evaluation of Ultrasonication Pre-Treatment Impact

3.6.1 Impact of Ultrasonication Pre-Treatment on POME

The physical morphology of the POME with and without ultrasonication pre-treatment was characterized using both non-imaging (particle size distribution) and imaging tools (microscopy analysis). These characterization tests were carried out to provide evidence in support of the hypothesis.

The particle size distribution of the non-treated and ultrasound-treated POME was determined using the laser light obscuration method. A small amount of sample was dispersed with distilled water in a *Hydro 2000G* dispersion unit before being injected into the particle size analyzer (PSA), *Malvern Mastersizer 2000*, for analysis. The particle size distribution in the sample was measured in triplicate as a percentage of volume in size ranges between 0.01 to 2,000 μm .



Figure 3.10: PSA (Malvern Mastersizer 2000)

Scanning electron microscopy (SEM) is one of the most popular techniques used to analyze the surface morphology of a material. In this study, the morphologies of POME with and without ultrasonication pre-treatment were analyzed using a field emission scanning electron microscope (FESEM), *JEOL JSM6701F*. The high-resolution SEM images of the POME samples were captured digitally at 1000x magnification.



Figure 3.11: FESEM (JEOL JSM6701F)

The presence of solids particles and residual oil droplets in non-treated and ultrasound-treated POME was investigated using light microscopy analysis. The POME was initially mixed with a few drops of Sudan (III) dye, a micelle marker to increase the contrast and transferred onto a clean microscope slide. The solid particles and oil droplets were observed using an *Optika B-190* binocular microscope equipped with a 10x objective lens.



Figure 3.12: Binocular Microscope (Optika B-190)

3.6.2 Impact of Ultrasonication Pre-Treatment on Recovered Oil

Process modifications to improve oil recovery are commercially crucial to palm oil mills. These sorts of interventions, designed to boost oil recovery, should not adversely impact the quality of recovered oil. Hence, the properties of residual oil recovered from POME (Section 3.5) with and without ultrasonication pre-treatment were evaluated.

Fourier-Transform Infrared Spectrometry is a common method for analyzing the functional groups present in the samples. The functional groups of the recovered oil obtained from POME with and without ultrasonication pre-treatment were analyzed using Fourier Transform Infrared Spectroscopy-Attenuated Total Reflectance (FTIR-ATR), *Model PerkinElmer Spectrum Two*. The recovered oil was loaded onto the diamond crystal iATR reflectance cell, equipped with a deuterated triglycine sulphate (DTGS) detector. The spectra

were measured over a frequency range of $400 - 4000 \text{ cm}^{-1}$ using an accumulation of 16 scans at a resolution of 4 cm^{-1} .



Figure 3.13: FTIR-ATR (PerkinElmer Spectrum Two)

Gross calorific value (GCV) is the amount of thermal energy generated when a unit mass of fuel is burned completely in a constant volume of the enclosure. The GCV can be determined using an oxygen bomb calorimeter (IKA Calorimeter system C200), which adheres to the ASTM D2015. The stainless-steel combustion crucible was filled with a known amount of fuel. The fuse wire was knotted with cotton thread and placed above the fuel surface. To ensure sufficient oxygen for the combustion process, the sample was sealed and subjected to 30 bars of pressure from pure oxygen gas for 30 seconds. The assembled bomb was contained in an adiabatic container filled with 2 L of water. Upon thermal equilibrium of the system, the sample was burned in a sealed chamber. The system is equipped with automatic data collection via the *CalWin* calorimeter software, which is responsible for the calorific value calculations.

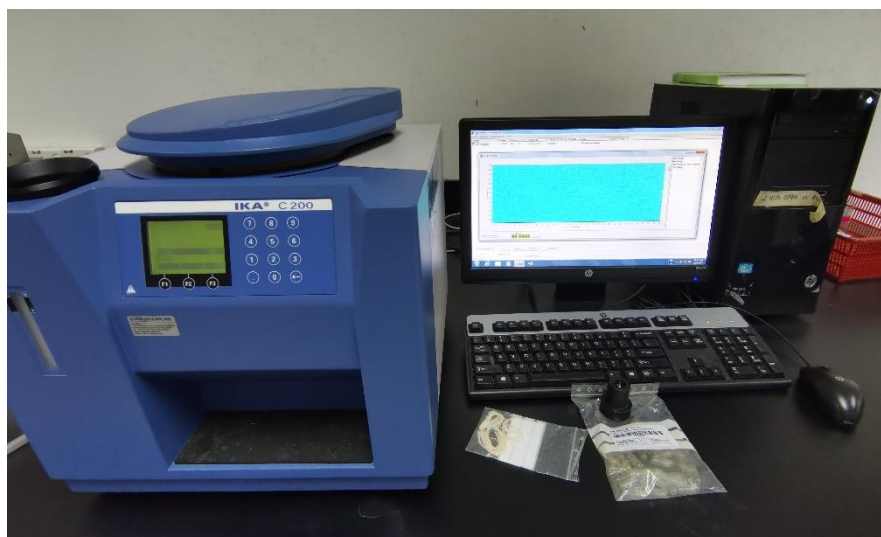


Figure 3.14: Oxygen Bomb Calorimeter (IKA Calorimeter System C200)

This study assessed several essential oil qualities, including deterioration of bleachable index (DOBI), acid value (AV), free fatty acid (FFA) content, iodine value (IV), as well as peroxide value (PV). The oil samples were analyzed in accordance with the official test methods by the American Oil Chemists' Society (AOCS) and MPOB. A detailed description of the experiments is outlined in Appendix D. The analyzed samples were compared to the quality standards for CPO in compliance with MS 814:2007 (Table 2.10) to evaluate its prospective usage.

3.7 Cost-Benefit Analysis

Cost-benefit analysis is a quantitative descriptive analysis that evaluates the viability of a project based on the projected costs and benefits. Figure 3.15 shows the overall flow for the cost-benefit analysis. The cost-benefit analysis of this study is just a preliminary estimate, focused on the enhancement of oil recovery from POME using the ultrasonication technique.

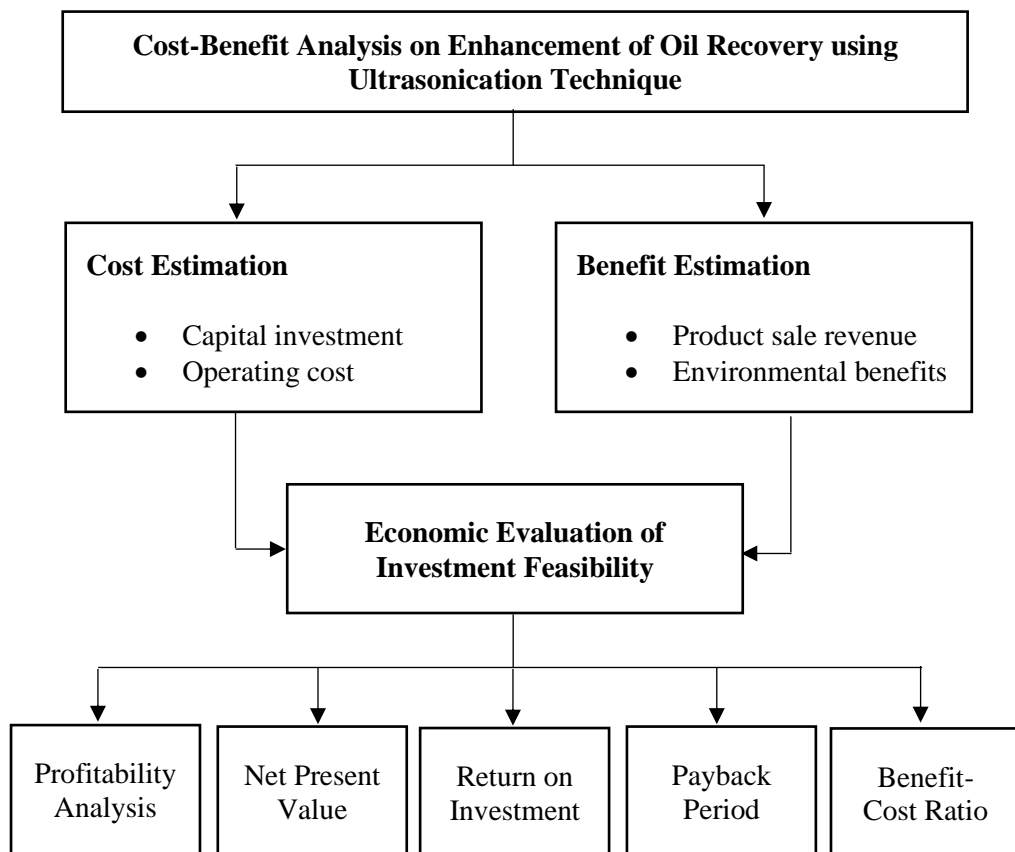


Figure 3.15: Process Flow of Cost-Benefit Analysis

The location of interest for this case study is Tian Siang Oil Mill (Air Kuning) Sdn. Bhd, which typically processes 80 to 120 MT/hr of FFB. This is a milling plant (midstream process) that did not involve any subsequent downstream process, such as refining or biodiesel production. Also, the operational cost of the oil recovery was not considered in this analysis as the objective was to assess the feasibility of utilizing ultrasonication as a pre-treatment to enhance the oil content.

As shown in Equation 3.3, ultrasonication dosage is defined as the amount of energy supplied per unit of volume sludge and is commonly used for power consumption computation. Under the optimal ultrasonication conditions of 30 % amplitude and 10 seconds duration (Section 4.3.3), the optimized ultrasonication dosage of 7.5 kW/L will result in an additional 42.5 % improvement of oil content.

$$\text{Ultrasonication dosage} = \frac{\text{Power (kW)} \times \text{Time (s)}}{\text{Volume (L)}} \quad (3.3)$$

Table 3.3 summarizes the assumptions made for the computation of the cost-benefit analysis. The typical oil extraction rate (OER) of a palm oil mill is 20 %, with POME accounting for 60 % of the plant's capacity. In an average 100 MT/hr FFB processing plant, 60 MT of POME was generated hourly. The milling plant operates on an intermittent basis, depending on the demand and pricing. With 16 hours of operation per day and 320 working days per year assumed, the annualized rate of FFB processing was 512,000 MT/year, with 307,200 MT of POME generated annually per mill.

Table 3.3: Assumptions for Cost-Benefit Analysis

Assumptions		
FFB processed	100 MT/hr	
POME generation	60 MT/hr	
Operating hours	16 hours per day	
Operating days	320 working days per year	
Ultrasonication dosage	7.5 kW/L	
Method	Non-treated	Ultrasound-treated
Oil content (%)	0.155	0.221

3.7.1 Cost Estimation

The projected expenditures of this project were capital investment and operating costs. Capital investments are estimated based on the percentage of delivered-equipment cost method (Peters, Timmerhaus and West, 2003). Equipment costs can be estimated through scaling when actual costs for the targeted capacity are unavailable. Commonly, the power relationship, known as the *six-tenths factor rule* indicated in Equation 3.4, is widely used in approximations of cost when one cost data for known capacity is available. A 3-kW power ultrasonic processor costs \$ 1,185 and has a capacity to treat 1,440 L of wastewater per hour (Equation E.1). Presuming a treatment rate of 60 MT of POME per hour, the estimated based purchase cost of the ultrasonic processor is \$ 11,106.87, which is equivalent to RM 49,203.42 using the conversion rate (\$ 1 = RM 4.43) as of 10th July 2022.

$$Cost_2 = \left(\frac{Capacity_2}{Capacity_1} \right)^{0.6} \times Cost_1 \quad (3.4)$$

Computations of equipment costs based on charts, equations, or vendor quotes are only valid for a defined period, as prices fluctuate from year to year due primarily to inflation. As a result, the Chemical Engineering Plant Cost Index (CEPCI) is commonly used to update the project's cost. The present purchase cost after considering inflation can be approximated using Equation 3.5, where the current CEPCI for 2022 is 797.6.

$$C_p = \text{Base purchase cost} \times \frac{I}{I_{base}} \quad (3.5)$$

Where I represents the current cost index (797.6), and I_{base} represents the historical cost index (567).

Table E.1 illustrates the percentage for estimating the capital investment items based on delivered-equipment cost. There were three sorts of processes: (1) solid, (2) solid-liquid, and (3) liquid. The solid-liquid processing plant factor was employed in this investigation since POME is a multiphase sample.

Operating costs encompass all expenses directly related to the equipment operation. These expenses are classified into three types: (1) variable costs, (2) overhead costs, and (3) fixed charges. Variable costs included the expenditures for raw materials, utilities, labor, as well as operating supplies. Overhead costs account for approximately 50 to 70 % of the total labor expenses and categorized into two types: payroll and plant overhead. Payroll overhead

includes employee benefits such as insurance and retirement plans, whereas plant overhead includes safety services and general plant maintenance. Fixed charges, on the other hand, are expenses substantially independent of the production rate, such as property taxes and insurance.

3.7.2 Benefit Estimation

The projected benefits can be a combination of both tangible and intangible benefits. In contrast to tangible benefits, which can be assessed in economic terms, intangible benefits cannot be quantified into the monetary unit but nonetheless have a major impact. In this study, the tangible benefit is the revenue from the sales of recovered oil, while the intangible benefits are environmental sustainability.

3.7.3 Economic Evaluation of Investment Feasibility

Profitability analysis is an evaluation of the value of a company's output after deducting expenses from revenue generated. Generally, there are four investment criteria to be assessed: (1) net present value, (2) payback period, (3) return on investment, and (4) benefit-cost ratio. Table 3.4 summarizes the computation for the profitability analysis and four investment criteria.

Table 3.4: Computation for Profitability Analysis and Four Investment Criteria

Criteria	Computation
Annual depreciation	1.2 % of FCI
Annual profit before tax	Revenue – (Depreciation + Operating Cost)
Tax	8 % of annual profit before tax
Net annual profit after tax	Annual profit before tax – Tax
Net present value	$NPV = \frac{\text{Cash flow}}{(1 + \text{discount rate})^{\text{time}}} - TCI$
Payback period	$PbP = \frac{TCI}{\text{Net annual profit}}$
Return on investment	$ROI = \frac{\text{Net annual profit}}{TCI} \times 100\%$
Benefit-cost ratio	$BCR = \frac{\text{Present value benefit}}{\text{Present value cost}}$

Net present value (*NPV*) refers to the current worth of a future stream of payments and is used to estimate whether an investment made today will result in positive cash flow in the future. A positive *NPV* at the end of the project indicates feasibility; a negative *NPV* implies infeasibility. The payback period (*PbP*) is the time required for the cash inflows received from a project to reimburse the initial expenditures necessitated by the investment. Return on investment (*ROI*) is a performance metric used to evaluate an investment's efficiency. The benefit-cost ratio (*BCR*) represents the relationship between a project's relative costs and benefits based on the *NPV* per unit of the initial investment. The investment is only viable if the *BCR* is greater than one.

3.8 Feasibility Study of Using Recovered Oil from POME as Biodiesel Feedstock

This section describes the second stage of the research, which is biodiesel production using recovered oil from POME to create industrial symbiosis possibilities. Figure 3.16 depicts the flowchart for the feasibility study of using recovered oil from POME as biodiesel feedstock.

Initially, the recovered oil from POME (Section 3.5) will undergo the assessment of acid value (AV) in line with AOCS official method Cd 3d-63. In case of the AV is less than 4 mg KOH/g oil, the feedstock can proceed directly to the conventional single-step alkaline transesterification biodiesel production. However, the recovered oil from POME possesses a high concentration of AV (19.59 mg KOH/g oil), which is incompatible with the conventional biodiesel production method. Hence, acid-esterification is required as a pre-treatment prior to alkaline transesterification to produce biodiesel using POME-recovered oil. Nevertheless, these reactions are mass-transfer restricted processes. Thus, this study will also investigate the potential of ultrasonication technique as a process intensifier (Section 3.8.1) to enhance the FFA conversion.

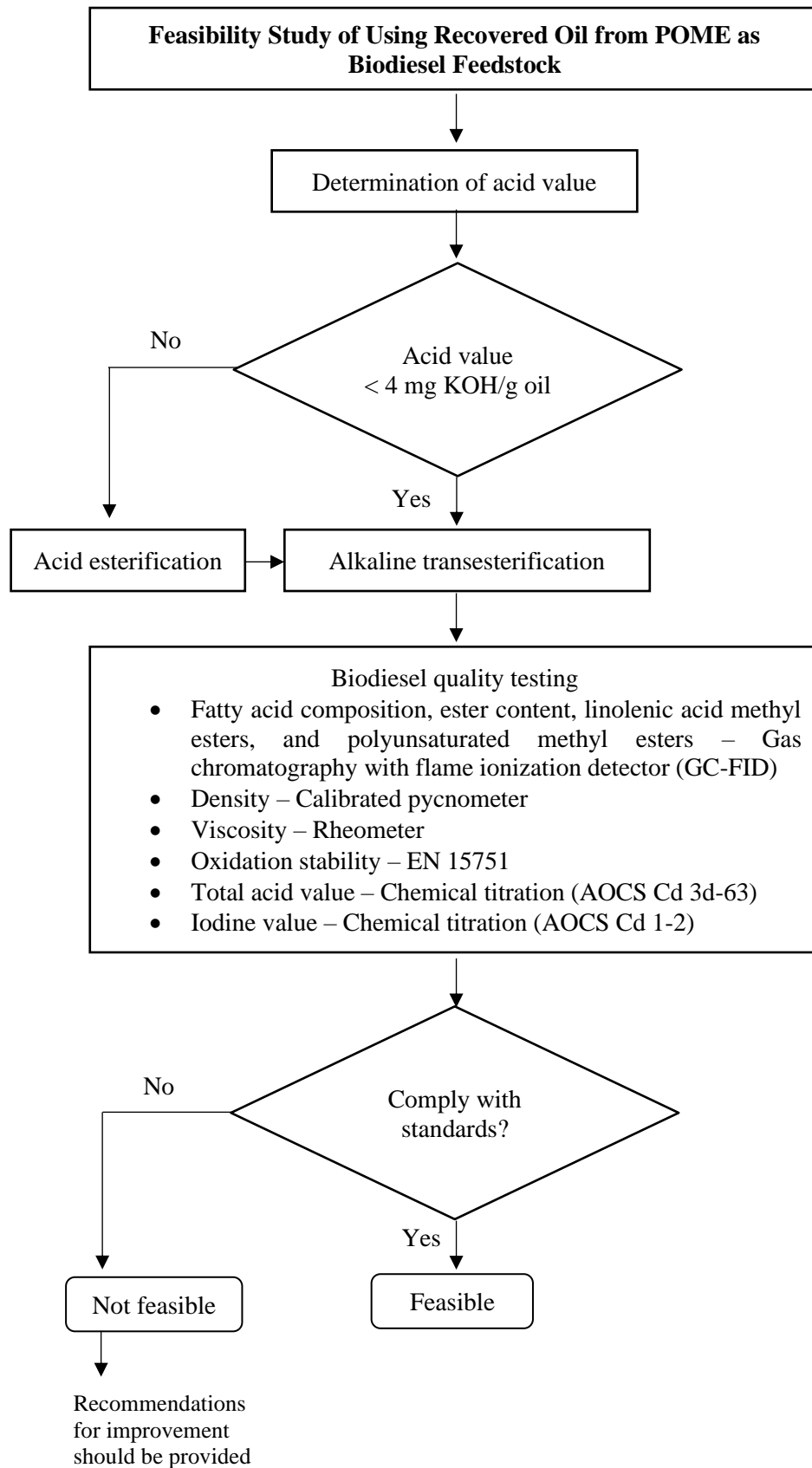


Figure 3.16: Process Flow of Feasibility Study of Using Recovered Oil from POME for Biodiesel Production

3.8.1 Potential of Using Ultrasonication Technique as a Process Intensifier for FFA Conversion

A comparison of three distinct approaches (i.e., conventional method, ultrasonic bath, and ultrasonic probe) was conducted in the case of acid-catalyzed esterification under the constant conditions. All the experiments were carried out using 5 g of recovered oil from POME. The reaction was carried out for 60 minutes using a methanol-to-oil molar ratio of 8:1 and an H₂SO₄ loading of 0.75 wt%. These conditions were selected based on the literature by Hayyan, et al. (2011), which involves acid-esterification of high FFA sludge palm oil, that has identical qualities as recovered oil from POME. The annotations of different types of approaches and reaction temperatures are listed in Table 3.5.

Table 3.5: Annotations for the Approaches and its Operating Temperature

Annotation	Approach	Reaction temperature
CT	Conventional method	60 °C
UBT	Ultrasonic bath	60 °C
UBWT	Ultrasonic bath	Room temperature
UPWT	Ultrasonic probe	Room temperature

Conventional esterification (CT) was performed on a stirring hot plate (*Thermo Scientific Cimarec*) at 60 °C with a stirring speed of 400 rpm, as a comparison to the ultrasonic-assisted reaction. An ultrasonic bath or an ultrasonic probe can be used to induce an ultrasonic-assisted reaction. However, there has been relatively little research on the comparability of these two

techniques in FFA conversion. This section will also compare the effectiveness of the ultrasonic bath and probe on FFA conversion.

Ultrasonic-bath-assisted reaction (UB) was performed in a temperature-controlled ultrasonic bath (*Elma S180 H*) with an operating frequency of 37 kHz and power consumption of 1000 W. These reactions were performed at two different operating temperatures (UBT and UBWT) to assess their efficacy in FFA conversion, while other parameters such as reaction time, methanol-to-oil molar ratio and H₂SO₄ loading were kept constant.

On the other hand, ultrasonic-probe-assisted reaction (UP) was carried out using a different ultrasonic processor (*Hielscher UP 400S*) located at UTAR Sungai Long Campus, which was equipped with a 3 mm microtip probe. This equipment operates at a frequency of 24 kHz and has a maximum power input and amplitude of 400 W and 166 μm, respectively. The reason for utilizing a different ultrasonic processor is that the existing ultrasonic processor (*Qsonica Q500*) used for improving oil recovery from POME does not support the small volume of samples that require microtips processing.

The process performance was assessed by monitoring the FFA conversion (Equation 3.6). The approaches with the highest FFA conversion would be subjected to further studies (Section 3.8.2).

$$FFA \text{ conversion } (\%) = \frac{\text{Initial FFA} - \text{Final FFA}}{\text{Initial FFA}} \times 100\% \quad (3.6)$$

3.8.2 Ultrasonication Conditions for the Esterification Process

Based on the results in Section 4.6.1, ultrasonic probe is preferable. Thus, a single factor experiment design was adopted to evaluate the influence of ultrasonication probe conditions, such as ultrasonication amplitude and duration, on the AV (Equation D.2) and FFA conversion (Equation 3.6). Table 3.6 illustrates the independent and dependent variables of ultrasonication conditions for the esterification process.

Table 3.6: Range of Independent Variables for Esterification Process

Independent variables	Dependent variables
Ultrasonication amplitude (20 – 40 %)	AV and FFA conversion
Ultrasonication duration (15 – 60 minutes)	

The AV and FFA conversion were studied by varying the ultrasonication amplitude (20 %, 30 % and 40 %) during the esterification process. Other parameters, such as a methanol-to-oil molar ratio of 8:1, H₂SO₄ loading of 0.75 wt%, and ultrasonication duration of 15 minutes, were kept constant during the experiment.

The effect of ultrasonication duration on AV and FFA conversion was also studied. In each batch of the experiment, different ultrasonication duration (15 min, 30 min, 45 min, and 60 min) were investigated while other parameters, such as the methanol-to-oil molar ratio of 8:1, H₂SO₄ loading of 0.75 wt% and ultrasonication amplitude of 30 %, were kept constant during the experiment.

3.8.3 Biodiesel Analysis

Prior to biodiesel analysis, the esterified oil is further derivatized by going through an alkaline-catalyzed transesterification reaction with a 10:1 methanol-to-oil molar ratio and 1 wt% KOH loading to improve its volatility. The fatty acids methyl esters composition of recovered oil from POME was determined using gas chromatography (GC-2010 Plus, Shimadzu) (Figure 3.17). Chromatographic separation was performed using an SGE Analytical Science BPX-70 column (60 m length \times 0.25 mm internal diameter \times 0.25 μ m film thickness) equipped with a flame ionization detector (FID). Helium gas was employed as the carrier gas at 3 mL/min. The temperature of the injector and detector was maintained at 230 °C. The initial temperature of the oven held at 80 °C for 2 min, was subsequently increased to 180 °C at a rate of 4 °C/min (held for 5 min) and further raised to 230 °C at a rate of 2 °C/min (held for 10 min). One microliter of the sample was injected in split mode with a split ratio of 40:1. Data was collected and analyzed using *GC Solution* software.

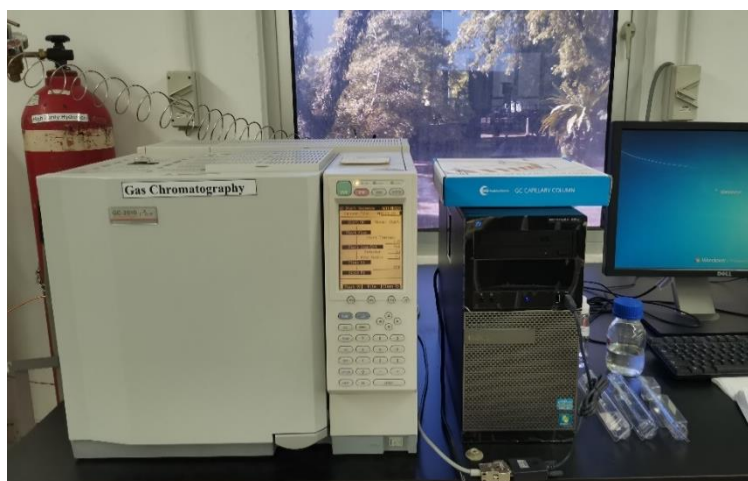


Figure 3.17: GC-FID (Shimadzu, GC-2010 Plus)

Several important biodiesel properties were evaluated in this study, including density, ester content, iodine value, linoleic acid methyl ester, polyunsaturated methyl ester, oxidation stability, total acid value, as well as viscosity. The density of the biodiesel was measured using a calibrated pycnometer (Figure 3.18), whereas the viscosity was measured at 40 °C using a Discovery Hybrid Rheometer, DHR-1 (Figure 3.19) at flow peak hold mode. The acquired results were compared to the international and local standard specifications listed in Table 2.13 to evaluate its potential as a feedstock for biodiesel production.



Figure 3.18: Calibrated Pycnometer



Figure 3.19: Discovery Hybrid Rheometer (DHR-1)

CHAPTER 4

RESULTS AND DISCUSSIONS

4.1 Raw POME Sample Characterization

Table 4.1 summarizes the properties of raw POME that were measured monthly for over six months to provide a comprehensive overview of its pollution potential. Even if the sample was obtained from the same mill, the composition of POME fluctuates over time due to various factors such as different batches of palm oil fruit utilized in the process, factory processing techniques, as well as the quality control of individual mills. Seasonal public holidays and mill closures for maintenance will also impact the quality and quantity of discharged POME.

Table 4.1: Characteristics of POME for Sample Collected for Six Months

Parameters	Range	Mean
pH	4.19 – 4.66	4.37 ± 0.18
BOD (mg/L)	21,200 – 41,367	34,183 ± 7,848
COD (mg/L)	62,333 – 141,667	106,667 ± 35,794
TS (mg/L)	37,500 – 53,000	43,917 ± 6,032
SS (mg/L)	11,100 – 34,000	21,223 ± 10,274
TVS (mg/L)	15,900 – 34,283	25,378 ± 8,274
O&G (mg/L)	1,537 – 4,670	3,014 ± 1,531

The analyzed parameters were found to be non-conforming to the POME standard discharged limits, as shown in Table 2.2. POME from this mill is a brownish, colloidal suspension composed of 95 – 97 % liquid and 3 – 5 % solids. POME is classified as high-strength wastewater due to its elevated organic matters and solids concentrations, making it one hundred times more polluted than municipal sewage. Even though Tian Siang Oil Mill has enhanced oil extraction system, those improvements are still not optimal, as evidenced by the high concentration of O&G contained in POME. Oil losses could be attributed to leakage or process instabilities. The presence of a considerable concentration of residual oil in the effluent indicated that POME is an excellent oil source with the potential to be processed into renewable fuels by considering the huge amount of POME generated annually.

As shown in Table 4.2, Pearson correlation coefficient analysis was conducted to measure the closeness of the association between two variables. The main emphasis will be placed on O&G since it is the focus of our research. BOD and COD are positively related to O&G; therefore, a rise in O&G will increase BOD and COD. This also postulated that the organic content might be considerably reduced by removing the oil from POME, resulting in a more efficient subsequent treatment process. In contrast, pH, TS, and SS are inversely associated with O&G. Since the acidic nature of wastewater favors demulsification and coalescence of larger oil droplets (Wahi, et al., 2017), lower pH indicates a higher O&G content. A high solid content will result in decreased O&G, as it is believed that most of the oil is adsorbed on these fibers due to their high oil adsorption capacity.

Table 4.2: Pearson Correlation Coefficient Analysis

	pH	BOD	COD	TS	SS	O&G
O&G	-0.57	0.83	0.97	-0.42	-0.06	1.00

4.2 Preliminary Study of Ultrasonication Conditions for Oil Enhancement

Process using OFAT

Since majority of the oil is emulsified and entrapped in the solids (Figure 4.13(A)), the oil content in POME cannot be entirely recovered using a stand-alone approach. Alternatively, ultrasonication pre-treatment on POME is believed to lead to a slightly higher fraction of easily extractable oil. This is because of the cavitation effect on the cells, which causes additional shattering of the undisrupted cell wall structure. The following subsections will describe how various ultrasonic parameters (i.e., ultrasonication amplitude, ultrasonication duration, and probe immersion depth) affect the oil content using the OFAT method.

4.2.1 Influence of Ultrasonication Amplitude on Oil Content

The ultrasonic probe generates a concentrated sound pressure field that radiates from its tips, and the amplitude of ultrasonication influences its propagation. Figure 4.1 presents the influence of ultrasonication amplitude on the oil content from POME under a constant condition. The red dotted line represents the oil content obtained from non-treated POME (4,340 mg/L) and serves as a control.

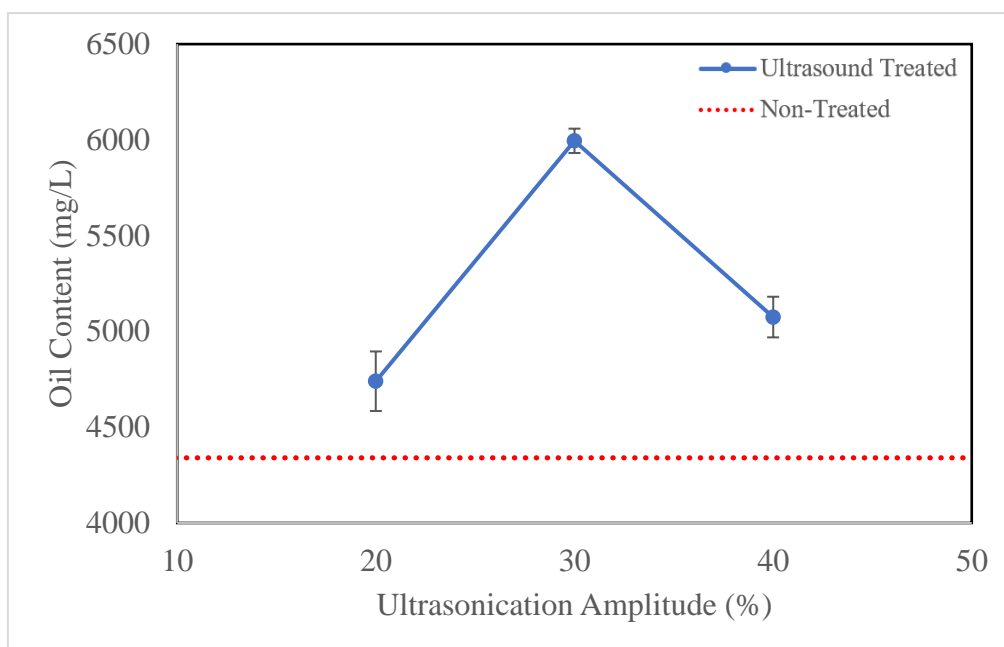


Figure 4.1: Effect of Different Ultrasonication Amplitude on Oil Content from POME (Conditions: Ultrasonication Duration: 30 seconds and Probe Immersion Depth: 2 cm)

Even at the lowest practicable ultrasonication amplitude of 20 %, the oil content from POME can be improved, resulting in a total of 4,740 mg/L. With an increase in ultrasonication amplitude from 20 % to 30 %, the oil content increased significantly, reaching a peak at 5,995 mg/L. In contrast, further application of higher ultrasonication amplitude may not necessarily generate desirable results. As the ultrasonication amplitude increased from 30 % to 40 %, the oil concentration declined from 5,995 mg/L to 5,075 mg/L.

The rise in oil content was attributed to the cavitation phenomenon induced by ultrasonic waves, which provoke a rapid local increase in pressure and temperature, resulting in microjets that shatter the cell. The cell wall disruption aided in the release of entrapped oil, thereby enhancing the oil

content. At a lower amplitude of 20 %, microbubbles are unable to achieve the maximum critical size during the collapse phase (Ong, et al., 2019). As a result, it exerts a weaker impact on the surface and decreases oil recovery yield compared to higher amplitude. Hashemi, Khaneghah and Akbarirad (2016) reported this observation in their research of ultrasound-assisted solvent extraction of Pistacia khinjuk hull oil, where an increase in ultrasonication amplitude increased oil yield. These findings can be explained by the fact that higher ultrasonication amplitude induces more rapid form of cavitations, which aided in the disruption of biological membranes by high-speed fluid microjets and expedited oil diffusion from disrupted plant tissue.

However, application beyond the optimal ultrasonication amplitude will form a high concentration of larger and more persistent bubbles clouds around the probe, acting as a barrier to acoustic energy transmission. Likewise, the cushioning effect of collapse caused by excessive bubbles may reduce the intensity of cavitation implosion on the surface matrix. Jadhav, et al. (2016) discovered a similar scenario in oil extraction from waste date seeds with ultrasound assistance, where there is no further increment in oil extraction yield detected when ultrasonication amplitude exceeds 30 %. Based on the current findings, it is recommended that the ultrasonication amplitude be adjusted to a low but sufficient level so that the propagation of ultrasound waves is less impeded.

4.2.2 Influence of Ultrasonication Duration on Oil Content

Since ultrasonic cavitation induces pyrolysis and free radicals, it is vital to strike a balance in the ultrasonication duration to maximize the facilitation of oil while limiting the deterioration of the targeted compounds. Figure 4.2 demonstrates the influence of ultrasonication duration in terms of minutes on oil content from POME.

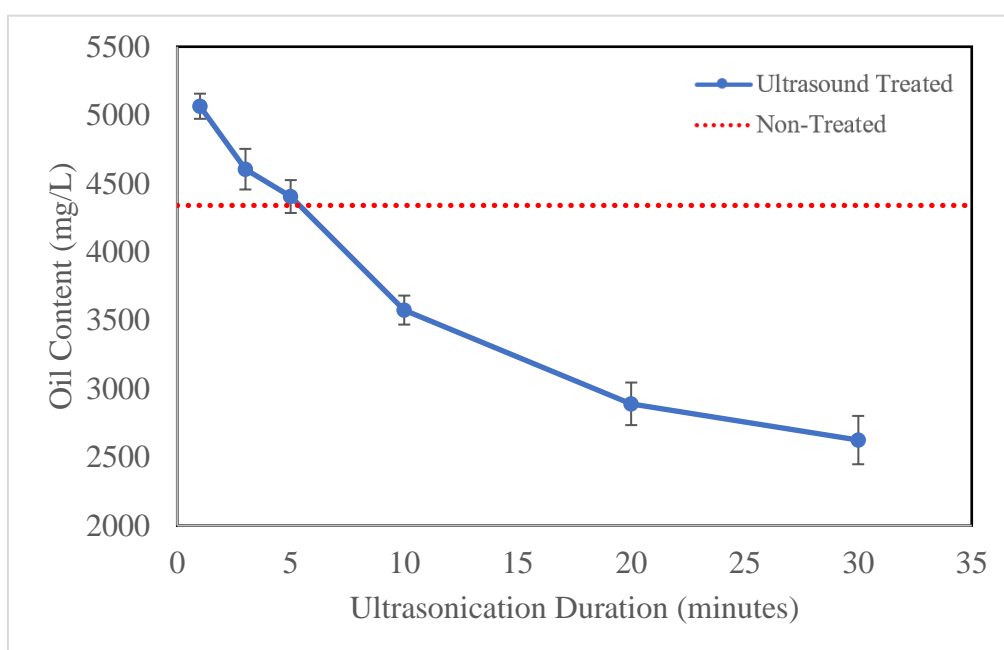


Figure 4.2: Effect of Different Ultrasonication Duration (Minutes) on Oil Content from POME (Conditions: Ultrasonication Amplitude: 30 % and Probe Immersion Depth: 2 cm)

In general, an increase in ultrasonication duration often results in a higher concentration of released components as cell disruption takes time. However, there is an obvious decreasing trend in the oil content when ultrasonication duration increases from 1 minute to 30 minutes. It is worth noting that sonicating for more than 5 minutes does not enhance oil recovery; rather, it has the opposite effect and reduces the oil concentration in POME. Prolonged exposure to ultrasonication induced the development of highly reactive hydroxyl radicals and increased localized temperature, which could cause the decomposition of oil, and as a result, a loss in oil content. This finding is consistent with that of Suksaroj, Yaeed and Suksaraj (2020), who also discovered that POME pre-treated with ultrasound for an extended period yielded lower O&G content. Another possible explanation for the decrease in oil content with extended ultrasonication application is that the targeted oil constituents tend to reabsorb into the oil-bearing ruptured particles owing to their comparatively large specific surface area (Buddin, et al., 2018).

Since prolonged ultrasonication would not improve oil recovery and would contradict our research goal of enhancing oil recovery, the effect of ultrasonication duration in terms of seconds was investigated and illustrated in Figure 4.3. The oil content increases considerably as the ultrasonication period increases from 15 seconds to 30 seconds. However, a declining trend was observed when the ultrasonication duration was extended beyond 45 seconds.

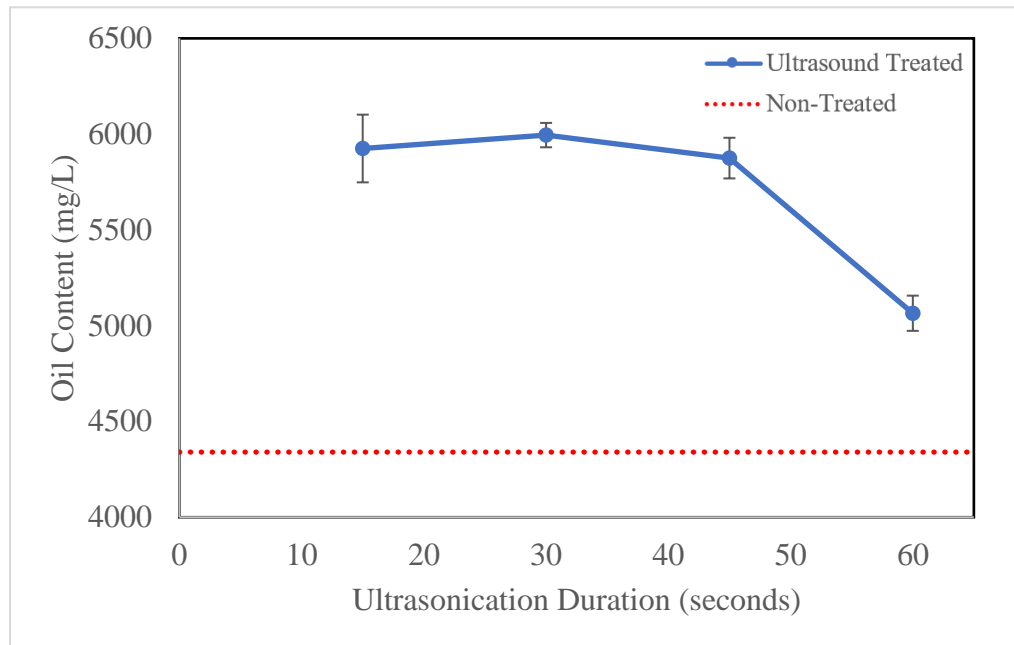


Figure 4.3: Effect of Different Ultrasonication Duration (Seconds) on Oil Content from POME (Conditions: Ultrasonication Amplitude: 30 % and Probe Immersion Depth: 2 cm)

In contrast to those oil enhancements from oleaginous seed slurries and crude oil tank sludge (Table 2.5), which contain a higher proportion of less-degradable cellulosic materials, the increase in oil content from POME was more intense during the early stage (seconds). This is probably because POME contains predominantly microbial cells with low mechanical resistance glands, which are easily disrupted by ultrasonication. Bigelow, et al. (2014) evaluated the influence of ultrasonication duration on the lipid extractability of *Chlamydomonas reinhardtii* cells and concluded that complete cell lysis is unnecessary for lipid improvement. The findings of this study suggested that ultrasonication can be carried out in seconds to a few minutes to enhance oil recovery from POME.

4.2.3 Influence of Probe Immersion Depth on Oil Content

Figure 4.4 depicts the effect of varying probe immersion depth on the oil content. It is observed that the probe position has a non-negligible influence on the oil content. The oil content increased from 4,845 mg/L to 5,995 mg/L as the immersion depth increased from 1 cm to 2 cm. However, the oil yield dropped slightly when the depth was further increased to 5 cm.

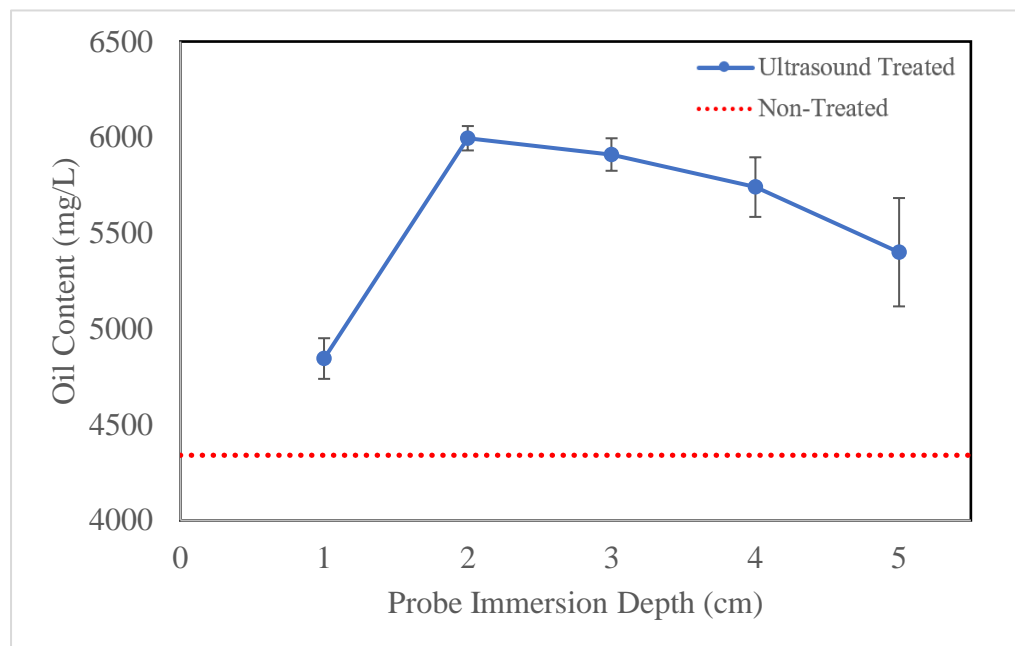


Figure 4.4: Effect of Different Probe Immersion Depth on Oil Content from POME (Conditions: Ultrasonication Amplitude: 30 % and Ultrasonication Duration: 30 seconds)

When the probe is brought too close to the surface of a liquid, air is introduced into the sample. As a result, the foam will be produced, and the effect of ultrasonic cavitation will be diminished. According to No and Son (2019), the luminol method revealed a significant increase in sonochemistry activity and intensity as probe immersion depth increased. This explains why the oil content increases as the probe immersion depth increase from 1 to 2 cm.

However, when the probe is immersed to a great depth, it may sonicate against the bottom of the vessel, resulting in an uneven distribution of acoustic energy in the sample. Furthermore, the vessel's wall and transducer's surface may be damaged in the long term. According to the operation manual by Qsonica, the probe should be submerged to a depth of at least 1.5 times the diameter of the tip. In this instance, the probe's diameter is 1.3 cm, and a minimum depth of 1.95 cm is sufficient.

4.3 Optimization Study of Ultrasonication Conditions for Maximum Improvement of Oil Yield using RSM

According to the preceding analysis (Section 4.2), all the variables listed influence the oil content from POME using ultrasonication. However, these factors were analyzed independently. It should be emphasized that these factors interact together within a system, and the OFAT method does not account for these interactions. Hence, the implementation of RSM is more advantageous as it enables the analysis of the variable's simultaneous effect.

Based on the preliminary study, the ultrasonication conditions (independent variables) employed in the design were specified as: (A) ultrasonication amplitude, 20 – 40 %; (B) ultrasonication duration, 10 seconds – 4 minutes; and (C) probe immersion depth, 2 – 4 cm. The improvement of oil yield (dependent variable) in terms of percentage was used to evaluate the process performance.

Twenty proposed experiments by CCD, including six replications of central points (Run 1, 2, 10, 13, 15 and 20), were conducted randomly to limit the effect of inexplicable variables in the observed response. The experimental results are tabulated in Table 4.3. The negative value in the table implies no improvement in oil yield over POME without ultrasonication pre-treatment, but a decrease in oil concentration. This trend was observed in trials conducted at 4 minutes of ultrasonication, with the most likely cause being the agglomeration of solid particles, which aids in trapping oil (Section 4.4.1).

Table 4.3: CCD: Experimental Parameters and Responses

Run	Variables			Response
	A: Ultrasonication amplitude (%)	B: Ultrasonication duration (min)	C: Probe immersion depth (cm)	Improvement of oil yield (%)
1	30	2.0835	3	10.97
2	30	2.0835	3	15.48
3	20	0.167	2	29.05
4	30	4	3	-7.10
5	40	2.0835	3	3.50
6	30	2.0835	4	19.55
7	40	0.167	2	27.37
8	40	4	4	-29.05
9	30	2.0835	2	12.85
10	30	2.0835	3	16.77
11	40	4	2	-31.60
12	30	0.167	3	40.22
13	30	2.0835	3	5.16
14	20	4	4	-12.29
15	30	2.0835	3	15.48
16	20	0.167	4	7.74
17	20	2.0835	3	-0.58
18	20	4	2	-12.88
19	40	0.167	4	16.77
20	30	2.0835	3	17.42

When the one-factor plots from the preliminary study (Section 4.2) and RSM (Figure 4.5) are compared, both share a similar trend in the effect of ultrasonication conditions.

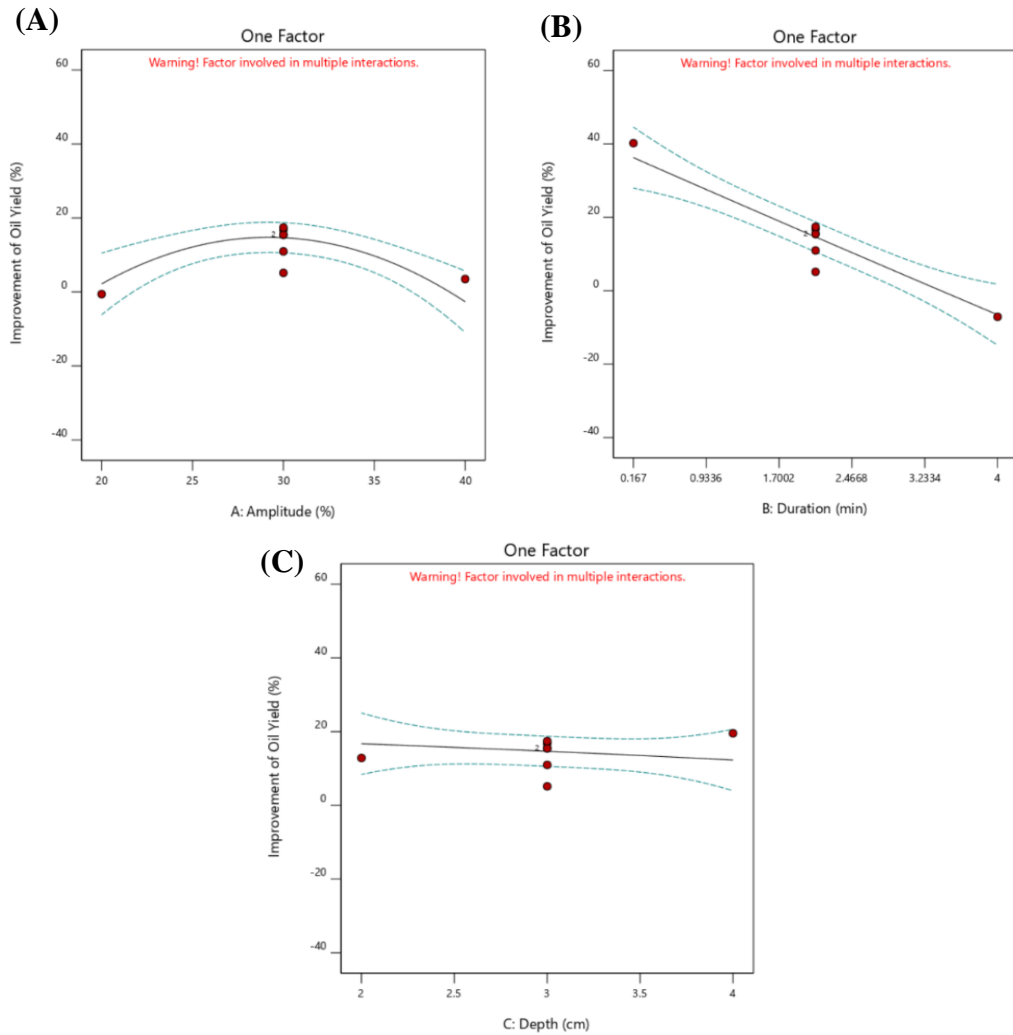


Figure 4.5: Effect of Different (A) Ultrasonication Amplitude, (B) Ultrasonication Duration, and (C) Probe Immersion Depth on the Improvement of Oil Yield from POME using RSM

4.3.1 Fit Summary, ANOVA, and Diagnostic Plots

The software proposes a quadratic model to reflect the improvement of oil yield from POME using the ultrasonication technique. This option is supported by the reports presented in Table 4.4 and 4.5. The fit summary in Table 4.4 shows that the quadratic model is significant since it matches the circumstances where the sequential p-value is less than 0.05. Similarly, the probability of lack of fit is greater than 0.05, indicating that it is insignificant and implying that the observed results are well aligned with the suggested model. The R^2 for this model was calculated to be 0.9561, suggesting that the model does not explain only 4.39 % of the total variation. Values greater than 0.80 show that the quadratic model and the experimental data are in satisfactory agreement. The adjusted coefficient of determination (R^2_{adj}) is 0.9166, which is close to one, indicating a reasonable degree of linear fit between the experimental and projected values.

Table 4.4: Fit Summary

Source	Linear	2FI	Quadratic	Cubic
Sequential p-value	< 0.0001	0.3303	0.0009	0.2795
Lack of Fit p-value	0.0220	0.0213	0.3110	0.3251
Lack of Fit F-value	6.97	7.29	1.59	1.19
R^2	0.7232	0.7854	0.9561	0.9790
Adjusted R^2	0.6713	0.6863	0.9166	0.9336
Predicted R^2	0.4902	-0.2514	0.7602	-3.9742

Table 4.5: Coefficient of Variables in the Regression Models and Their Significance

Sources	Sum of Squares	df	Mean Square	F-value	p-value
Model	6199.64	9	688.85	24.19	<0.0001
A-Amplitude	57.89	1	57.89	2.03	0.1844
B-Duration	4583.02	1	4583.02	160.92	<0.0001
C- Depth	48.66	1	48.66	1.71	0.2204
AB	229.41	1	229.41	8.06	0.0176
AC	20.10	1	20.10	0.7057	0.4205
BC	153.65	1	153.65	5.40	0.0426
A ²	610.60	1	610.60	21.44	0.0009
B ²	0.1090	1	0.1090	0.0038	0.9519
C ²	0.0712	1	0.0712	0.0025	0.9610

Based on Table 4.5, the model had a high F-value of 24.19 and a low p-value ($p < 0.0001$), implying that this model was very significant. Model terms with p-values less than 0.05 are considered significant. According to the ANOVA analysis in Table 4.5, the independent variable (B); two-level interactions (AB and BC); and the quadratic factor (A²) are the significant model terms. The experimental finding reveals an adequate precision (AP) value of 18.391, which is larger than 4, indicating a satisfactory signal-to-noise ratio.

Figure 4.6 shows the Design-Expert plots, which aid in judging the model satisfactoriness by assessing the pattern of all data points. As illustrated in Figure 4.6(A), the observed results are distributed reasonably close to the 45° regression line, showing a modest deviation between actual and anticipated values. Figure 4.6(B) indicates the residuals versus run for improvement of oil yield. Although the highlighted run differs, there is no cause for concern as it is within the red control boundaries. Both plots are satisfactory, implying that the empirical model adequately describes the enhancement of oil recovery using ultrasonication pre-treatment. In other words, the existing model was precise enough; hence, no further model modification was necessary.

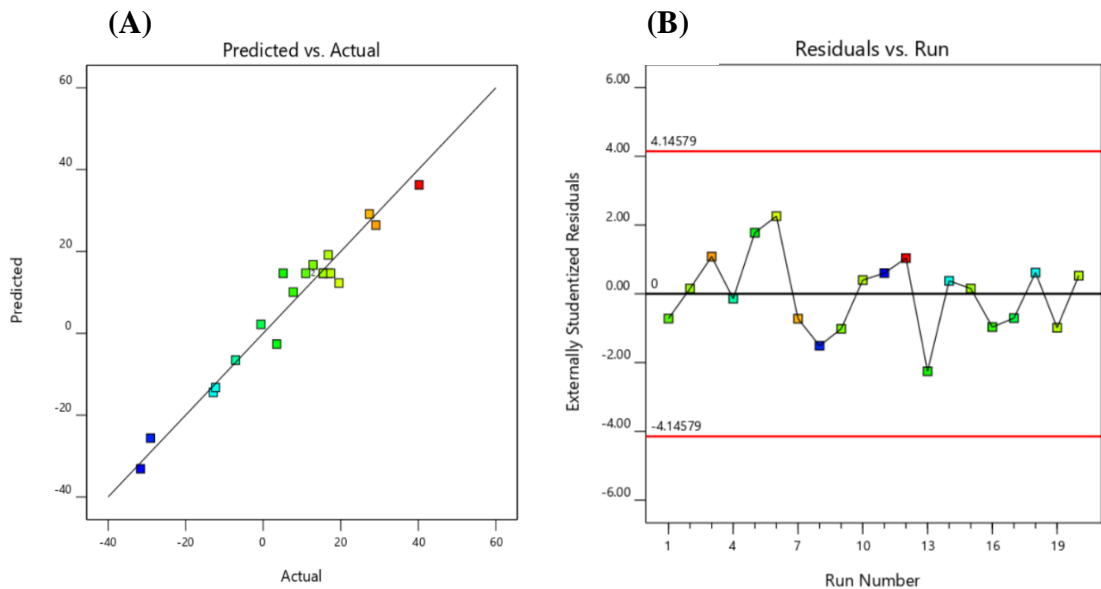


Figure 4.6: Design-Expert Plots: (A) Predicted Versus Actual and (B) Residual Versus Run

4.3.2 3D Response Surface Plots

The 3D response surface plots were generated to visualize the combined impact of two independent variables on the dependent ones. In comparison to the other interactions (AC and BC), the interaction between ultrasonication amplitude and ultrasonication duration (AB) demonstrated the most significant effect on the response variable, provided by the high F-value (8.06).

Figure 4.7 shows the 3D plot on the improvement of residual oil recovery in terms of ultrasonication amplitude and ultrasonication duration (AB) at a fixed probe immersion depth of 3 cm. The ultrasonication amplitude and duration varied from 20 to 40 % and 0.167 to 4 mins, respectively. It was discovered that with the increment of ultrasonication amplitude to 30% at an ultrasonication duration of 10 seconds, the percentage of improved oil recovery reached the maximum at 40.22 %. The amount of residual oil recovered was more remarkable at a shorter ultrasonication period.

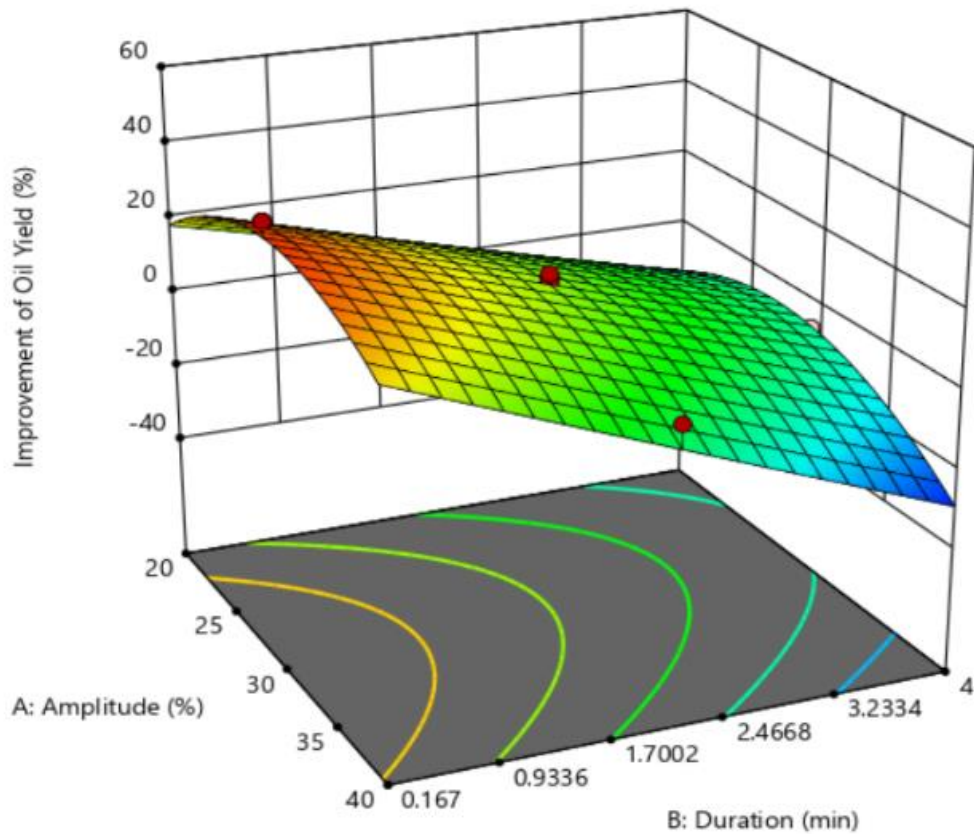


Figure 4.7: 3D Response Surface Plot for Interaction Between AB

Figure 4.8 depicts a 3D plot of oil recovery as a function of ultrasonication amplitude and probe immersion depth (AC) at a constant ultrasonication time of 10 seconds. There is no discernible difference in the improvement of oil yield regardless of amplitude or depth. Overall, the plot reveals that the interaction has a negligible effect on improving oil recovery from POME, as evidenced by the low F-value (0.7057) and high p-value (0.4205).

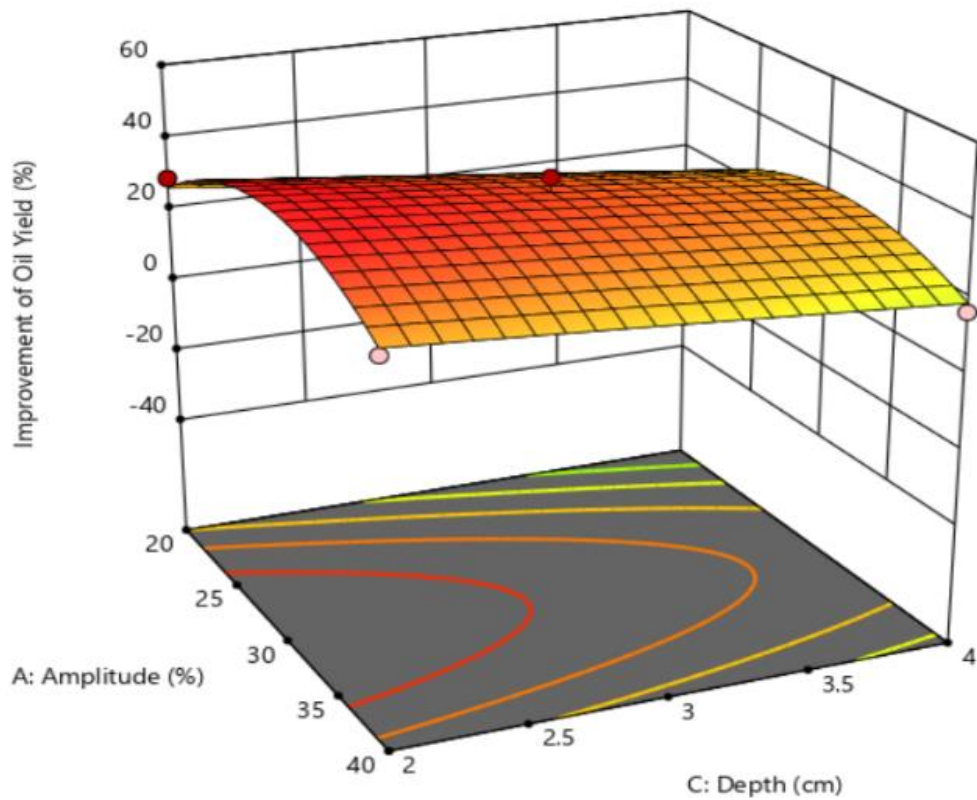


Figure 4.8: 3D Response Surface Plot for Interaction Between AC

Figure 4.9 illustrates the combined effect of ultrasonication duration and probe immersion depth (BC) on oil recovery improvement at a constant ultrasonication amplitude of 30 %. The 3D surface plot shows that the oil yield reached a maximum gain of 40.59 % at the ultrasonication duration of 10 seconds and probe immersion depth of 2 cm. In other words, the oil recovery increased with decreasing ultrasonication duration and probe immersion depth. The interaction between ultrasonication duration and probe immersion depth (BC) also demonstrated a significant effect on the response variable, provided by the high F value (5.40).

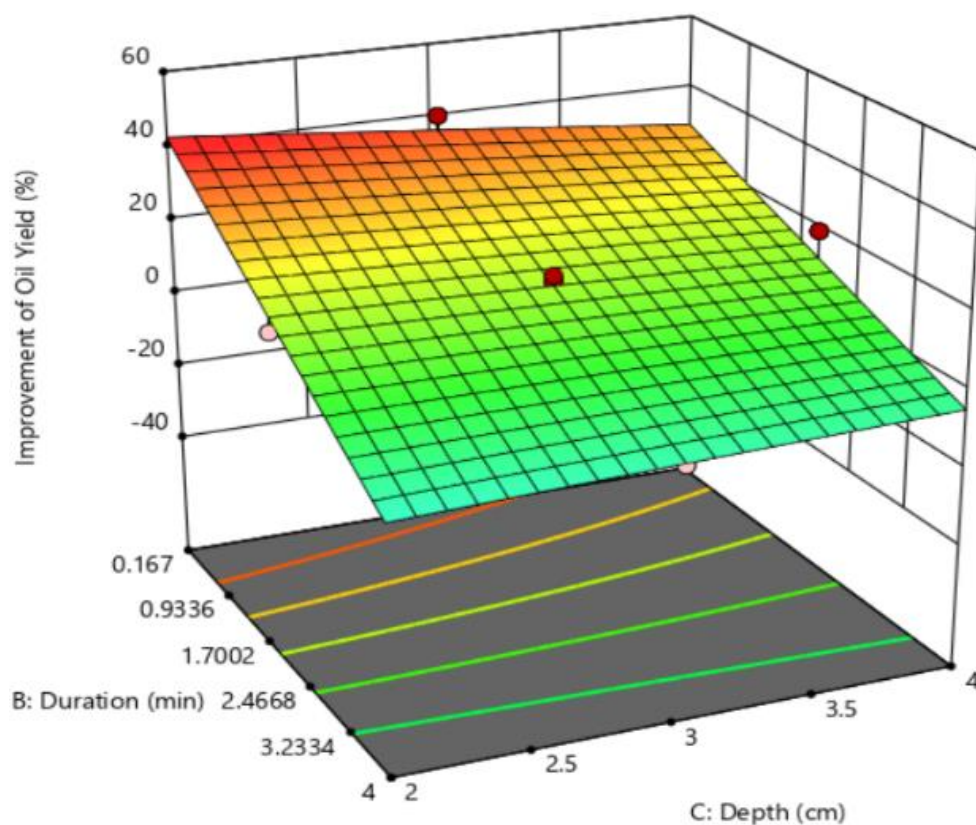


Figure 4.9: 3D Response Surface Plot for Interaction Between BC

The perturbation plot in Figure 4.10 displays all independent variables' effects on the improvement of oil yield. A steep slope observed in the ultrasonication duration (B) indicates that the response was very sensitive to the variable. The curvature of ultrasonication amplitude (A) similarly exhibits response sensitivity, albeit in different patterns. In contrast, the comparatively flat line of probe immersion depth (C) shows insensitivity to change in that factor on response. Overall, ultrasonication duration (B) exhibited the greatest effect, followed by ultrasonication amplitude (A), and finally the probe immersion depth (C).

Factor Coding: Actual

Improvement of Oil Yield (%)

Actual Factors

A: Amplitude = 30

B: Duration = 2.0835

C: Depth = 3

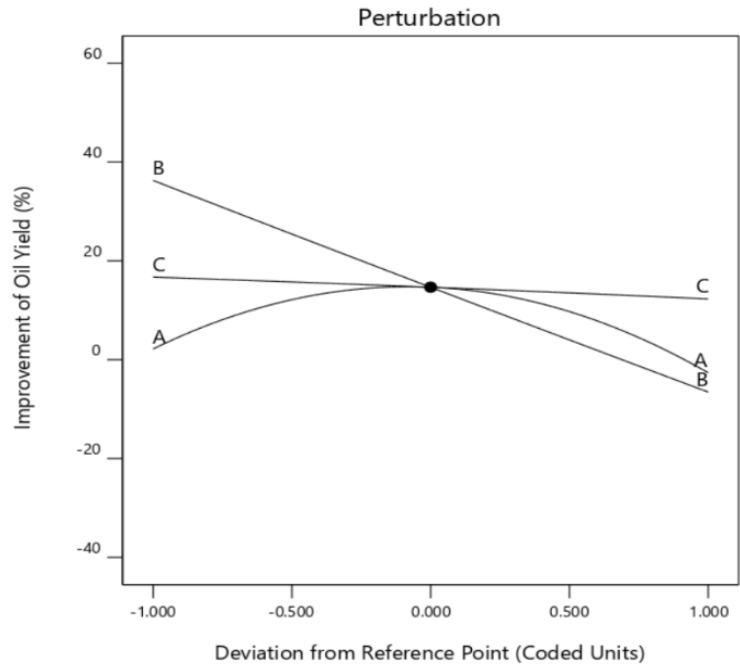


Figure 4.10: Perturbation Plot for Improvement of Oil Yield

4.3.3 Optimization and Validation of Model

Process optimization is critical for maximizing throughput while incurring the least expenses in the process operation. Equation 4.1 shows the final empirical model for the improvement of residual oil recovery (Y , %). The model equation was utilized to forecast the optimum ultrasonication performance. The equation's sign indicates whether the corresponding factors positively or negatively affect the responses.

$$Y = 14.67 - 2.41A - 21.41B - 2.21C - 5.35AB + 1.58AC + 4.38BC - 14.90A^2 + 0.1991B^2 - 0.1609C^2 \quad (4.1)$$

The optimal ultrasonication conditions for the response were determined via numerical optimization. The factors were set to be in the range, whereas the response was aimed to be maximized. Three RSM-proposed conditions with high desirability, ranging from 83.7 % to 85.2 %, were chosen to check the accuracy of the models. The experiments were conducted in accordance with the proposed operating conditions, and the experimental results were compared with the predicted results. As illustrated in Table 4.6, there is only a minor difference between the predicted and observed values, which are less than 5 % of the error rate, implying that the model was satisfactory for forecasting performance. In short, the optimum conditions of 30.074 % ultrasonication amplitude, 0.167 min ultrasonication duration, and 2 cm probe immersion depth resulted in an additional 42.5 % improvement in oil yield.

Table 4.6: Verification of Forecasted Responses for Ultrasonication Pre-Treatment on POME

Ultrasound Condition			Desirability	Predicted	Experimental	Error rate (%)
Amplitude (%)	Duration (min)	Depth (cm)		Improvement (%)	Improvement (%)	
30.454	0.167	2.000	0.852	42.738	40.50	5
30.074	0.167	2.000	0.851	42.716	42.50	1
31.397	0.210	2.000	0.837	42.008	41.32	2

4.4 Evaluation of Ultrasonication Pre-Treatment Impact on POME and Recovered Oil

Ultrasonication is an acoustic green technology that can induce physical, chemical, and biological effects on the sonicated materials. The following subsections will describe the impact of ultrasonication pre-treatment on POME and recovered oil at optimized ultrasonication conditions (30.074 % ultrasonication amplitude, 0.167 min ultrasonication duration, and 2 cm probe immersion depth).

4.4.1 Impact of Ultrasonication Pre-Treatment on POME

In line with the previous study, it has been speculated that the enhancement of oil recovery may be attributable to the pressure difference during ultrasonication pre-treatment, which exerted extreme physical disruption on the biomass surface, causing fragmentation and particle size reduction. Particle size distribution and microscopy analysis have been widely employed as physical evaluation tools to estimate the effectiveness of ultrasound disruption.

As illustrated in Figure 4.11, the particle size distribution demonstrates that the POME particles range in size from 0.030 μm to 954.993 μm , with an asymmetric behavior curve. In the case of an ultrasound-treated POME, it was observed that the peak distribution of particles is oriented towards smaller particles.

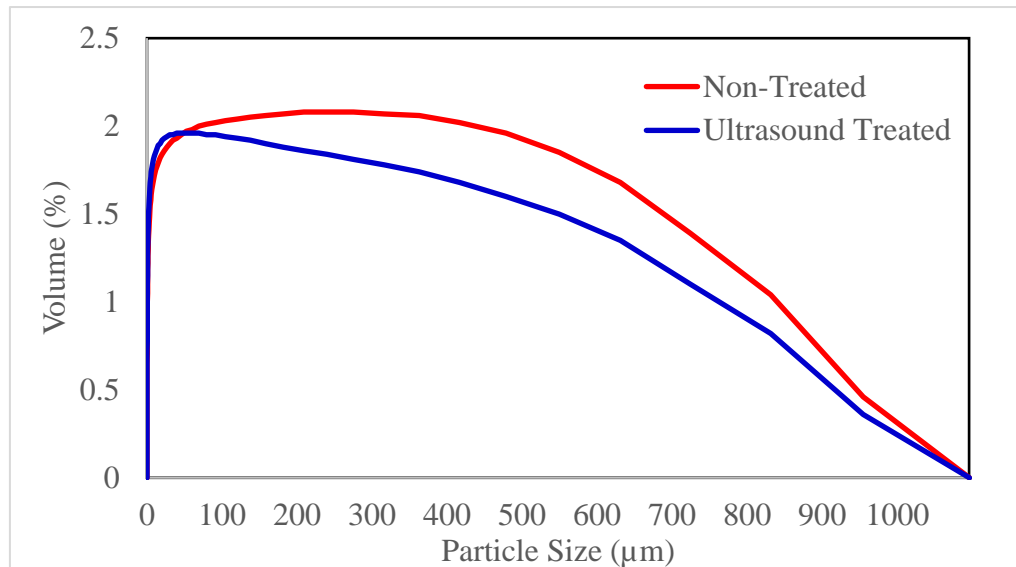


Figure 4.11: Particle Size Distribution of Non-Treated and Ultrasound-Treated POME

Table 4.7 shows the effect of increasing ultrasonication dosages (Equation 3.3) with fixed ultrasonication volume (200 mL) and duration (0.167 minutes) on the POME particle size profiles. The mean particle size of the POME sample reduced as soon as ultrasonication was incorporated.

Table 4.7: POME Particle Size Profiles of Different Ultrasonication Dosage

Ultrasonic dosage (kWs/L)	Particle size, μm				Surface area, m^2/g	Particle size reduction, %
	Mean	$d_{(0.1)}$	$d_{(0.5)}$	$d_{(0.9)}$		
0 (Control)	110.772	0.605	23.928	373.199	4.10	-
5	100.394	0.555	19.699	339.071	4.37	9.37
7.5	95.047	0.533	17.894	319.985	4.50	14.20
10	99.903	0.553	19.528	337.352	4.38	9.81

$d_{(0.1)}$, $d_{(0.5)}$, and $d_{(0.9)}$ represent that 10 %, 50 % and 90 % of the particles are smaller than the column values.

When large particles in the liquid suspension are subjected to ultrasonication, they are prone to particle size reductions or surface erosion. Under the optimized ultrasonication dosage of 7.5 kW/L (Equation 3.3), the mean particle size decreases by 14.2 %. The drop in particle size demonstrated that the particles were broken up and free substances were liberated, contributing to improved oil recovery. In addition, these changes are concomitant with the increase of specific surface area as the particle size decreases. The increase in the surface area should correspond to a larger area for solvent contact.

Further increase in ultrasonication dosage only has little contribution to the particle size reduction. Still, it results in coarsening of agglomerates due to the increased release of intracellular polymers, which is advantageous for particle re-flocculation and entrapment of oil. These results reflect those of Wong, Isa and Bashir (2016), who also observed comparable changes in the particle size profile of POME after ultrasonic treatment. Table 4.8 compares the solid profiles of non-treated POME with ultrasound-treated POME at optimized conditions. Ultrasonic irradiation could enhance organic solids solubilization, which will be an added advantage for subsequent biological treatment.

Table 4.8: Solid Profiles of Non-Treated and Ultrasound-Treated POME

	Non-Treated	Ultrasound-Treated	Reduction (%)
TS (mg/L)	43,900 ± 990	42,800 ± 282	2.51
SS (mg/L)	27,000 ± 707	19,500 ± 1,414	27.78
TVS (mg/L)	37,400 ± 849	36,000 ± 1,131	3.74

As shown in Figure 4.12, the scanning electron micrographs (SEM) could provide detailed information about the cellular-level morphological alterations on the surface of POME. It is noticed that the surface of the non-treated POME sample, as shown in Figure 4.12(A), appeared to be smoother and more intact than the surface of the ultrasound-treated POME, as shown in Figure 4.12 (B), where there is a development of crevices, cracks, and microfractures. The appearance of pores and tears indicates that structure disruption occurred, which could account for the increased amount of oil retrieved. Wang, et al. (2019) also reported that ultrasonic sound waves induced structural disorganizations in the sample during their research. Ultrasound cavitation creates microjet impingement, which eventually leads to erosion, surface peeling, and particle breakdown.

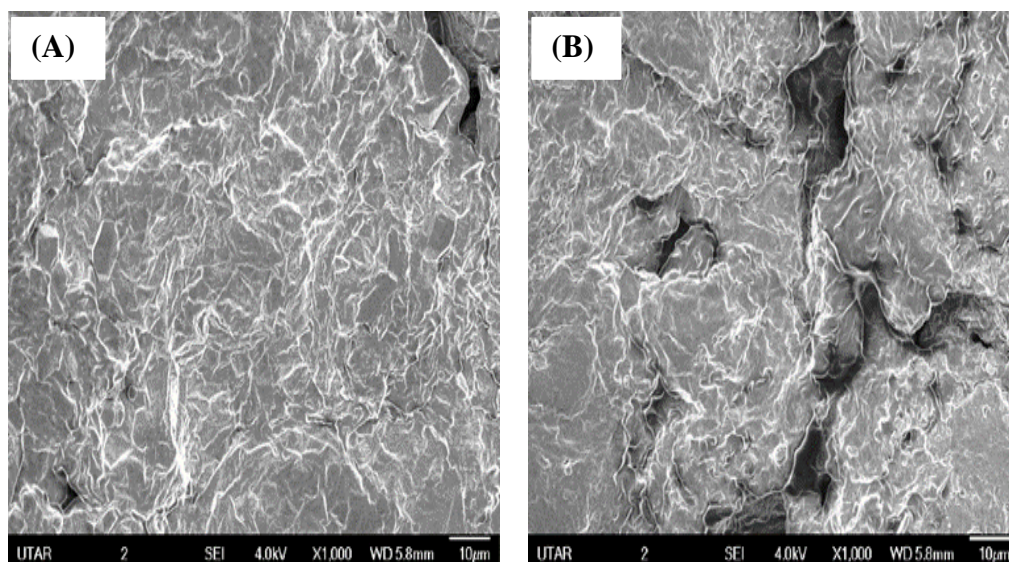


Figure 4.12: SEM Images of POME: (A) Non-Treated and (B) Ultrasound-Treated

The microscopic observation of POME, as depicted in Figure 4.13, could provide qualitative information about sludge disintegration, such as alteration in floc structure and disappearance of filaments. As illustrated in Figure 4.13(A), some of the oil is bound to and trapped within the fibers of non-treated POME. It is also worth noting that the size of the oil droplets was smaller than that of the solid particles. Without an efficient approach, they remain subsurface, resulting in more oil loss. Figure 4.13(B), on the other hand, demonstrates that ultrasound-treated POME disintegrates solids and releases oil in the free form, hence, facilitating increased oil recovery.

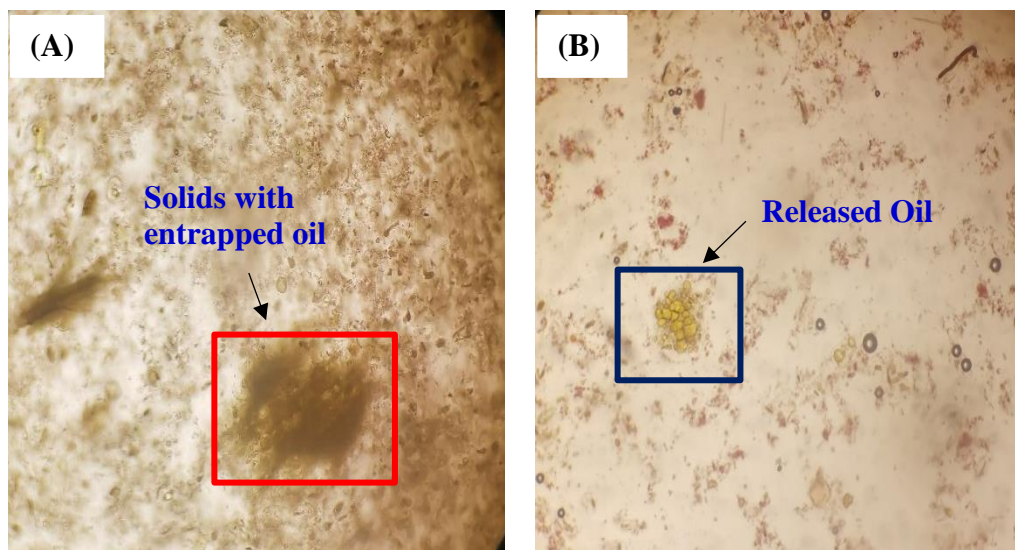


Figure 4.13: Microscopic Observation of POME: (A) Non-Treated and (B) Ultrasound-Treated

All these particle sizes and microscopy analyses demonstrated that structural disorganization occurred, providing support to the hypothesis that ultrasonication pre-treatment can disrupt complex particles in POME, facilitating the release of entrapped oil.

4.4.2 Impact of Ultrasonication Pre-Treatment on Recovered Oil

Undoubtedly, ultrasonication effectively alters a material's structural and physical aspects. However, if these alterations contribute to quality deterioration, they may be unfavorable. Hence, the characteristics of residual oil recovered from POME with and without ultrasonication pre-treatment will be evaluated in this section.

The ATR spectra of the recovered oil samples and the absorption frequency for the respective functional group, were exhibited in Figure 4.14 and Table 4.9. Triglycerides are the primary components in fats and oils; hence, they dominate the spectrum. Overall, the oil recovered from POME with and without ultrasonication pre-treatment had a comparable pattern of peaks in the ATR spectrum, indicating that acoustic cavitation generated by ultrasonication did not induce structural changes in the oil's compounds.

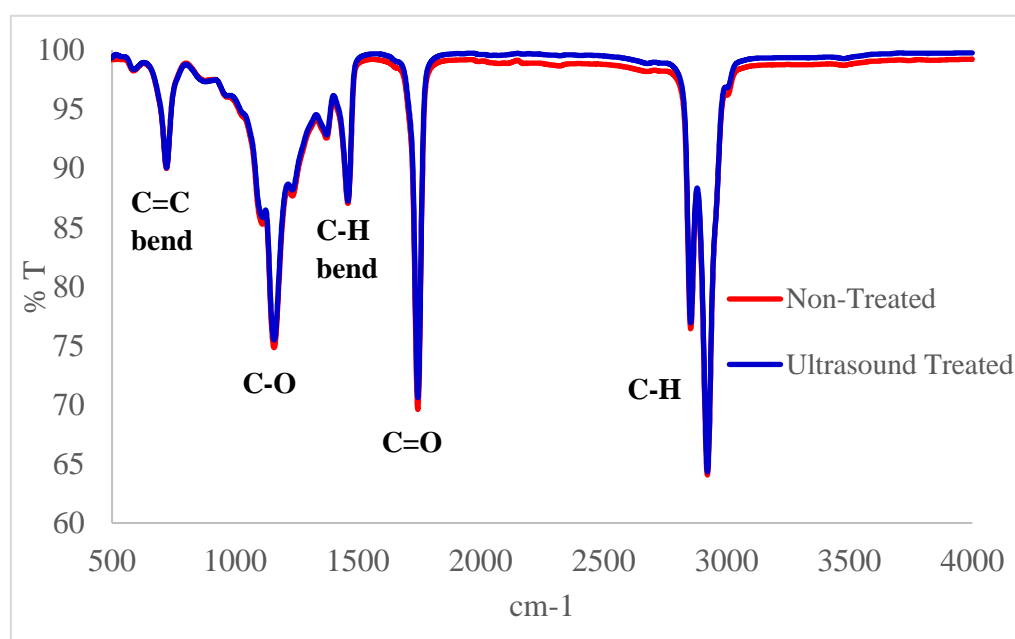


Figure 4.14: ATR Spectrum of Recovered Oil from POME

Table 4.9: Absorption Frequency for the Respective Functional Group in ATR Test Results

Functional group	Molecular motion	Frequency range (cm ⁻¹)	Peak frequency in sample (cm ⁻¹)
Alkenes	C=C bending	665 – 730	722
Esters	C-O stretching	1124 – 1250	1159
Alkanes	C-H bending	~1465	1460
Esters	C=O stretching	1735 – 1750	1744
Alkanes	C-H stretching	2840 – 3000	2854, 2922

The peak at 722 cm⁻¹ is attributable to the bending of C=C, whereas the peak at 1460 cm⁻¹ represents the bending of C-H. Esters were identified as the predominant class of lipids in the sample, with C-O and C=O vibration stretch peaks at 1159 cm⁻¹ and 1744 cm⁻¹, respectively. Strong duplet bands at peaks of 2854 cm⁻¹ and 2922 cm⁻¹ were assigned to C-H vibration stretch as lipid backbones. The ATR result confirms the presence of oil, and the functional groups identified in the sample are consistent with palm oil (Hashim, Zaki and Muhamad, 2017).

A series of oil quality indices were used to assess the impacts of ultrasonication pre-treatment on the oil quality. Table 4.10 compares the characteristics of residual oil recovered from non-treated POME to those recovered from ultrasound-treated POME.

Table 4.10: Characteristics of Residual Oil Recovered from Non-Treated and Ultrasound-Treated POME

Quality parameters	Standards	Non-Treated	Ultrasound-Treated	Differences
DOBI	Min 2.3	2.46	2.45	0.41 %
AV (mg KOH/g oil)	-	23.70	23.78	0.34 %
FFA (% lauric)	-	8.44	8.46	0.24 %
FFA (% oleic)	-	11.91	11.95	0.34 %
FFA (% palmitic)	Max 5	10.82	10.82	0.00 %
IV	-	44.46	41.07	8.26 %
PV (meq/kg)	Max 2	3.06	3.28	7.19 %
GCV (J/g)	-	39,300	39,651	0.89 %

Deterioration of bleachability index (DOBI) reflects the ease of refining, which involves the use of acid and bleaching earth to remove gums, impurities, color pigments, and FFA. The raw material qualities and processing conditions primary influence DOBI. A higher DOBI denotes better oil quality and a more efficient refining process. According to the grading scheme presented in Table 2.11, the DOBI of residual oil recovered from POME is around 2.4, which is a relatively fair grade. There were no statistically significant variations in DOBI between oil recovered from non-treated and ultrasound-treated POME samples. Both oils were within the specification of MS 814:2007, with a minimum DOBI of 2.3.

Fatty acids are typically in the form of triglycerides; however, they tend to hydrolyze into FFA during processing. The presence of FFA in oil can lead to possible deterioration or degradation of the oil as FFAs undergo oxidation more readily than triglycerides, leading to the formation of volatile compounds that contribute to the rancidity (Di Pietro, Mannu and Mele, 2020). Since AV is a measure of FFA content in oil, there is a direct relationship between both. A higher AV will result in a higher FFA content, thereby decreasing the oil's quality. The AV and FFA (% palmitic) of the residual oil recovered from POME are approximately 23.7 mg KOH/g oil and 10.8 %, respectively, with no notable difference between the oil recovered from non-treated and ultrasound-treated POME samples. It is classified as low-grade oil for non-edible applications since it exceeds the maximum permitted limit in the CPO specification standard (max 5 %). The high AV and FFA levels determined in this study also did not fulfil the minimum requirements for alkaline-transesterification biodiesel production to proceed smoothly (< 4 mg KOH/g oil of AV or < 2 % of FFA). As a result, acid-esterification is required as a pre-treatment prior to alkaline-transesterification, which is covered in more detail in Section 4.6.

Iodine value (IV) quantifies the degree of unsaturation, which influences the melting points, oxidative stability, and storage quality. A low IV suggests that oil is rich in saturated fatty acids such as palmitic (C16:0) and stearic (C18:0) acids. These fatty acids contribute to the solidification of the oil and reduce its susceptibility to oxidation. The stability of saturated fats, characterized by the fully loaded single bond carbon chains, contributes to this effect. On the other

hand, a high IV suggests that oil is primarily constituted of unsaturated fatty acids such as oleic (C18:1) and linoleic (C18:2) acids, which cause the oil to liquefy and are more prone to oxidation due to the availability of double bond carbon chains. In this investigation, the IV of oil recovered from ultrasound-treated POME was found to be 8 % lower than that of oil recovered from non-treated POME. In other words, recovered oil from POME with ultrasonication pre-treatment contains more saturated fatty acids and tends to solidify at room temperature. This is further demonstrated in Figure 4.15, where both oils are heated above the melting points and cooled to room temperature simultaneously, with the recovered oil from ultrasound-treated POME containing more solid fat deposited at the bottom.

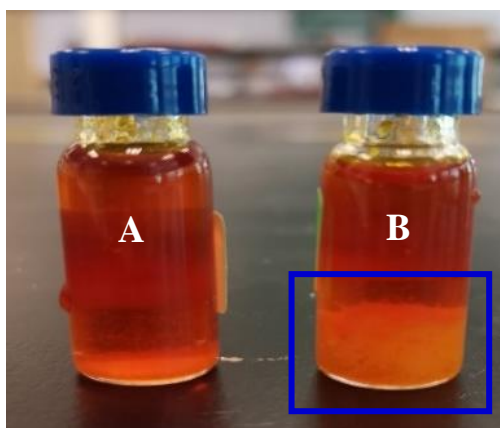


Figure 4.15: Residual Oil Recovered from (A) Non-Treated and (B) Ultrasound-Treated POME at Room Temperature

Geleta, Stymne and Bryngelsson (2011) stated that a significant amount of polyunsaturated fatty acids (PUFA) in triacylglycerol induces oxidative rancidity, reduces shelf life, and develops off-flavors. The heightened susceptibility to autoxidation observed in PUFA can be attributed to their

elevated amount of double bonds. These double bonds signify the presence of additional hydrogen atoms, which, upon the rupture of the carbon-carbon double bond, can readily participate in the process of autoxidation (Ayala, Muñoz and Argüelles, 2014; Boukandoul, et al., 2019). Peroxide value (PV) is also a key element in assessing the stability, phases of oxidation, as well as level of spoilage of oil by measuring the concentration of hydroperoxides. In short, higher IV increases oxidation susceptibility, which leads to increased PV.

The oil recovered from non-treated POME has a higher IV in this study; it is also expected to have a higher PV. However, contrary to expectations, the oil recovered from ultrasound-treated POME has a 7 % higher PV than the oil recovered from non-treated POME. The discrepancy could be ascribed to the acoustic cavitation by ultrasound, in which the microbubbles' implosion induces lipid oxidation through pyrolysis, free radical attacks, microstreaming, or a combination of these. Oil rancidity may be exacerbated by the simultaneous degradation and generation of hydroperoxides caused by the presence of oxygen and the metallic probe. These results reflect those of Halim and Thoo (2018), who also reported that ultrasound treatment in the form of an ultrasonic bath speeds up the process of lipid oxidation in sunflower oil and palm oil. According to the classification provided by Warner and Nelsen (1996), the residual oil recovered from POME has a PV of about 3 meq/kg, indicating a low oxidation state which shall not be of concern. The stability of palm oil can be attributed to the presence of significant levels of lipid-soluble antioxidants like carotenoids, Vitamin E, and ubiquinone in their composition (Edem, 2002).

The GCV, which can also be referred to as the gross heat of combustion (GHC) or higher heating value (HHV), measures the heat generated in complete combustion to determine the energy content of a substance. The GCV of residual oil recovered from POME is around 39,000 J/g, with oil recovered from ultrasound-treated POME slightly higher than oil recovered from non-treated POME. This indicates that the recovered oil from POME with ultrasonication pre-treatment combusts more efficiently and generates more heat when burned. The energy content of the fuel varies depending on the fuel composition, feedstock source, refinery technique, and processing time. According to Van Gerpen, et al. (2004), saturated fuels tend to have higher energy content than unsaturated fuels on a weight basis. This is consistent with our findings that oil recovered from ultrasound-treated POME has a greater degree of saturation, resulting in higher energy content.

Ultrasound cavitations induce free radical reactions, and the degree of the sonochemistry varies with frequency. The free radical formation is more evident at higher frequencies ranging from 100 to 1,000 kHz (Sancheti and Gogate, 2017). In this case, the applied frequency was 20 kHz, which did not fall within the frequency range that resulted in significant free radical reactions. Hence, there were no discernible effects on the quality of the oil recovered from non-treated and ultrasound-treated POME samples. Due to its high FFA and PV, the recovered oil from POME is best employed in non-edibles applications such as burner fuel, raw material for cosmetics, bioplastics, or biodiesel manufacturing.

4.5 Cost-Benefit Analysis on Enhancement of Oil Recovery using Ultrasonication Technique

An economic cost-benefit analysis was conducted to assess the feasibility of utilizing ultrasonication as a pre-treatment to enhance oil recovery from POME in Tian Siang Oil Mill (Air Kuning) Sdn. Bhd., which typically generates 60 MT of POME per hour.

4.5.1. Cost Estimation

The projected costs of this project are capital investment and operating expenses. Capital investments are estimated based on the percentage of delivered equipment cost method (Peters, Timmerhaus and West, 2003). The purchase cost of an ultrasonic processor was estimated using a vendor's quotation in conjunction with the *six-tenths factor rule* indicated in Equation 3.4. Table 4.11 presents the equipment purchase price adjusted for inflation, presuming a treatment rate of 60 MT of POME per hour.

Table 4.11: Purchase Cost of Equipment

Equipment	Base purchase cost	New purchase cost (Adjusted for inflation)
Ultrasonic processor	RM 49,203.42	RM 69,214.55

Table 4.12 outlines the estimation of capital investment for the enhancement of oil recovery using the ultrasonication technique. Fixed capital investment (FCI) is the summation of total direct and indirect costs. Direct costs are the expenses incurred in the fabrication and installation of permanent facilities. In contrast, indirect costs are the expenses that are not permanent but are essential for the orderly execution of a project. The estimated direct and indirect expenditures are RM 209,027.94 and RM 87,210.33, respectively, totaling RM 296,238.27 in the fixed capital investment. Total capital investment (TCI) is computed by summing up the project's FCI and working capital. The total capital investment of this project would be RM 348,149.18.

Table 4.12: Cost Estimation for Total Capital Investment

Subject	Cost (RM)	Total (RM)
Direct Costs		
<i>Onsite</i>		
Purchased equipment	RM 69,214.55	
Installation	RM 26,993.67	
Instrumentation and controls	RM 17,995.78	
Piping	RM 21,456.51	
Electrical system	RM 6,921.46	RM 142,581.97
<i>Offsite</i>		
Buildings	RM 20,072.22	
Yard improvement	RM 8,305.75	
Service facilities	RM 38,068.00	RM 66,445.97
<i>Total direct cost, DC</i>		RM 209,027.94
Indirect Costs		
Engineering and supervision	RM 22,148.66	
Construction expenses	RM 23,532.95	
Legal expenses	RM 2,768.58	
Contractor's fee	RM 13,150.76	
Contingency	RM 25,609.38	
<i>Total indirect cost, IC</i>		RM 87,210.33
Fixed Capital Investment, FCI		RM 296,238.27
Working capital, WC	RM 51,910.91	
Total Capital Investment, TCI		RM 348,149.18

Operating expenses include raw materials, utilities, labor, and indirect manufacturing costs. Table 4.13 shows a comprehensive annual operating cost for employing ultrasonication to improve oil recovery from POME. The by-product of the palm oil milling process, POME, serves as the raw material; it is obtained at no charge. Since the enhancement of oil recovery using ultrasonication does not involve the use of chemicals, electricity consumption would be the most concerning factor. The category of consumers and the supply voltage generally determine the rate of electricity charges. According to the low-voltage industrial electricity tariff rate provided by Tenaga Nasional Berhad (2022), electricity is charged at RM 0.38/kWh. To treat 60 MT of POME per hour, 125 kWh of electricity is required for the ultrasonication process (Equation E.2). The estimated hourly electrical cost for the process is RM 47.50, totaling RM 243,200 in annual utility bills.

The labor expenses are computed using an anticipated operating wage of RM 2,000 monthly and two working shifts daily (Aliff, 2022). Manufacturing operations always necessitate a certain amount of direct supervision and maintenance. Direct supervisory costs are typically a 15 % premium of operating wages, while maintenance costs are a 10 % premium. The total estimated annual labor cost is RM 156,000. Indirect costs like overhead, fixed, and administrative charges account for RM 107,525.96 annually. The total annual operating cost for ultrasound-enhanced oil recovery is expected to be RM 507,318.44.

Table 4.13: Cost Estimation for Operating Cost

Subject	Specifications	Cost (RM)	Total (RM/year)
Direct Operating Costs (Variable)			
Raw material	POME	-	
Utilities	Electricity	RM 243,200.00	RM 243,200.00
Direct Operating Costs (Semi variable)			
<i>Labor cost</i>			
Operating	1 staff per shift	RM 48,000.00	
Supervisory	1 staff per shift (15% premium of operating wages)	RM 55,200.00	
Maintenance	1 staff per shift (10% premium of operating wages)	RM 52,800.00	RM 156,000.00
Operating supplies	0.2% of FCI	RM 592.48	RM 592.48
Indirect Operating Costs			
Overhead (Payroll and plant)	60% of labor cost	RM 93,600.00	
Property taxes	1% of TCI	RM 3,481.49	
Insurance	1% of TCI	RM 3,481.49	
Administrative charges	2% of TCI	RM 6,962.98	RM 107,525.96
Operating cost, O	Direct + Indirect		RM 507,318.44

4.5.2. Benefit Estimation

The revenue of this project is through the sale of recovered residual oil. Considering 0.155 % as the current oil loss in POME, ultrasonication pre-treatment improves the oil recovery by 42.5 %, corresponding to 0.221 % of oil. Given that the market price per ton of CPO fluctuates between RM 5,345.50 to RM 6,873.00 from January to June 2022 (MPOB, 2022), the average CPO price is around RM 6,301.50/ton. With the assumption that residual oil recovered from POME can be sold for 50 % of the typical CPO price, the selling price is approximately RM 3,150.75/ton. The variation of O&G concentration in POME can range from 130 to 18,000 mg/L, depending on fruit batches, processing mechanisms, and weather conditions. Therefore, it should be noted that the revenue generated could be higher. Table 4.14 shows the product sales revenue of the oil recovered from non-treated and ultrasound-treated POME samples.

Table 4.14: Benefit Estimation from Product Sales Revenue

Method	Non-Treated	Ultrasound-Treated
Oil (%)	0.155	0.221
Oil (MT/year)	476.16	678.91
Sales revenue (RM/year)	RM 1,500,261.12	RM 2,139,075.68
Differences (RM/year)	RM 638,814.56	

Furthermore, there are potential benefits that cannot be quantified into the monetary unit, such as reduced COD content and improved organic solubilization. Table 4.8 and 4.15 show that ultrasound-treated POME and de-

oiled POME reduced SS content by 27.78 % and COD content by 17.14 %, respectively. This finding is consistent with those of Wong, et al. (2019), who discovered that pre-treatment of POME with ultrasound enhanced organic matter solubilization by 31.5 %. On the other hand, Liew, et al. (2017) reported that the removal of oil from raw sludge reduces COD content by 10 to 15 %. They further claimed that the removal of oil along with suspended solids could reduce COD and BOD concentrations by up to 70 %. Jahi, et al. (2020) also discovered that COD values decreased by 18 % after the treatment of oil waste by absorption. Organic matter solubilization and de-oiling contribute positively to anaerobic digestion rate and biomethane yield (Aziz, et al., 2020). This is attributed to a lesser proportion of recalcitrant biofibers, which is advantageous for subsequent biological treatment.

Table 4.15: COD Removal Efficiency After Oil Recovery

	COD (mg/L)
Before oil recovery	76,700 ± 1,980
After oil recovery	63,550 ± 2,758
Removal efficiency	17.14 %

Undoubtedly, oil recovery from POME converts negative externalities of POME into positive externalities, thereby progressing towards sustainable development. Oil recovery from POME could not only contribute to environmental sustainability through pollutant reduction and waste utilization, but it could also contribute to social sustainability through job creation and technology transfer.

4.5.3. Economic Evaluation of Investment Feasibility

Table 4.16 shows the profitability analysis for the residual oil enhancement using the ultrasonication technique. Enhancement of oil recovery from POME using ultrasonication pre-treatment will bring in additional revenue of RM 638,814 per mill per year, depending on the mill's oil loss. Even with the consideration of annual depreciation, operating costs, as well as tax, this pre-treatment can still generate a profit of RM 117,705.96 per year, making ultrasound pre-treatment a viable process.

Table 4.16: Profitability Analysis

Subject	Cost (RM/year)
Product sales revenue	RM 638,814.56
Annual depreciation	RM 3,554.86
Operating cost	RM 507,318.44
Tax	RM 10,235.30
Net annual profit after tax	RM 117,705.96

The TCI and potential savings of this project are RM 348,149.18 and RM 117,705.96, respectively. Assuming a discount rate of 3.8 % and the project is targeted to run up to 5 years, the net present value (NPV) calculation is shown in Table 4.17. The computation reveals that the NPV is positive by the end of the fifth year, indicating that the use of ultrasonication to improve oil recovery is feasible.

Table 4.17: Net Present Value Calculation

Year	Cash flow	Present value saving	Net present value
0	(RM 348,149.18)		
1	RM 117,705.96	RM 113,396.88	(RM 234,752.30)
2	RM 117,705.96	RM 109,245.55	(RM 125,506.75)
3	RM 117,705.96	RM 105,246.19	(RM 20,260.56)
4	RM 117,705.96	RM 101,393.25	RM 81,132.69
5	RM 117,705.96	RM 97,681.36	RM 178,814.05
Total		RM 526,963.23	

Table 4.18 presents this project's payback period, return on investment, and benefit-cost ratio. In general, this investment reaches a breakeven point at a payback period of 2.96 years with a 33.81 % of average rate of return. This project's benefit-cost ratio is more than one, indicating that the investment is feasible. In short, ultrasound pre-treatment not only reveals a new economic opportunity for palm oil millers but can also appreciably reduce the treatment operation footprint and subsequently save treatment costs. Hence, it seems plausible to integrate ultrasonication in the existing POME treatment facility.

Table 4.18: Payback Period, Return on Investment, and Benefit-Cost Ratio

$Payack\ period = \frac{RM\ 348,149.18}{RM\ 117,705.96}$	PbP = 2.96 years
$Return\ on\ investment = \frac{RM\ 117,705.96}{RM\ 348,149.18} \times 100\%$	ROI = 33.81 %
$Benefit\ cost\ ratio = \frac{RM\ 526,963.23}{RM\ 348,149.18}$	BCR = 1.51

4.6 Feasibility Study of Using Recovered Oil from POME as Biodiesel Feedstock

This section outlines the second stage of the research, which is biodiesel production using recovered oil from POME to develop industrial symbiosis potential. As discussed in Section 4.4.2, the high AV of the recovered oil from POME did not fulfil the minimal criterion for alkaline-transesterification biodiesel production to proceed smoothly. As a result, acid-esterification is required as a pre-treatment prior to alkaline-transesterification to reduce the high concentration of FFA.

4.6.1 Potential of Using Ultrasonication Technique as a Process Intensifier for FFA Conversion

Nonetheless, the esterification and transesterification reactions are mass-transfer-restricted processes due to the issues with the miscibility of reactants. To circumvent this obstacle, the ultrasonication technique was applied as a process intensifier and compared to the conventional approach to determine if ultrasonication would improve the conversion process. Figure 4.16 compares the three distinct strategies for the reduction of high FFA feedstock, namely the conventional method, ultrasonic bath, and ultrasonic probe, under the constant conditions of an 8:1 methanol-to-oil molar ratio, 0.75 wt% H₂SO₄ loading and 60-minute reaction time.

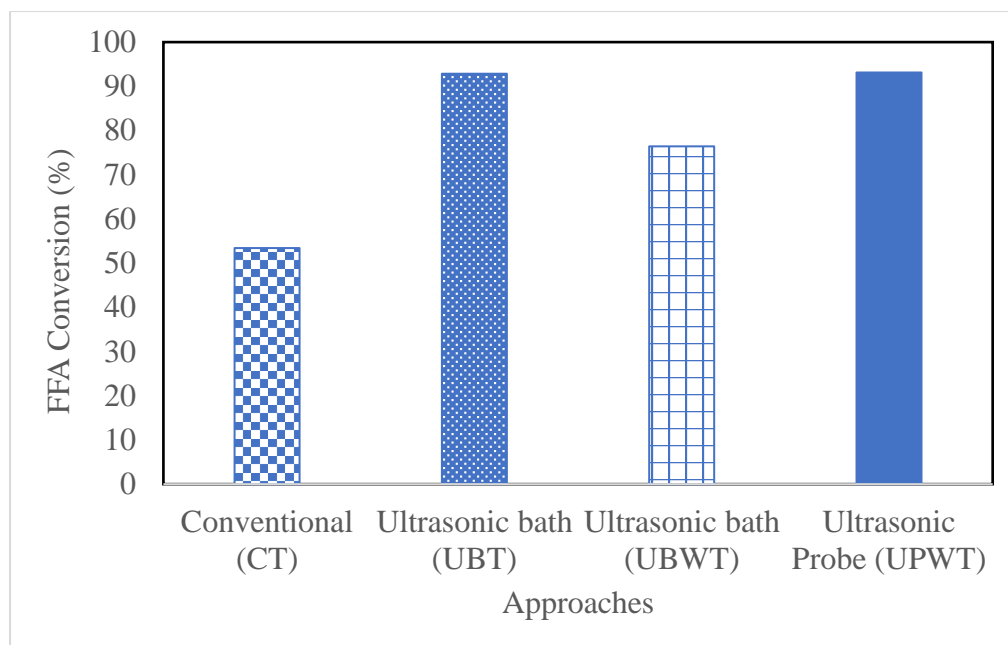


Figure 4.16: Comparison of Three Different Approaches for the Reduction of High FFA Feedstock

Under the fixed reaction parameters, ultrasound-intensified techniques (UBT, UBWT, and UPWT) had an FFA conversion of approximately 76 % to 93 %, whereas the conventional approach (CT) only had a conversion of 53 %. From this comparison, it can be clearly seen that the conversion attained using ultrasound-assisted techniques are 23 – 40 % greater than using the conventional approach. The process intensification by ultrasonic irradiation is mainly attributable to the enhanced mixing caused by the cavitation effects. Ultrasound causes the development of microemulsions between the immiscible phases, which improves the interfacial region and accelerates the reaction rates.

The FFA conversion achieved with an ultrasonic bath at 60 °C operating temperature (UBT) is 16.43 % higher than the conversion achieved with an ultrasonic bath at ambient temperature (UBWT). This is explained through the

theory of chemical reaction kinetics, where a higher temperature produces a greater proportion of fast-moving molecules, which in turn promotes a higher reaction rate.

In a comparison of FFA conversion between an ultrasonic bath (UBWT) and an ultrasonic probe (UPWT) at ambient temperature, the ultrasonic probe offers a 16.69 % greater conversion than the ultrasonic bath. This is probably due to the direct contact of the sample with the ultrasonic probe, which provides better energy dissipation than the indirect contact of the sample with the ultrasonic bath.

Besides, it is also worth noting that the conversion attained using an ultrasonic probe at ambient temperature (UPWT) and a bath at an operating temperature of 60°C (UBT) did not differ significantly. However, the power applied by an ultrasonic bath (1000 W) is more than that of an ultrasonic probe (max 400 W) due to an additional heating element, thus resulting in higher energy consumption. Ultrasonic probe-assisted esterification can be performed at ambient temperature, eliminating the need of external heating, and effectively reducing energy consumption due to the development of microjets and hot spots. For this reason, it is of interest to explore the impact of ultrasound probe parameters such as ultrasonication amplitude and duration on the FFA conversion.

4.6.2 Influence of Ultrasonication Amplitude on Acid Value and FFA Conversion

To investigate the influence of ultrasonication amplitude, experiments were carried out by altering the ultrasonication amplitude from 20 % to 40 %, while maintaining the other parameters at an ultrasonication duration of 15 minutes, methanol-to-oil molar ratio of 8:1, and H₂SO₄ loading of 0.75 wt%. Figure 4.17 presents the influence of ultrasonication amplitude on the AV and FFA conversion.

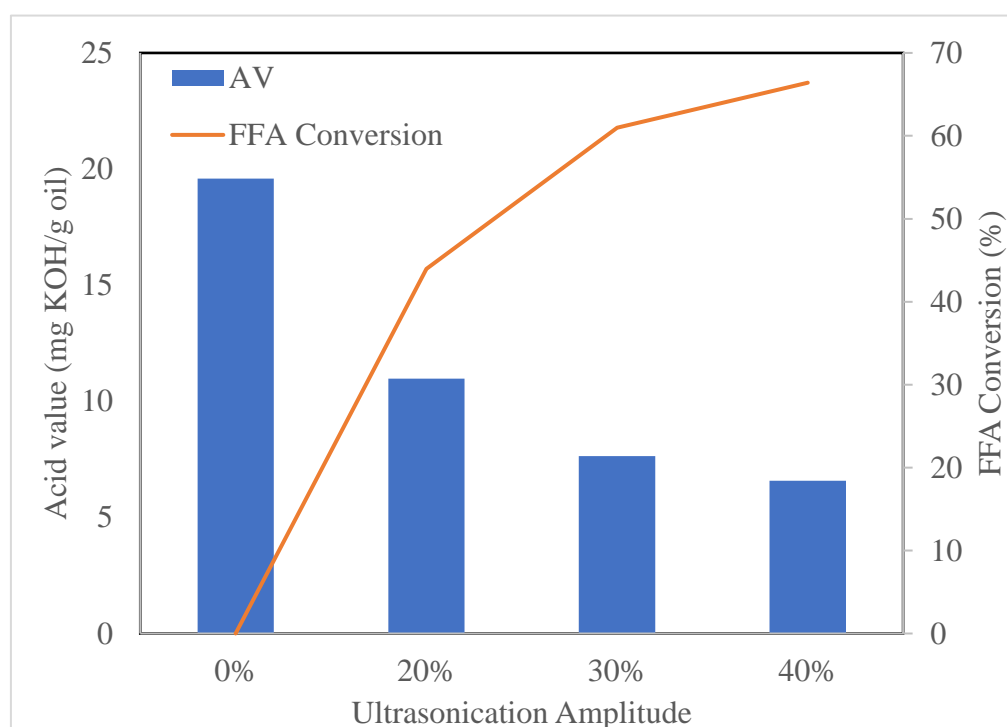


Figure 4.17: Effect of Different Ultrasonication Amplitude on AV and FFA Conversion (Conditions: Ultrasonication Duration: 15 minutes, Methanol-to-Oil Molar Ratio: 8:1, and H₂SO₄ Loading: 0.75 wt%)

Ultrasonic process intensification results in temperature and pressure hotspots due to the rapid disintegration of microbubbles subjected to adiabatic compression. This, in turn, triggers the generation of shockwaves, which subsequently increases both heat and mass transfers in the reaction. The ultrasonication amplitude is correlated with the cavitation effects. Even at the lowest practicable ultrasonication amplitude of 20 %, the AV reduced from 19.59 mg KOH/g oil to 10.98 mg KOH/g oil, with an FFA conversion of 43.95 %. The FFA conversion skyrocketed when ultrasonication amplitude was raised to 40 %, reaching 66.41 %. Increasing the ultrasonication amplitude resulted in a more prominent microstreaming effect, which aided in enhanced phase mixing.

A similar phenomenon was observed in the study of biodiesel synthesis from waste bio-oil using an ultrasound-assisted approach (Yasvanthrajan, et al., 2021), where an increase in ultrasonication amplitude increases the conversion. However, increasing the ultrasonication amplitude over the 40 % threshold has been shown to lower the conversion. A decreased cavitation activity is most likely the result of a high concentration of microbubbles at higher amplitude, which provides a cushion effect upon collapse and reduces energy transmission into the system. Since the maximum workable amplitude for a microtip probe is 40 %, a further increment in the ultrasonication amplitude is not recommended as it will damage the probe and increase the operating cost.

4.6.3 Influence of Ultrasonication Duration on Acid Value and FFA Conversion

Figure 4.18 demonstrates the influence of ultrasonication duration on the AV and FFA conversion. The reactions were initiated with a 15-minute reaction period, and subsequently raised to 60 minutes. Other parameters, such as ultrasonication amplitude of 30 %, methanol-to-oil molar ratio of 8:1, and H₂SO₄ loading of 0.75 wt%, were kept constant during the experiment.

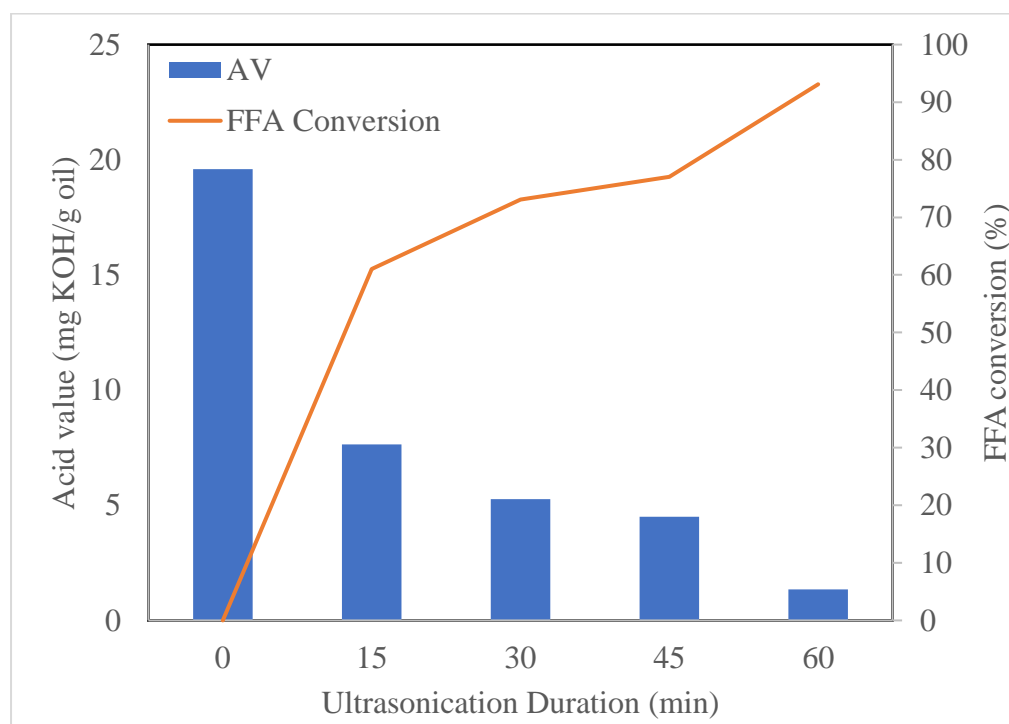


Figure 4.18: Effect of Different Ultrasonication Duration on AV and FFA Conversion (Conditions: Ultrasonication Amplitude: 30 %, Methanol-to-Oil Molar Ratio: 8:1, and H₂SO₄ Loading: 0.75 wt%)

A linearly increasing trend in the FFA conversion was observed as the ultrasonication duration increased. This occurs because FFA conversion requires adequate contact time between the reactants and catalysts. Takase, et al. (2014) investigated the effect of ultrasonic reaction time varying from 10 to 40 minutes on biodiesel synthesis from *Silybum marianum* oil and discovered that the reaction was reliant on the ultrasonication duration. However, allowing the reaction to continue for an extended period is not advisable. This is due to the possibility of catalyst deactivation caused by the buildup of water by-products, resulting in a modest fall in biodiesel yield (Mardhiah, et al., 2017). Variations in the biodiesel conversion were sometimes also observed, but at a smaller magnitude, with extended reaction duration (Dawodu, et al., 2014). The highest documented FFA conversion in this investigation (Figure 4.18) was 93.11 %, with an AV of 1.35 mg KOH/g oil during the reaction period of 60 minutes. This satisfied the minimum AV required for the transesterification to proceed smoothly (< 4 mg KOH/g oil).

4.6.4 Physicochemical Quality of Biodiesel

A maximum FFA conversion of 93 % can be achieved after 1 hour of ultrasonication at 30 % amplitude, using a methanol-to-oil molar ratio of 8:1 and an H₂SO₄ loading of 0.75 wt%. Prior to GC analysis, the esterified oil was subjected to alkaline transesterification to improve its volatility. Table 4.19 summarizes the fatty acid composition of biodiesel produced from POME-recovered oil.

According to Table 4.19, the biodiesel produced from POME-recovered oil contains approximately equal proportions of saturated and unsaturated fatty acids. Methyl palmitate (C16:0, 44 %) was the most prevalent saturated fatty acid in the oil, with methyl stearate (C18:0, 4 %) coming in second. Unsaturated fatty acids can be classified into two distinct types: monounsaturated fatty acids (MUFAs, 39 %) and polyunsaturated fatty acids (PUFAs, 10 %). The predominant monounsaturated fatty acid was methyl oleate (C18:1, 38 %), while the polyunsaturated fatty acid was methyl linoleate (C18:2, 10 %). Overall, the fatty acid composition of POME residual oil is comparable to the fatty acid composition of CPO in accordance with MS 814:2007 in Table 2.12.

Table 4.19: Fatty Acid Composition of POME-Methyl Ester

Fatty acid composition	wt%	Concentration (mg/g)
Methyl butyrate (C4:0)	0.24	1.93
Methyl hexanoate (C6:0)	0.01	0.06
Methyl octanoate (C8:0)	0.02	0.13
Methyl decanoate (C10:0)	0.02	0.16
Methyl laurate (C12:0)	0.25	1.98
Methyl myristate (C14:0)	0.96	7.61
Methyl pentadecanoate (C15:0)	0.06	0.51
Methyl palmitate (C16:0)	44.21	350.60
Methyl palmitoleate (C16:1)	0.17	1.33
Methyl stearate (C18:0)	4.33	34.33
Methyl oleate (C18:1)	38.90	308.52
Methyl linoleate (C18:2)	9.81	77.84
Methyl-gamma-linoleate (C18:3)	0.31	2.44
Methyl eicosanoate (C20:1)	0.36	2.82
Methyl linolenate (C18:3)	0.12	0.98
Methyl eicosatrienoate (C20:3)	0.06	0.49
Methyl eicosatetraenoate (C20:4)	0.07	0.56
Methyl docosadienoate (C22:2)	0.02	0.15
Methyl eicosapentaenoate (C20:5)	0.08	0.63
Total saturated fatty acids (SFAs)	50.26	398.62
Total unsaturated fatty acids (UFAs)	49.74	394.43
Total monounsaturated fatty acids (MUFAs)	39.26	311.35
Total polyunsaturated fatty acids (PUFAs)	10.48	83.08

A series of fuel properties indices were carried out to evaluate the quality of biodiesel produced. Table 4.20 summarizes the physicochemical quality parameters of POME biodiesel produced through two-step esterification and transesterification process. The results were compared to the standard specifications as well as the properties of conventional palm-based biodiesel produced in Malaysia listed in Table 2.13.

Table 4.20: Comparison of Physicochemical Properties of POME Biodiesel with Standard Specifications

Properties	This study	Standards
Density at 15°C (kg/m ³)	861	860 – 890
Ester content (%)	92.9	Min 96.5
Iodine value	51.5	Max 110
Linolenic acid methyl ester (wt%)	0.44	Max 12
Oxidation stability at 110°C (hours)	29.3	Min 8
Polyunsaturated methyl ester (wt%)	0.15	Max 1
Total acid value (mg KOH/ g oil)	0.07	Max 0.5
Viscosity at 40°C (mm ² /s)	4.55	1.9 – 6.0

POME methyl ester has a density of 861 kg/m³, which is within the acceptable range of 860 – 890 kg/m³. It has a lower density than conventional biodiesels like soybean (880 kg/m³) and canola (883 kg/m³) (Şahin and Aydın, 2018; Joshi, et al., 2017). A fuel with reduced density and viscosity enhances atomization efficiency (Wan Ghazali, et al., 2015).

The purity of biodiesel is measured in terms of ester content. In this study, the ester content of POME biodiesel is 92.9 %, which is lower than the standard specifications (min 96.5 %). The low ester content in biodiesel can be attributable to the presence of impurities in oil or an incomplete reaction of glycerides (Etim, et al., 2022). Non-decomposable glycerol, residual alcohols, as well as unsaponifiable matters are all the examples of contaminations that substantially lower the FAME content below the permissible value. These pollutants, however, can be eliminated using a distillation or filtration procedure. Conversely, a high concentration of mono-, di- and triglycerides is an indication of an inefficient reaction. Thus, there is a need to improve the biodiesel production process.

POME biodiesel has an iodine value of 51.5, well below the maximum allowable limit of 110. Similarly, linolenic acid methyl esters and polyunsaturated methyl esters also fall within the standard specifications. Unsaturated fatty acids in biodiesel should be kept to a minimum to prevent oxidation. Oxidation stability is vital for decent engine performance as oxidized products lead to issues, including the build-up of deposits, filter clogging, and corrosion. Since the oxidation stability of POME methyl ester is 29.3 hours, well over the minimum required criteria of 8 hours, there is no cause for concern.

Fuel deterioration and fuel supply system corrosion have been linked to the total acid value. This investigation discovered a total acid value of 0.07 mg KOH/g oil, which meets the biodiesel criteria. Viscosity refers to a fluid's internal resistance, which is crucial to its combustibility and the production of

deposits and soot. Incomplete combustion occurs when the fuel's viscosity is so high that it cannot be atomized efficiently. POME methyl ester has a viscosity of 4.55 mm²/s, which is commensurate with the requirement of 1.9 – 6 mm²/s.

In general, except for the ester content, all these results meet the international standards (EN 14214 and ASTM D6751) as well as the local standard (MS 2008:2008). Furthermore, the attributes of POME methyl ester are comparable to those of palm-based biodiesel produced in Malaysia, demonstrating that the residual oil from POME is a viable feedstock for biodiesel synthesis, with the biggest advantage of its non-interference with the food supply chain.

CHAPTER 5

CONCLUSIONS AND RECOMMENDATIONS

5.1 Conclusions

5.1.1 General Conclusion

Conclusively, this research identifies a novel strategy for enhancing oil recovery from POME. The effect of various ultrasonication operating parameters on oil yield improvement was investigated. Additionally, the impacts of ultrasonication pre-treatment on POME and recovered oil were discussed. A cost-benefit analysis was incorporated to determine its feasibility as well. The scope of the research was further extended to biodiesel production using recovered oil from POME. The biodiesel produced was analyzed and compared to international and local standards. Several key findings were deduced:

1. The residual oil in POME is mainly bound to and trapped within the fibers. Low-frequency ultrasound can enhance oil recovery yield by disrupting the cell structure.
2. The application of ultrasonication as a pre-treatment affects POME particle size reduction and SS solubilization.

3. The intervention of ultrasonication pre-treatment enhances the oil content from POME without compromising its oil quality.
4. The cost-benefit analysis reveals that ultrasonication pre-treatment is a viable alternative that not only benefits the environment, but also offers an economic opportunity.
5. Ultrasound-assisted biodiesel production enhances the FFA conversion over the conventional method.
6. The properties of biodiesel produced from POME-recovered oil achieve the requirements of the standards.

5.1.2 Conclusion for Objective 1

An optimized study on the ultrasound-enhanced oil recovery from POME was conducted using RSM. The optimized conditions were obtained at 30.074 % ultrasonication amplitude, 0.167 minutes ultrasonication duration, and 2 cm probe immersion depth. This resulted in an additional 42.50 % improvement in oil recovery yield over non-treated POME, which is in close agreement with the model's prediction.

5.1.3 Conclusion for Objective 2

Particle size distribution and microscopy analyses of ultrasound-treated POME samples indicate structural disorganization, supporting the assertion that ultrasonication could disrupt the complex particles, and subsequently release of entrained oil. The ATR spectrum and quality assessment reveal that ultrasonication had no significant effect on the recovered oil's functional group, DOBI, AV, FFA, and GCV, indicating that the ultrasonication does not impair the oil's quality.

5.1.4 Conclusion for Objective 3

The economic cost-benefit analysis revealed that ultrasonication pre-treatment is viable for improving oil from POME, with a positive NPV and a BCR greater than one. This investment reaches a breakeven point at a payback period of 2.96 years and an ROI of 33.81 %. Enhancing oil recovery from POME using ultrasonication could contribute not only to environmental sustainability through pollutant reduction and waste utilization, but also to social sustainability through job creation and technology transfer.

5.1.5 Conclusion for Objective 4

The FFA conversion achieved by ultrasound-intensified techniques are 23 – 40 % greater than the conventional approach. The ultrasonic probe achieved a better performance than the ultrasonic bath. The ultrasonic probe-

assisted reaction can be performed at ambient temperature, eliminating the need of external heating, and effectively reducing energy consumption. A maximum FFA conversion of 93 % can be achieved after 1 hour of ultrasonication at 30 % amplitude, using a methanol-to-oil molar ratio of 8:1, and an H₂SO₄ loading of 0.75 wt%. A series of fuel properties indices were carried out to evaluate the quality of biodiesel produced. Except for the ester content, all these results meet international and local standards. The low ester content may be attributable to contaminants in the oil or an incomplete reaction. Overall, the attributes of POME methyl esters are comparable to those of palm-based biodiesel produced in Malaysia, demonstrating its potential as an alternative source.

5.2 Recommendations

In this study, lab-scale and batch-mode experiments were carried out. A comprehensive study on the scale-up process, such as the ability to transfer the application of ultrasonication from a batch to continuous, can be undertaken as one of the preparatory steps for the industrialization of this application. Additionally, larger-scale applications require the consideration of system design and ultrasound field patterns. It is also suggested to study the applicability of ultrasonication pre-treatment for enhancement of oil recovery in other oily wastewater, such as plant oil mill effluent and food processing effluent. Moreover, it is worth noting that the current study solely concentrated on comparing the oil content from ultrasound-treated POME with non-treated POME on a laboratory scale. Thus, it is highly recommended to undertake a comprehensive comparative study to evaluate the efficacy of ultrasonication

pre-treatment as an enhanced oil recovery technique, in relation to other pertinent technologies.

Cost-benefit analysis of this study is just a preliminary estimate in which the capital investment was computed as a percentage of delivered equipment cost, with the equipment cost scaled using the *six-tenths factor rule*. For a more accurate cost analysis, extra investigation on the sizing and material specifications of the essential equipment, as well as the material and energy balances, can be considered.

In view of the low ester content and limited biodiesel's quality explored in this study, additional research is necessary to determine the uncertainties. Other operating parameters for biodiesel production from POME-recovered oil, such as the amount of catalyst and alcohol-to-oil molar ratio, can be investigated to improve the ester content and obtain the optimum conditions. More research is required to ascertain the other undetermined quality of biodiesel, such as flash point, cetane number, total contamination, and so on, to ensure that they fulfill all the standard specifications. In addition to serving as a feedstock for biodiesel production, researchers can also expand their horizons and explore new possibilities and applications for the recovered oil.

REFERENCES

Agi, A., Junin, R., Shirazi, R., Afeez, G. and Yekeen, N., 2019. Comparative study of ultrasound assisted water and surfactant flooding. *Journal of King Saud University - Engineering Sciences*, [e-journal] 31(3), pp. 296-303. <https://doi.org/10.1016/j.jksues.2018.01.002>.

Ahmad, A.L., Sithamparam, K., Zulkali, M.M.D. and Ismail, S., 2003. Extraction of residue oil from palm oil mill effluent (POME) using organic solvent. *ASEAN Journal on Science and Technology for Development*, 20(3&4), pp.385–394.

Ahmad, A.L., Bhatia, S., Ibrahim, N. and Sumathi, S., 2005. Adsorption of residual oil from palm oil mill effluent using rubber powder. *Brazilian Journal of Chemical Engineering*, 22(3), pp.371–379.

Ahmad, A.L., Sumathi, S. and Hameed, B.H., 2005. Adsorption of residue oil from palm oil mill effluent using powder and flake chitosan: Equilibrium and kinetic studies. *Water Research*, 39(12), pp.2483-2494.

Al-Husaini, I.S. and Sakthipandi, K., 2020. Improvements in electrospun nanofibrous membranes and their applications in water treatments. *Journal of Applied Membrane Science & Technology*, 24(3), pp.31–56.

Aliff, S., 2022. No problem for RM1,500 minimum wage in plantation sector. *The Malaysian Reserve*, [online] 15 March. Available at: <<https://themalaysianreserve.com/2022/03/15/plantation-sector-has-no-problem-to-implement-rm1500-minimum-wage/#:~:text=For the palm oil industry%2C in particular%2C Zuraida said the,to RM2%2C500 per month>> [Accessed 5 July 2022].

Altaf, U., Rouf, A., Kanojia, V., Ayaz, Q. and Zargar, I., 2018. Ultrasound treatment: A novel processing technique for food preservation. *The Pharma Innovation Journal*, 7(2), pp.234–241.

Altun, N.E., Hwang, J.Y. and Hicyilmaz, C., 2018. *Use of ultrasound to enhance flotation performance: Flotation cleaning of oil shale after ultrasonic pre-treatment*. In: International ASET Inc. (International Academy of Science, Engineering and Technology), Proceedings of the 4th World Congress on Mechanical, Chemical, and Material Engineering, Madrid, Spain, 16-18 August 2018. Orleans: Canada.

American Public Health Association, 2017. *Standard methods for the examination of water and wastewater (23rd ed.)*. Washington DC: APHA.

Ayala, A., Muñoz, M.F. and Argüelles, S., 2014. Lipid peroxidation: Production, metabolism, and signaling mechanisms of malondialdehyde and 4-hydroxy-2-nonenal. *Oxidative Medicine and Cellular Longevity*, [e-journal] 2014, <https://doi.org/10.1155/2014/360438>.

Aziz, M.M.A., Kassim, K.A., ElSergany, M., Anuar, S., Jorat, M.E., Yaacob, H., Ahsan, A., Imteaz, M.A. and Arifuzzaman, 2020. Recent advances on palm oil mill effluent (POME) pretreatment and anaerobic reactor for sustainable biogas production. *Renewable and Sustainable Energy Reviews*, [e-journal] 119, p.109603. <https://doi.org/10.1016/j.rser.2019.109603>.

Bigelow, T.A., Xu, J., Stessman, D.J., Yao, L., Spalding, M.H. and Wang, T., 2014. Lysis of *Chlamydomonas reinhardtii* by high-intensity focused ultrasound as a function of exposure time. *Ultrasonics Sonochemistry*, [e-journal] 21(3), pp.1258–1264. <http://doi.org/10.1016/j.ultsonch.2013.11.014>.

Boffito, D.C., Galli, F., Pirola, C., Bianchi, C.L. and Patience G.S., 2014. Ultrasonic free fatty acids esterification in tobacco and canola oil. *Ultrasonics Sonochemistry*, [e-journal] 21(6), pp.1969–1975. <http://doi.org/10.1016/j.ultsonch.2014.01.026>.

Boukandoul, S., Santos, C.S.P., Casal, S. and Zaidi, F., 2019. Oxidation delay of sunflower oil under frying by moringa oil addition: more than just a blend. *Journal of the Science of Food and Agriculture*, 99(12), pp.5483–5490.

Brotchie, A., Grieser, F. and Ashokkumar, M., 2009. Effect of power and frequency on bubble-size distributions in acoustic cavitation. *Physical Review Letters*, [e-journal] 102(8), pp.1–4. <https://doi.org/10.1103/physrevlett.102.084302>.

Buddin, M.M.H.S., Rithuan, M.Z.A., Surni, M.S.A., Jamal, N.H.M. and Faiznur, M.F., 2018. Ultrasonic assisted extraction (UAE) of Moringa oleifera seed oil: Kinetic study. *ASM Science Journal*, 11(3), pp.158–166.

Cao, P., Hao, C., Ma, C., Yang, H. and Sun, R., 2021. Physical field simulation of the ultrasonic radiation method: An investigation of the vessel, probe position and power. *Ultrasonics Sonochemistry*, [e-journal] 76, p.105626. <https://doi.org/10.1016/j.ultsonch.2021.105626>.

Cercado, A.P.I., Ballesteros, F.C. and Capareda, S.C., 2018. Biodiesel from three microalgae transesterification processes using different homogenous catalysts. *International Journal of Technology*, [e-journal] 9(4), pp.645–651. <https://doi.org/10.14716/ijtech.v9i4.1145>.

Chuah, L.F., Bokhari, A., Yusup, S., Klemeš, J.J., Abdullah, B. and Akbar M.M., 2016. Optimisation and kinetic studies of acid esterification of high free fatty acid rubber seed oil. *Arabian Journal for Science and Engineering*, [e-journal] 41, pp.2515–2526. <https://doi.org/10.1007/s13369-015-2014-1>.

Da Porto, C., Natolino, A. and Decorti, D., 2015. Effect of ultrasound pretreatment of hemp (*Cannabis sativa* L.) seed on supercritical CO₂ extraction of oil. *Journal of Food Science and Technology*, 52(3), pp.1748–1753.

Dawodu, F.A., Ayodele, O., Xin, J., Zhang, S. and Yan D., 2014. Effective conversion of non-edible oil with high free fatty acid into biodiesel by sulphonated carbon catalyst. *Applied Energy*, 114, pp.819-826.

Department of Environment Malaysia, 1977. *Environmental Quality (Prescribed Premises) (Crude Palm Oil) (Amendment) Regulation 1977. Environmental Quality Act 1974 (Act 127)*. Malaysia: DOE.

Di Pietro, M.E., Mannu, A. and Mele, A., 2020. NMR determination of free fatty acids in vegetable oils. *Processes*, [e-journal] 8(4), <https://doi.org/10.3390/pr8040410>.

Edem, D.O., 2002. Palm oil: Biochemical, physiological, nutritional, hematological, and toxicological aspects: A review. *Plant Foods for Human Nutrition*, [e-journal] 57(3–4), pp.319–341. <https://doi.org/10.1023/a:1021828132707>.

Etim, A.O., Jisieike, C.F., Ibrahim, T.H. and Betiku, E., 2022. Biodiesel and its properties. In: A. Arumugam, ed. 2022. *Production of Biodiesel from Non-Edible Sources: Technological Updates*, Amsterdam: Elsevier Science. pp.39-79.

Faisal, M., Machdar, I., Gani, A. and Daimon, H., 2016. The combination of air flotation and a membrane bioreactor for the treatment of palm oil mill effluent. *International Journal of Technology*, [e-journal] 7(5), pp.767–777. <http://doi.org/10.14716/ijtech.v7i5.3163>.

Fukunaga, S., Higashi, S., Horie, T., Sugiyama, H., Kanda, A., Hsu, T.Y., Tung, K.L., Taniya, K., Nishiyama, S. and Ohmura, N., 2019. Effect of geometrical configuration of reactor on a ZrP nano-dispersion process using ultrasonic irradiation. *Ultrasonics Sonochemistry*, [e-journal] 52, pp.157–163. <https://doi.org/10.1016/j.ultsonch.2018.11.008>.

Gallo, M., Ferrara, L. and Naviglio, D., 2018. Application of ultrasound in food science and technology: A perspective. *Foods*, [e-journal] 7(10), pp.1–18. <https://doi.org/10.3390/foods7100164>.

Geleta, M., Stymne, S. and Bryngelsson, T., 2011. Variation and inheritance of oil content and fatty acid composition in niger (*Guizotia abyssinica*). *Journal of Food Composition and Analysis*, [e-journal] 24(7), pp.995–1003. <http://doi.org/10.1016/j.jfca.2010.12.010>.

Goh, S.H., Choo, Y.M. and Ong, S.H., 1985. Minor constituents of palm oil. *Journal of the American Oil Chemists' Society*, [e-journal] 62(2), pp.237–240. <https://doi.org/10.1007/BF02541384>.

Goula, A.M., Papatheodorou, A., Karasavva, S. and Kaderides, K., 2018. Ultrasound-assisted aqueous enzymatic extraction of oil from pomegranate seeds. *Waste and Biomass Valorization*, [e-journal] 9(1), pp.1–11. <https://doi.org/10.1007/s12649-016-9740-9>.

Halim, H.H. and Thoo, Y.Y., 2018. Effect of ultrasound treatment on oxidative stability of sunflower oil and palm oil. *International Food Research Journal*, 25(5), pp.1959–1967.

Hamidi, H., Haddad, A.S., Otumudia, E.W., Rafati, R., Mohammadian, E., Azdarpour, A., Pilcher, W.G., Fuehrmann, P.W., Sosa, L.R., Cota, N., García, D.C., Ibrahim, R.M., Damiev, M. and Tanujaya, E., 2021. Recent applications of ultrasonic waves in improved oil recovery: A review of techniques and results. *Ultrasonics*, [e-journal] 110, p.106288. <https://doi.org/10.1016/j.ultras.2020.106288>.

Han, H., Wang, S., Rakita, M., Wang, Y. Han, Q. and Xu, Q., 2018. Effect of ultrasound-assisted extraction of phenolic compounds on the characteristics of walnut shells. *Food and Nutrition Sciences*, [e-journal] 9(8), pp.1034–1045. <https://doi.org/10.4236/fns.2018.98076>.

Hashemi, S.M.B., Khaneghah, A.M. and Akbarirad, H., 2016. The effects of amplitudes ultrasound-assisted solvent extraction and pretreatment time on the yield and quality of Pistacia Khinjuk hull oil. *Journal of Oleo Science*, [e-journal] 65(9), pp.733–738. <https://doi.org/10.5650/jos.ess15252>.

Hashim, Z., Zaki, S.S.A.M. and Muhamad, I.I., 2017. Quality assessment of fried palm oils using fourier transform infrared spectroscopy and multivariate approach. *Chemical Engineering Transactions*, [e-journal] 56, pp.829–834. <http://doi.org/10.3303/CET1756139>.

Hassan, M.A., Yacob, S., Shirai, Y. and Hung, Y.T., 2005. Treatment of palm oil wastewaters. In: L.K., Wang, H.H., Lo and C., Yapijakis, eds. 2006. *Waste Treatment in the Food Processing Industry*. Boca Raton: CRC Press. pp. 101–118.

Hassan, M.I., Mariati, R. and Ng, D., 2021. *Overview of the global palm oil sector in 2020 and outlook for 2021*. [online] Available at: <<https://mpoc.org.my/overview-of-the-global-palm-oil-sector-in-2020-and-outlook-for-2021/>> [Accessed: 8 August 2022].

Hayyan, A., Alam, M.Z., Mirghani, M.E.S., Kabbashi, N.A., Hakimi, N.I.N.M., Siran, Y.M. and Tahiruddin, S., 2011. Reduction of high content of free fatty acid in sludge palm oil via acid catalyst for biodiesel production. *Fuel Processing Technology*, [e-journal] 92(5), pp.920–924. <http://dx.doi.org/10.1016/j.fuproc.2010.12.011>.

Hii, K.L., Yeap, S.P. and Mashitah, M.D., 2012. Cellulase production from palm oil mill effluent in Malaysia: Economical and technical perspectives. *Engineering in Life Sciences*, [e-journal] 12(1), pp.7–28. <https://doi.org/10.1002/elsc.201000228>.

Hosseini, S.E. and Wahid, M.A., 2015. Pollutant in palm oil production process. *Journal of the Air and Waste Management Association*, [e-journal] 65(7), pp.773–781. <http://dx.doi.org/10.1080/10962247.2013.873092>.

Hsiao, M.C., Lin, W.T., Chiu, W.C. and Hou, S.S., 2021. Two-stage biodiesel synthesis from used cooking oil with a high acid value via an ultrasound-assisted method. *Energies*, [e-journal] 14(12), p.3703. <https://doi.org/10.3390/en14123703>.

Ishak, S. and Kamari, A., 2019. A review of optimum conditions of transesterification process for biodiesel production from various feedstocks. *International Journal of Environmental Science and Technology*, [e-journal] 16(5), pp.2481–2502. <https://doi.org/10.1007/s13762-019-02279-6>.

Jadhav, A.J., Holkar, C.R., Goswami, A.D., Pandit, A.B. and Pinjari D.V., 2016. Acoustic cavitation as a novel approach for extraction of oil from waste date seeds. *ACS Sustainable Chemistry and Engineering*, [e-journal] 4(8), pp.4256–4263. <https://doi.org/10.1021/acssuschemeng.6b00753>.

Jahi, N., Ling, E.S., Othaman, R. and Ramli, S., 2015. Modification of oil palm plantation wastes as oil adsorbent for palm oil mill effluent (POME). *Malaysian Journal of Analytical Sciences*, 19(1), pp.31–40.

Jahi, N., Othaman, R., Lazim, A.M. and Ramli, S., 2020. Empty fruit bunch cellulose-based sorbent for oil sorption in palm oil mill effluent. *Sains Malaysiana*, 49(9), pp.2323–2333.

Joshi, S., Gogate, P.R., Moreira, P.F. and Giudici, R., 2017. Intensification of biodiesel production from soybean oil and waste cooking oil in the presence of heterogeneous catalyst using high speed homogenizer. *Ultrasonics Sonochemistry*, [e-journal] 39, pp.645–653. <http://dx.doi.org/10.1016/j.ultsonch.2017.05.029>.

Kamyab, H., Chelliapan, S., Din, M.F.M., Rezanian, S., Khademi, T. and Kumar, A., 2018. Palm oil mill effluent as an environmental pollutant. *Palm Oil*, pp.13–28.

Kara, K., Ouanji, F., Lotfi, E.M, Mahi., M.E., Kacimi, M. and Ziyad, M., 2018. Biodiesel production from waste fish oil with high free fatty acid content from Moroccan fish-processing industries. *Egyptian Journal of Petroleum*, [e-journal] 27(2), pp.249–255. <https://doi.org/10.1016/j.ejpe.2017.07.010>.

Kayanan, B.U.R. and Sagum, R.S., 2021. Microwave and ultrasound pretreatment of moringa oleifera lam. seeds: Effects on oil expression, oil quality, and bioactive component. *Journal of Oleo Science*, 70(7), pp.875–884.

Kumar, K., Srivastav, S. and Sharanagat, V.S., 2021. Ultrasound assisted extraction (UAE) of bioactive compounds from fruit and vegetable processing by-products: A review. *Ultrasonics Sonochemistry*, [e-journal] 70, p.105325. <https://doi.org/10.1016/j.ultsonch.2020.105325>.

Kusumaningtyas, R.D., Akbar, M.H. and Widjanarko, D., 2019. Reduction of FFA in Kapok Randu (*Ceiba pentandra*) seed oil via esterification reaction using sulfuric acid catalyst: experimental and kinetics study. *Jurnal Bahan Alam Terbarukan*, 8(2), pp.156–166.

Laohaprapanon, T., Prasertsan, P. and Kittikun, A.H., 2005. Physical and chemical separation of oil and suspended solids from palm oil mill effluent. *Asian Journal on Energy and Environment*, 6(1), pp.39–55.

Liew, A.S.B., Hadi, N.A., Halim, R.M, Yap, A. and Rahman, Z.A., 2017. Methane avoidance via zero effluent discharge using aquaeco plant. *PIPOC Proceedings*. pp.1–15.

Liu, Y., Liu, X., Cui, Y. and Yuan, W., 2022. Ultrasound for microalgal cell disruption and product extraction: A review. *Ultrasonics Sonochemistry*, [e-journal] 87, p.106054. <https://doi.org/10.1016/j.ultsonch.2022.106054>.

Loh, S.K., Lai, M.E., Ngatiman, M., Lim, W.S., Choo, Y.M., Zhang, Z. and Salimon, J., 2013. Zero discharge treatment technology of palm oil mill effluent. *Journal of Oil Palm Research*, 25(3), pp.273–281.

Loh, S.K., Nasrin, A.B., Mohamad Azri, S., Nurul Adela, B., Muzzammil, N., Daryl Jay, T., Stasha Eleanor, R.A., Lim, W.S., Choo, Y.M. and Kaltschmitt, M., 2017. First report on Malaysia's experiences and development in biogas capture and utilization from palm oil mill effluent under the economic transformation programme: Current and future perspectives. *Renewable and Sustainable Energy Reviews*, [e-journal] 74, pp.1257–1274. <http://dx.doi.org/10.1016/j.rser.2017.02.066>.

López-Bascón, M.A. and Luque de Castro, M.D., 2020. Soxhlet extraction. *Liquid-Phase Extraction*, pp.327-354. <https://doi.org/10.1016/B978-0-12-816911-7.00011-6>.

Luna, C., Luna, D., Calero, J. Bautista, F.M., Romero, A.A., Posadillo, A. and Verdugo-Escamilla, C., 2016. Biochemical catalytic production of biodiesel. *Handbook of Biofuels Production: Processes and Technologies*, pp.165-199.

Mahmod, S.S., Arisht, S.N., Jahim, J.M., Takriff, M.S., Tan, J.P., Luthfi, A.A.I. and Abdul, P.M., 2021. Enhancement of biohydrogen production from palm oil mill effluent (POME): A review. *International Journal of Hydrogen Energy*, [e-journal] 47(96), pp.40637-40655. <https://doi.org/10.1016/j.ijhydene.2021.07.225>.

Mardhiah, H.H., Ong, H.W., Masjuki, H.H., Lim, S. and Pang, Y.L., 2017. Investigation of carbon-based solid acid catalyst from *Jatropha curcas* biomass in biodiesel production. *Energy Conversion and Management*, [e-journal] 144, pp.10–17. <https://doi.org/10.1016/j.enconman.2017.04.038>.

Mohamed Anuar, M.A., Amran, N.A. and Ruslan, M.S.H., 2020. *Effect of stirring rate and freezing time on the percentage of recovery of residual oil from palm oil mill effluent via a stirred freeze crystallizer*. In: RSCE, 26th Regional Symposium on Chemical Engineering (RSCE 2019). Kuala Lumpur, Malaysia, 30-31 October 2019. United Kingdom: IOP Publishing Ltd.

Mohammad, S., Baidurah, S., Kobayashia, T., Ismail, N. and Leh, C.P., 2021. Palm oil mill effluent treatment processes—A review. *Processes*, [e-journal] 9(5), pp.1–22. <https://doi.org/10.3390/pr9050739>.

Mohammed, M.E.A. and Alhajhoj, M.R, 2020. Importance and applications of ultrasonic technology to improve food quality. *Food Processing*, pp.1–16.

Malaysian Palm Oil Board, 2022. *MPOB daily Malaysia prices of crude palm oil (RM/tonne)*. [online] Available at: <https://bepi.mpob.gov.my/admin2/price_local_daily_view_cpo_msia.php?more=Y&jenis=1Y&tahun=2022> [Accessed: 1 July 2022].

Mecpro Heavy Engineering Limited, 2022. *Palm oil mill - Oil recovery from effluent water*. [online] Available at: <<https://www.mecpro.com/oil-recovery-from-pome.html>> [Accessed: 14 June 2021].

Ngarmkam, W., Sirisathitkul, C. and Phalakornkule, C., 2011. Magnetic composite prepared from palm shell-based carbon and application for recovery of residual oil from POME. *Journal of Environmental Management*, [e-journal] 92(3), pp.472–479. <http://doi.org/10.1016/j.jenvman.2010.08.031>.

Nizam, A.F.A. and Mahmud, M.S., 2021. Food quality assurance of crude palm oil: A review on toxic ester feedstock. *OCL - Oilseeds and fats, Crops and Lipids*, [e-journal] 28, pp.1-14. <http://doi.org/10.1051/ocl/2021011>.

No, Y. and Son, Y., 2019. Effects of probe position of 20 kHz sonicator on sonochemical oxidation activity. *Japanese Journal of Applied Physics*, [e-journal] 58(SGGD02), pp.2–6. <https://doi.org/10.7567/1347-4065/ab0adb>.

Nur Aisha, A.W., 2021. MPOB: Palm oil industry remains resilient under MCO. *Malay Mail*, [online] 28 August. Available at: <<https://www.malaymail.com/news/malaysia/2021/08/28/mpob-palm-oil-industry-remains-resilient-under-mco/2001119>> [Accessed 5 March 2022].

Ogunkunle, O. and Ahmed, N.A., 2019. A review of global current scenario of biodiesel adoption and combustion in vehicular diesel engines. *Energy Reports*, [e-journal] 5, pp.1560–1579. <https://doi.org/10.1016/j.egy.2019.10.028>.

Oil World, 2021. *Independent global market analyses & forecasts since 1958*. [online] Available at: <<https://www.oilworld.biz/p/monthly-november-11-2022#monthly-november-11-2022>> [Accessed: 17 July 2022].

Ong, V.Z., Wu, T.Y, Lee, C.B.T.L., Cheong, N.W.R. and Shak, K.P.Y., 2019. Sequential ultrasonication and deep eutectic solvent pretreatment to remove lignin and recover xylose from oil palm fronds. *Ultrasonics Sonochemistry*, [e-journal] 58, p.104598. <https://doi.org/10.1016/j.ultsonch.2019.05.015>.

Panadare, D.C., Gondaliya, A. and Rathod, V.K., 2020. Comparative study of ultrasonic pretreatment and ultrasound assisted three phase partitioning for extraction of custard apple seed oil. *Ultrasonics Sonochemistry*, [e-journal] 61, p.104821. <https://doi.org/10.1016/j.ultsonch.2019.104821>.

Parkar, P.A., Choudhary, H.A. and Moholkar, V.S., 2012. Mechanistic and kinetic investigations in ultrasound assisted acid catalyzed biodiesel synthesis. *Chemical Engineering Journal*, [e-journal] 187, pp.248–260. <http://doi.org/10.1016/j.cej.2012.01.074>.

Patricio, A., Fernandez, C., Mota, A.M. and Capelo, J.L., 2006. Dynamic versus static ultrasonic sample treatment for the solid-liquid pre-concentration of mercury from human urine. *Talanta*, [e-journal] 69(3), pp.769–775. <https://doi.org/10.1016/j.talanta.2005.11.007>.

Peters, M.S., Timmerhaus, K.D. and West, R.E., 2003. *Plant Design and Economics for Chemical Engineers*. 5th ed. New York: McGraw-Hill.

Photaworn, S., Tongurai, C. and Kungsanunt, S., 2017. Process development of two-step esterification plus catalyst solution recycling on waste vegetable oil possessing high free fatty acid. *Chemical Engineering and Processing: Process Intensification*, [e-journal] 118, pp.1–8. <http://doi.org/10.1016/j.cep.2017.04.013>.

Rajesh, K., Natarajan, M.P., Devan, P.K. and Ponnuvel, S., 2021. Coconut fatty acid distillate as novel feedstock for biodiesel production and its characterization as a fuel for diesel engine. *Renewable Energy*, [e-journal] 164, pp.1424–1435. <https://doi.org/10.1016/j.renene.2020.10.082>.

Ritchie, H. and Roser, M., 2021. *Palm Oil*. [online] Available at: <<https://ourworldindata.org/palm-oil#citation>> [Accessed: 8 April 2022].

Rokhina, E. V., Lens, P. and Virkutyte, J., 2009. Low-frequency ultrasound in biotechnology: state of the art. *Trends in Biotechnology*, 27(5), pp.298–306.

Sahar, Sadaf, S., Iqbal, J., Ullah, I., Bhatti, H.N., Nouren, S., Rehman, H., Nisar, J. and Iqbal, M., 2018. Biodiesel production from waste cooking oil: An efficient technique to convert waste into biodiesel. *Sustainable Cities and Society*, [e-journal] 41, pp.220–226. <https://doi.org/10.1016/j.scs.2018.05.037>.

Şahin, T. and Aydın, F., 2018. Investigation of fuel properties of canola oil biodiesel, bioethanol, and diesel fuel mixture. *International Journal of Automotive Engineering and Technologies*, 7(4), pp.158–163.

Salaheldeen, M., Mariod, A.A., Aroua, M.K., Rahman, S.M.A., Soudagar, M.E.M. and Fattah, I.M.R., 2021. Current state and perspectives on transesterification of triglycerides for biodiesel production. *Catalysts*, [e-journal] 11(9), pp.1–37. <https://doi.org/10.3390/catal11091121>.

Sancheti, S.V. and Gogate, P.R., 2017. A review of engineering aspects of intensification of chemical synthesis using ultrasound. *Ultrasonics Sonochemistry*, 36, pp.527–543. <https://doi.org/10.1016/j.ultsonch.2016.08.009>.

Semilin, V., Janaun, J., Chung, C.H., Touhami, D., Haywood, S.K., Chong, K.P., Yaser, A.Z. and Zein, S.H., 2021. Recovery of oil from palm oil mill effluent using polypropylene micro/nanofiber. *Journal of Hazardous Materials*, [e-journal] 404, p.124144. <https://doi.org/10.1016/j.jhazmat.2020.124144>.

Shojaeiarani, J., Bajwa, D. and Holt, G., 2020. Sonication amplitude and processing time influence the cellulose nanocrystals morphology and dispersion. *Nanocomposites*, [e-journal] 6(1), pp.41–46. <https://doi.org/10.1080/20550324.2019.1710974>.

Singh, A. and Kumar, G., 2018. Advancement in catalysts for transesterification in the production of biodiesel: a review. *Journal of Biochemical Technology*, 9(1), p.17-27.

Suksaroj, T.T., Yaeed, S. and Suksaroj, C., 2020. The effect of pome ultrasonication pretreatment on biogas production and reduction of greenhouse gases emissions from wastewater treatment units of palm oil mills. *Desalination and Water Treatment*, 202, pp.86–94.

Sulin, S.N. and Mokhtar, M.N., 2019. *Residual crude palm oil resources and recovery method: A Review*. In: MSAE (Malaysian Society of Agricultural and Food Engineers), Konvensyen Kebangsaan Kejuruteraan Pertanian Dan Makanan 2019. Putrajaya, Malaysia, 21 March 2019. Putrajaya: MSAE.

Sungnat, C. and Wongwuttanasatian, T., 2018. *Esterification of crude palm oil with low ultrasonic intensity*. Chendu, China, 25-26 March 2018. Pennsylvania: DEStech Transactions on Environment, Energy and Earth Sciences.

Suslick, K.S., 1998. *Kirk-Othmer encyclopedia of chemical technology*. 4th ed. New York: John Wiley & Sons, Inc.

Suwanno, S., Rakkan, T., Yunu, T., Paichid, N., Kimtun, P., Prasertsan, P. and Sangkharak, K., 2017. The production of biodiesel using residual oil from palm oil mill effluent and crude lipase from oil palm fruit as an alternative substrate and catalyst. *Fuel*, [e-journal] 195, pp.82–87. <http://dx.doi.org/10.1016/j.fuel.2017.01.049>.

Suzuki, D., Sato, Y., Kamasaka, H., Kuriki, T. and Tamura, H., 2020. Oiling-out effect improves the efficiency of extracting aroma compounds from edible oil. *NPJ Science of Food*, [e-journal] 4(1), pp.4-6. <https://doi.org/10.1038/s41538-020-00079-8>.

Takase, M., Chen, Y., Liu, H., Zhao, T., Yang, L. and Wu, X., 2014. Biodiesel production from non-edible *Silybum marianum* oil using heterogeneous solid base catalyst under ultrasonication. *Ultrasonics Sonochemistry*, [e-journal] 21(5), pp.1752–1762. <http://doi.org/10.1016/j.ultsonch.2014.04.003>.

Tan, S.X., Lim, S., Ong, H.C. and Pang, Y.L., 2019. State of the art review on development of ultrasound-assisted catalytic transesterification process for biodiesel production. *Fuel*, [e-journal] 235, pp.886–907. <https://doi.org/10.1016/j.fuel.2018.08.021>.

Tavizón-Pozos, J.A., Chavez-Esquivel, G., Suárez-Toriello, V.A., Santolalla-Vargas, C.E., Luévano-Rivas, O.A., Valdés-Martínez, O.U., Talavera-López, A. and Rodriguez, J.A., 2021. State of art of alkaline earth metal oxides catalysts used in the transesterification of oils for biodiesel production. *Energies*, [e-journal] 14, pp. 1–24. <https://dx.doi.org/10.390/en14041031>.

Tenaga National Berhad, 2022. *Pricing & Tariff*. [online] Available at: <<https://www.tnb.com.my/commercial-industrial/pricing-tariffs1/>> [Accessed: 16 August 2022].

Thaiyasuit, P., Pianthong, K. and Worapun, I., 2012. Acid esterification-alkaline transesterification process for methyl ester production from crude rubber seed oil. *Journal of Oleo Science*, 61(2), pp.81–88.

Thoai, D.N., Tongurai, C., Prasertsit, K. and Kumar, A., 2019. Review on biodiesel production by two-step catalytic conversion. *Biocatalysis and Agricultural Biotechnology*, [e-journal] 18, p.101023. <https://doi.org/10.1016/j.bcab.2019.101023>.

Tran, N.N., McMurchie, E.J. and Ngothai, Y., 2018. Biodiesel production from recycled grease trap waste: A case study in South Australia. Part 1: The pre-treatment of high free fatty acid feedstock. *ChemistrySelect*, 3(9), pp.2509–2514.

Trinh, H., Yusup, S. and Uemura, Y., 2018. Optimization and kinetic study of ultrasonic assisted esterification process from rubber seed oil. *Bioresource Technology*, [e-journal] 247, pp.51–57. <http://doi.org/10.1016/j.biortech.2017.09.075>.

United States Environmental Protection Agency, 1982. *EPA handbook for sampling and sample preservation of water and wastewater*, Ohio: USEPA.

Van Gerpen, J., Shanks, B., Pruszko, R., Clements, D. and Knothe, G., 2004. *Biodiesel analytical methods*, Colorado: National Renewable Energy Laboratory (NREL).

Wahi, R., Abdullah, L.C., Mobarekeh, M.N., Ngaini, Z. and Yaw, T.C.S., 2017. Utilization of esterified sago bark fibre waste for removal of oil from palm oil mill effluent. *Journal of Environmental Chemical Engineering*, 5(1), pp.170–177.

Wan Ghazali, W.N.M., Mamat, R., Masjuki, H.H. and Najafi, G., 2015. Effects of biodiesel from different feedstocks on engine performance and emissions: A review. *Renewable and Sustainable Energy Reviews*, 51, pp.585–602.

Wan Sharifudin, W.S.S.A., Sulaiman, A., Mokhtar, N., Baharuddin, A.S., Tabatabaei, M., Busu, Z. and Subbian, K., 2015. Presence of residual oil in relation to solid particle distribution in palm oil mill effluent. *BioResources*, 10(4), pp.7591–7603.

Wang, H., Xu, K., Ma, Y., Liang, Y., Zhang, H. and Chen, L., 2019. Impact of ultrasonication on the aggregation structure and physicochemical characteristics of sweet potato starch. *Ultrasonics Sonochemistry*, [e-journal] 63, p.104868. <https://doi.org/10.1016/j.ultsonch.2019.104868>.

Wang, J., Mahmood, Q., Qiu, J.P., Li, Y.S., Chang, Y.S., Chi, L.N. and Li, X.D., 2015. Zero discharge performance of an industrial pilot-scale plant treating palm oil mill effluent. *BioMed Research International*, [e-journal] 2015. <https://doi.org/10.1155/2015/617861>.

Warner, K. and Nelsen, T., 1996. AOCS collaborative study on sensory and volatile compound analyses of vegetable oils. *Journal of the American Oil Chemists' Society*, 73(2), pp.157–166.

Wen, C., Zhang, J., Zhang, H., Dzah, C.S., Zandile, M., Duan, Y., Ma, H. and Luo, X., 2018. Advances in ultrasound assisted extraction of bioactive compounds from cash crops – A review. *Ultrasonics Sonochemistry*, [e-journal] 48, pp.538–549. <https://doi.org/10.1016/j.ultsonch.2018.07.018>.

Wondi, M.H., Shamsudin, R., Yunus, R., Alsultan, G.A. and Iswardi, A.H., 2020. Centrifugal separation-assisted and extraction of crude palm oil from separated mesocarp fiber: Central composite design optimization. *Journal of Food Process Engineering*, 43(7).

Wong, L.P., Isa, M.H. and Bashir, M.J.K., 2016. Use of low frequency ultrasound for solids solubilization in palm oil mill effluent. In: N.A.W.A. Zawawi, ed. 2016. *Engineering Challenges for Sustainable Future*. pp. 221–224.

Wong, L.P., Isa, M.H. and Bashir, M.J.K., 2018. Disintegration of palm oil mill effluent organic solids by ultrasonication: Optimization by response surface methodology. *Process Safety and Environmental Protection*, [e-journal] 114, pp.123–132. <https://doi.org/10.1016/j.psep.2017.12.012>.

Wong, L.P., Isa, M.H., Bashir, M.J.K. and Guo, X.X., 2019. *Optimization of ultrasound irradiation for palm oil mill effluent*. In: C.H. Weng, 5th International Conference on Water Resource and Environment (WRE 2019). Macao, China, 16-19 July 2019. United Kingdom: IOP Publishing Ltd.

Wu, P., Bai, L., Lin, W. and Wang, X., 2018. Mechanism and dynamics of hydrodynamic-acoustic cavitation (HAC). *Ultrasonics Sonochemistry*, [e-journal] 49, pp.89–96. <https://doi.org/10.1016/j.ultsonch.2018.07.021>.

Yasvanthrajan, N., Sivakumar, P., Muthukumaer, L., Murugesan, T. and Arunagiri, A., 2021. Production of biodiesel from waste bio-oil through ultrasound assisted transesterification using immobilized lipase. *Environmental Technology and Innovation*, [e-journal] 21, p.101199. <https://doi.org/10.1016/j.eti.2020.101199>.

Zahan, K.A. and Kano, M., 2018. Biodiesel production from palm oil, its by-products, and mill effluent: A review. *Energies*, [e-journal] 11(8), pp.1–25. <https://doi.org/10.3390/en11082132>.

Zhang, J., Li, J., Thring, R.W., Hu, X. and Song, X., 2012. Oil recovery from refinery oily sludge via ultrasound and freeze/thaw. *Journal of Hazardous Materials*, [e-journal] 203–204, pp.195–203. <http://doi.org/10.1016/j.jhazmat.2011.12.016>.

Zulqarnain, Mohd Yusoff, M.H, Ayoub, M., Ramzan, N., Nazir, M.H., Zahid, I., Abbas, N., Elboughdiri, N., Mirza, C.R. and Butt, T.A., 2021. Overview of feedstock for sustainable biodiesel production and implementation of the biodiesel program in Pakistan. *ACS Omega*, [e-journal] 6(2), pp. 19099-19114. <https://doi.org/10.1021/acsomega.1c02402>.

APPENDICES

Appendix A: List of Chemicals and Instruments

Table A.1: List of Chemicals Involved in the Research

Chemicals	Source	Purpose
BOD nutrient buffer pillow	HACH	Dilution water for BOD
COD digestion vials, HR+	HACH	Reagent for COD
Hexane	Chemiz	Solvent for O&G and GC analysis
Anhydrous sodium sulphate	Bendosen	Absorb moisture
Sudan (III) dye	CHEMSOLN	Micelle marker
Isopropyl alcohol	GENE Chemical	Solvent for AV
Toluene	EMSURE [®]	Solvent for AV
Potassium hydroxide	FRIENDEMANN SCHMIDT	Titrant for AV and catalyst for alkaline transesterification
Phenolphthalein	R&M Chemicals	Indicator for AV
Potassium iodide	QRëC [®]	Reagent for IV and PV
Wijs reagent	Sigma-Aldrich	Reagent for IV
Starch solution	R&M Chemicals	Indicator for IV and PV
Sodium thiosulphate	QRëC [®]	Titrant for IV and PV
Glacial acetic acid	HmbG [®] Chemicals	Solvent for IV and PV
Cyclohexane	R&M Chemicals	Solvent for IV and PV
Potassium dichromate	EMSURE [®]	Standardization of sodium thiosulfate
Hydrochloric acid	Fisher Chemicals	Standardization of sodium thiosulfate
Sulfuric acid	R&M Chemicals	Catalyst for acid esterification
Methanol	LiChrosolv [®]	Reagent for biodiesel production
37 Component FAME Mix	Sigma-Aldrich	Calibration standard for GC
Methyl heptadecanoate	RESTEK	Internal standard for GC

Table A.2: List of Instruments Involved in the Research

Instruments	Specifications	Purpose
Portable multiparameter	Eutech PCD 650	Determination of pH
DO meter	Eutech DO 2700	Determination of DO
BOD incubator	VELP, FOC 225E	BOD incubation
Vial thermo-reactor	HANNA HI 839800	COD digester
Portable colorimeter	HACH DR/890	Determination of COD
Universal oven	Memmert UF 110	Sample drying
Vacuum pressure pump	GAST	Determination of SS
Analytical balance	Shimadzu AUX320	Determination of mass
Muffle furnace	LabTech LEF-103S-1	Determination of TVS
Centrifuge	HERMLE Z 326K	Centrifugation of emulsion
Rotary evaporator	Büchi R-215	Solvent recovery
Ultrasonic probe with 13 mm tip	Qsonica Q500	Pre-treatment for enhanced oil recovery
Particle size analyzer	Malvern 2000	Particle size distribution analysis
Field emission scanning electron microscope	JEOL JSM6701F	Surface morphology analysis
Binocular microscope	Optika B-190	Surface morphology analysis
Fourier transform infrared spectroscopy-attenuated total reflectance	PerkinElmer Spectrum Two	Functional group analysis
Oxygen bomb calorimeter	IKA Calorimeter C200	Determination of GCV
Ultraviolet-visible spectrophotometer	Jasco V-730	Determination of DOBI
Stirring hot plate	Thermo Scientific Cimarec	Conventional reaction for FFA conversion
Ultrasonic bath	Elma S180 H	Ultrasonic bath-assisted reaction for FFA conversion
Ultrasonic probe with 3 mm tip	Hielscher UP 400S	Ultrasonic probe-assisted reaction for FFA conversion
Gas chromatography with flame ionization detector	Shimadzu GC-2010 Plus	Determination of fatty acid composition, linoleic methyl ester, and polyunsaturated methyl ester
Rheometer	Discovery Hybrid, DHR-1	Determination of viscosity

Appendix B: Methods for Preserving Samples

Table B.1: Preservation Methods and the Maximum Holding Time for Each Parameters (United States Environmental Protection Agency, 1982)

Parameters	Preservative	Maximum holding time
pH	-	15 mins
BOD	Cool at 4°C	48 hours
COD	Acidified with H ₂ SO ₄ to pH < 2 and cool at 4°C	28 days
TS	Cool at 4°C	7 days
SS	Cool at 4°C	7 days
TVS	Cool at 4°C	7 days
O&G	Acidified with H ₂ SO ₄ to pH < 2 and cool at 4°C	28 days

Appendix C: Methods for Characterization of POME

Determination of pH (APHA 4500 H⁺)

On a scale of 0 to 14, pH describes the degree of acidity or alkalinity of a solution, with high numbers indicating more alkaline conditions and lower numbers indicating more acidic condition. Meanwhile, a pH of 7 implies neutral characteristics. Prior to measurement, the pH electrode was cleaned with distilled water and patted dry with a paper towel. The pH electrode tip was then immersed in the sample, and the pH reading was recorded once it had stabilized.



Figure C.1: Portable Multiparameter (Eutech CyberScan PCD 650)

Determination of BOD (APHA 5210 B)

BOD is defined as the amount of oxygen required by the microbes to breakdown the organic compounds. To begin, dilution water was prepared by diluting a BOD nutrient buffer pillow in 3L of distilled water. The dilution water was then mixed vigorously to dissolve the nutrients.

Two BOD bottles with similar volumes of diluted samples were prepared. The initial DO of a diluted sample was measured using a DO meter, whereas the other diluted sample was sealed airtight and placed in the BOD incubator for 5 days at a controlled temperature of 20°C. The BOD bottles were periodically inspected during the incubation time to ensure that the dilution water was constantly at the bottle's lip and, if necessary, topped up with distilled water. After 5 days, the sample was taken out to determine the final DO reading. The general equation for determination of BOD₅ value is:

$$BOD_5(mg/L) = \frac{\text{Initial DO} - \text{Final DO}}{\text{Dilution factor}} \quad (\text{Equation C.1})$$



Figure C.2: DO Meter (Eutech DO 2700)



Figure C.3: BOD Incubator (VELP, FOC 225E)



Figure C.4: BOD Bottles with Stopper in BOD Incubator

Determination of COD (APHA 5220 B)

COD is an indicative measure of the oxygen required to chemically oxidize the particulate matter under reflux conditions with the aid of a strong chemical oxidant. A 0.2 mL of diluted sample was pipetted at 45° angle into a COD HR+ vial. To create a blank, a similar volume of distilled water was added to another vial. The vials were gently tilted numerous times to thoroughly mix the sample. The vials were then placed in the pre-heated vial thermo-reactor for 2 hours of reflux at 150°C. After 2 hours, the vials were allowed to cool in the reactor for around 20 minutes to bring the temperature down to 120°C. The vials were inverted several times while still warm. The vials were then placed in a tube rack to cool to ambient temperature. Finally, the COD values were determined using a portable colorimeter.



Figure C.5: Vial Thermo-Reactor (HANNA HI 839800) and Portable Colorimeter (HACH DR/890)

Determination of TS (APHA 2540 B)

Total solids comprise both dissolved and suspended particles. The mass of an empty evaporating dish was first measured. A known volume of sample was pipetted into the evaporating dish and dried in the oven at 105°C for 1 hour. The dried sample was placed in the desiccator and cooled to room temperature before being weighed. The drying procedure was repeated until a constant value was obtained. The general equation for determination of TS is:

$$TS(mg/L) = \frac{(A-B) \times 1000}{\text{Sample volume, L}} \quad (\text{Equation C.2})$$

Where:

A = mass of evaporating dish + dried residue, g

B = mass of evaporating dish, g



Figure C.6: Universal Oven (Mettmert Universal UF 110)

Determination of SS (APHA 2540 D)

A filter paper of known mass was placed in a Büchner funnel on top of a Büchner flask with a vacuum pressure pump connected. Then, a known volume of sample was poured through the filter paper. The portion that passed through the filter paper was dissolved solids, while suspended solids was the portion that was retained by the filter paper. The residue-containing filter paper was then dried in an oven at 105°C for 1 hour. The filter paper with residual was cooled and weighed after drying. The general equation for determination of SS is:

$$SS(mg/L) = \frac{(A-B) \times 1000}{\text{Sample volume, L}} \quad (\text{Equation C.3})$$

Where:

A = mass of filter paper + dried residue, g

B = mass of filter paper, g



Figure C.7: Vacuum Filtration Setup for SS Determination

Determination of TVS (APHA 2540 E)

The pre-weighed dried total solids test sample was ignited in a furnace at 550°C for 15 minutes. The ignited sample was then cooled to room temperature in a desiccator before being weighed. The general equation for determination of TVS is:

$$TVS(mg/L) = \frac{(A-B) \times 1000}{\text{Sample volume, L}} \quad (\text{Equation C.4})$$

Where:

A = mass of crucible + sample before ignition, g

B = mass of crucible + sample after ignition, g



Figure C.8: Muffle Furnace (LabTech LEF-103S-1)

Appendix D: Methods for Evaluating the Quality of Recovered Oil

Determination of DOBI (MPOB Test Method p2.9:2004)

DOBI is acquired by performing a simple spectrometric measurement using an ultraviolet-visible (UV-Vis) spectrophotometer. As demonstrated by Equation D.1, the DOBI value was determined by calculating the absorbance ratio at 446 nm to 269 nm for 0.5 – 1 % of the oil sample in hexane solvent.

$$DOBI \text{ value} = \frac{\text{Absorbance at 446 nm}}{\text{Absorbance at 269 nm}} \quad (D.1)$$



Figure D.1: UV-Vis Spectrophotometer (Jasco V-730)

Determination of AV and FFA content (AOCS Official Method Cd 3d-63)

The AV denotes the amount of KOH in milligrams that is necessary to neutralize the FFA present in one gram of sample. The AV was determined using the chemical titration of neutralized alcoholic solution of oil with 0.1 M KOH using phenolphthalein as an indicator until a pink end point was attained. The AV was computed by Equation D.2, in which S represents the volume of titrant used in sample titration and B represents the volume of titrant used in the blank titration, both in millimeters (mL).

$$AV (mg KOH/g oil) = \frac{(S-B) \times \text{Molarity of KOH} \times 56.1}{\text{Mass of sample (g)}} \quad (D.2)$$

To express in terms of FFA (% lauric, oleic, or palmitic), the acid value was divided by 2.81, 1.99, or 2.19, respectively.

Determination of IV (AOCS Official Method Cd 1-25)

The IV expresses the degree of unsaturation in terms of number centigrams of iodine absorbed per gram of sample. The IV can be determined using Wijs (cyclohexane-acetic acid solvent) method. This approach involves a chemical titration with 0.1 M of standardized sodium thiosulphate ($\text{Na}_2\text{S}_2\text{O}_3$) and starch as an indicator until the blue color was faded. The IV was computed by Equation D.3.

$$IV = \frac{(B-S) \times \text{Molarity of } \text{Na}_2\text{S}_2\text{O}_4 \times 12.69}{\text{Mass of sample (g)}} \quad (D.3)$$

Determination of PV (AOCS Official Method Cd 8b-90)

The PV denotes the amount of peroxide in milliequivalents of active oxygen per kilogram of sample. The PV was determined by titrating the glacial acetic acid-cyclohexane and potassium iodide solutions of oil with 0.01 M $\text{Na}_2\text{S}_2\text{O}_3$ using starch as an indicator until a faint yellow or color endpoint was achieved.

$$PV (\text{meq } O_2/\text{kg}) = \frac{(S-B) \times \text{Molarity of } Na_2S_2O_3 \times 1000}{\text{Mass of sample (g)}} \quad (\text{D.4})$$

Appendix E: Cost-Benefit Analysis

Sample Calculation for Operating Capacity

The following is the sample calculation for the operating capacity of a 3-kW power ultrasonic processor based on the ultrasonication dosage of 7.5 kW/L.

$$\begin{aligned} \text{Operating capacity } \left(\frac{L}{hr} \right) &= 3kW \times \frac{L}{7.5 \text{ kW/L}} \times \frac{3600s}{hr} & (E.1) \\ &= 1,440L/hr \end{aligned}$$

A 3-kW power ultrasonic processor has a capacity to treat 1,440 L of POME per hour.

Sample Calculation for Utilities

Assuming that electricity is charged at RM 0.38/kWh and a treatment rate of 60 MT of POME per hour, the following is the sample calculation for the electricity charges per hour:

$$\begin{aligned} \text{Electricity Cost (RM/hr)} &= \frac{7.5kW/L}{L} \times 60,000L \times \frac{hr}{3600s} \times \frac{RM0.38}{kWh} & (E.2) \\ &= RM 47.50/hr \end{aligned}$$

With 16 hours of operation per day and 320 working days per year assumed, the annual electricity costs would be:

$$\begin{aligned} \text{Annual Electricity Cost } \left(\frac{RM}{\text{year}} \right) &= \frac{RM\ 47.50}{hr} \times \frac{16\ \text{hours}}{\text{day}} \times \frac{320\ \text{days}}{\text{year}} \quad (\text{E.3}) \\ &= RM\ 243,200/\text{year} \end{aligned}$$

Sample Calculation for Labor Expenses

The labor expenses are computed using an anticipated operating wage of RM2,000 monthly and two working shifts daily. Assuming that the direct supervisory costs are typically a 15 % premium of operating wage, the annual direct supervisory cost would be:

$$\begin{aligned} \text{Annual Cost } \left(\frac{RM}{\text{year}} \right) &= 1.15 \times \frac{RM\ 2,000}{\text{month}} \times \frac{12\ \text{months}}{\text{year}} \times 2\ \text{shifts} \quad (\text{E.4}) \\ &= RM\ 55,200/\text{year} \end{aligned}$$

Sample Calculation for Product Sales Revenue

The annualized rate of POME generation is 307,200 MT/year. Considering 0.155 % as the current oil loss in POME, the annualized oil loss would be 476.16 MT/year. With the assumption that residual oil can be sold for RM 3,150.75/MT. The sales revenue would be:

$$\begin{aligned} \text{Sales Revenue } \left(\frac{RM}{\text{year}} \right) &= \frac{RM\ 3,150.75}{MT} \times \frac{476.16\ MT}{\text{year}} \quad (\text{E.5}) \\ &= RM\ 1,500,261.12/\text{year} \end{aligned}$$

Table E.1: Percentage for Estimating Capital Investment Items Based on Delivered-Equipment Cost (Peters, Timmerhaus and West, 2003)

	Percentage of delivered equipment cost for		
	Solid	Solid liquid	Liquid
Direct Costs			
Purchased equipment	100	100	100
Installation	45	39	47
Instrumentation and controls	18	26	36
Piping	16	31	68
Electrical system	10	10	11
Buildings	25	29	18
Yard improvements	15	12	10
Service facilities	40	55	70
Total direct plant cost	269	302	360
Indirect Costs			
Engineering and supervision	33	32	33
Construction expenses	39	34	41
Legal expenses	4	4	4
Contractor's fee	17	19	22
Contingency	35	37	44
Total indirect plant cost	128	126	144
Fixed capital investment	397	428	504
Working capital	70	75	89
Total capital investment	467	503	593

Appendix F: Preparation of Methanol-to-Oil Molar Ratio and Catalyst Loading for Biodiesel Production

Sample Calculation for Preparation of Methanol-to-Oil Molar Ratio

The acid-esterification reaction required a methanol-to-oil molar ratio of 8:1. The molecular weight of methanol and oil are 32.04 g/mol and 845.8 g/mol, respectively. Assuming that the reaction was carried out using 5 g of oil, the mass of methanol required will be:

$$\begin{aligned} \text{Mass of methanol} &= \frac{\text{Mass of oil} \times \text{Ratio} \times \text{Molecular weight of methanol}}{\text{Molecular weight of oil}} \quad (\text{F.1}) \\ &= \frac{5 \text{ g} \times 8 \times 32.04 \text{ g/mol}}{845.8 \text{ g/mol}} = 1.515 \text{ g methanol} \end{aligned}$$

Equation F.2 is used to convert the required mass to required volume. Methanol has a density of 0.791 g/mL.

$$\text{Volume} = \frac{\text{Mass}}{\text{Density}} \quad (\text{F.2})$$

$$\text{Volume of methanol} = \frac{1.515 \text{ g}}{0.791 \text{ g/mL}} = 1.915 \text{ mL}$$

In the acid-esterification of 5 g of oil, the total volume of methanol required is 1.915 mL.

Sample Calculation for Preparation of Catalyst Loading

The acid-esterification reaction required an H₂SO₄ loading of 0.75 wt%. In other words, 0.0075 g of H₂SO₄ is required for every 1 g of oil. Assuming that the reaction was carried out using 5 g of oil, the mass of H₂SO₄ required will be 0.0375 g. To convert the required mass to required volume, Equation F.2 is used, where H₂SO₄ has a density of 1.84 g/mL.

$$\text{Volume of } H_2SO_4 = \frac{0.0375 \text{ g}}{1.84 \text{ g/mL}} = 0.02 \text{ mL}$$

In the acid-esterification of 5 g of oil, the total volume of H₂SO₄ required is 0.02 mL.

Appendix G: Characterization Results of POME

Table G.1: Properties of POME for Sample Collected for Six Months

Month	July 2021	* ^P August 2021	September 2021	October 2021	* ^O November 2021	December 2021	Average
pH	4.25 ± 0.01	4.19 ± 0.01	4.37 ± 0.02	4.49 ± 0.02	4.27 ± 0.01	4.66 ± 0.01	4.37 ± 0.18
BOD	39,733 ± 2,397	39,200 ± 2,000	41,367 ± 451	35,000 ± 1,769	21,200 ± 819	28,600 ± 2,553	34,183 ± 7,848
COD	136,333 ± 5,508	141,667 ± 7,234	137,667 ± 577	86,333 ± 3,055	62,333 ± 2,082	75,667 ± 577	106,667 ± 35,794
TS	40,000 ± 8,660	40,000 ± 8,660	43,833 ± 1,258	49,167 ± 1,041	37,500 ± 2,500	53,000 ± 4,272	43,917 ± 6,032
SS	11,100 ± 2,751	14,400 ± 6,773	34,000 ± 2,646	30,633 ± 4,041	11,100 ± 2,000	26,167 ± 1,674	21,233 ± 10,274
TVS	34,283 ± 5,000	30,000 ± 5,000	33,000 ± 866	15,900 ± 800	15,967 ± 2,779	23,117 ± 284	25,378 ± 8,274
O&G	4,197 ± 186	4,340 ± 262	4,670 ± 223	1,537 ± 277	1,550 ± 36	1,790 ± 56	3,014 ± 1,531

*^PPOME sample used for preliminary study; *^OPOME sample used for optimization study

Appendix H: Pearson Correlation Coefficient Analysis

Pearson correlation coefficient analysis is a tool used to measure the closeness of the association between two variables at a time. A positive sign denotes a proportional relationship, whereas a negative sign denotes an inverse proportional relationship. The unitless value reflects the strength of the relationship, with a greater value indicating a stronger link.

$$r = \frac{N(\sum xy) - (\sum x)(\sum y)}{\sqrt{[N\sum x^2 - (\sum x)^2][N\sum y^2 - (\sum y)^2]}} \quad (\text{H.1})$$

Where

r = Pearson correlation coefficient

N = number of values in each data set

The sample calculation of Pearson correlation coefficient for O&G and BOD is demonstrated:

Table H.1: Characterization Data on O&G and BOD

Set	1	2	3	4	5	6
O&G (x)	4,197	4,340	4,670	1,537	1,550	1,790
BOD (y)	39,733	39,200	41,367	35,000	21,200	28,600

Where

$$N = 6$$

$$\Sigma xy = 667,996,510$$

$$\Sigma x = 18,084$$

$$\Sigma y = 205,100$$

$$\Sigma x^2 = 66,228,278$$

$$\Sigma y^2 = 7,318,979,978$$

$$r = \frac{6(667,996,510) - (18,084)(205,100)}{\sqrt{[(6 \times 66,228,278) - (18,084)^2][(6 \times 7,318,979,978) - (205,100)^2]}} = 0.83$$

BOD is positively related to O&G.

Appendix I: Biodiesel Analysis

Determination of Fatty Acid Composition

According to the modified standard test method described in EN 14103, the fatty acid composition was determined using 37 component FAME mix as the calibration standard and methyl heptadecanoate as the internal standard. The type of methyl ester was identified by comparing the retention time of the calibration standard, whereas the concentration of methyl ester was quantified by comparing the peak area of the internal standard. The concentration of each individual component of sample in terms of mg/g was calculated by Equation I.1, whereas the content of each individual component of sample in terms of percentage was calculated by Equation I.2.

$$C_i(\text{mg/g}) = \frac{A_i}{A_{IS}} \times \frac{C_{IS} \times V_{IS}}{m} \quad (\text{Equation I.1})$$

$$C_i(\%) = \frac{A_i}{\sum A - A_{IS}} \times 100\% \quad (\text{Equation I.2})$$

Where

A_i = peak area for product of interest

A_{IS} = peak area of internal standard

C_{IS} = concentration of internal standard used, mg/mL

V_{IS} = volume of internal standard used, mL

m = mass of the sample analyzed, g

$\sum A$ = total peak area for methyl ester

The analysis of 8 mg of biodiesel was conducted using 0.2 mL of methyl heptadecanoate (C17) with a concentration of 10 mg/mL as an internal standard. Methyl palmitate (C16:0) was used to demonstrate the sample computation of the component's concentration and content. The peak area for C16:0 is 6,500,763. The peak area for C17 and total peak area are 4,635,503 and 1,934,0335, respectively.

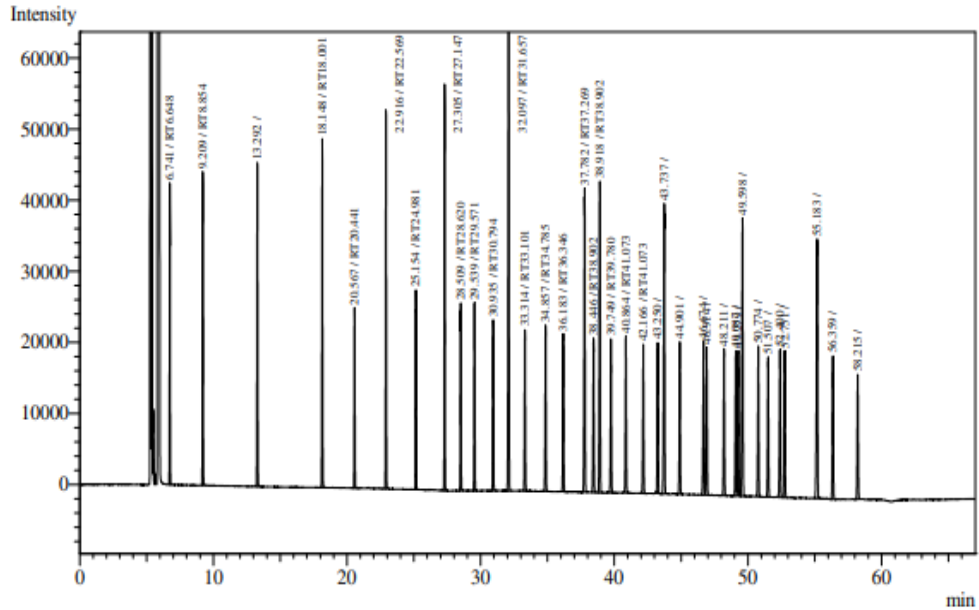
$$C_i(\text{mg/g}) = \frac{6500763}{4635503} \times \frac{\frac{10\text{mg} \times 0.2\text{ mL}}{\text{mL}}}{0.008\text{ g}} = 350.60\text{ mg/g}$$

$$C_i(\%) = \frac{6500763}{19340335 - 4635503} \times 100\% = 44.21\%$$

Total saturated fatty acids (SFAs) are methyl esters ranging from C4:0 to C18:0. Monounsaturated fatty acids (MUFAs) are C18:1 and C20:1. Polyunsaturated fatty acids (PUFAs) are C18:2, C18:3, C20:3, C20:4, C22:2 and C20:5. The computation for linolenic acid methyl ester is from the content of C18:3, whereas polyunsaturated methyl esters are from the content of C20:4, C20:5, C22:5 and C22:6.

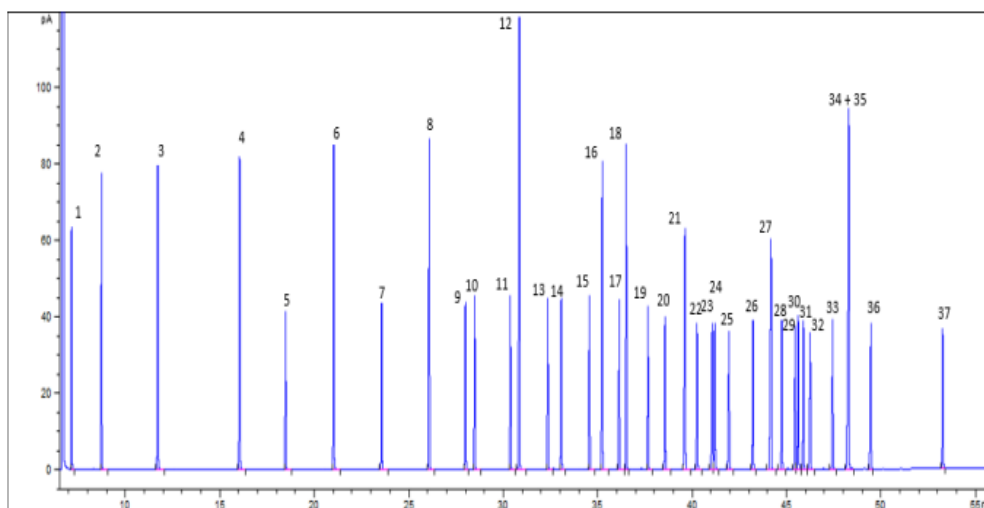
Analysis Date & Time : 14/9/2022 10:01:52 AM
 User Name : Admin
 Vial# : 1
 Sample Name : TYM FAME Standard 10,000ppm
 Sample ID : TYM FAME Standard 10,000ppm
 Sample Type : Unknown
 Injection Volume :
 ISTD Amount :

Data Name : C:\GCsolution\Data\DEV FYP(W.L.P) Tang yee Mun\TYM FAME Standard 10,000ppm.gcd
 Method Name : C:\GCsolution\Data\DPE FYP\GC Method\Method - STD FAME BPX70\BPX 70 STD FAME Supplier.gcm



Peak#	Ret.Time	Area	Height	Conc.	Unit	Mark	ID#	Cmpd Name
1	6.741	119941	42297	0.000	ppm		3	RT6.648
2	9.209	149810	43894	0.000	ppm		4	RT8.854
3	13.292	162321	45316	0.000	ppm			
4	18.148	166025	48897	0.000	ppm		9	RT18.001
5	20.567	83988	25200	0.000	ppm		11	RT20.441
6	22.916	172849	53146	0.000	ppm		13	RT22.569
7	25.154	88559	27870	0.000	ppm		15	RT24.981
8	27.305	182962	56866	0.000	ppm		18	RT27.147
9	28.509	90399	26243	0.000	ppm		20	RT28.620
10	29.539	93958	26370	0.000	ppm		21	RT29.571
11	30.935	92239	23942	0.000	ppm		23	RT30.794
12	32.097	288153	66261	0.000	ppm		24	RT31.657
13	33.314	94866	22621	0.000	ppm		26	RT33.101
14	34.857	97987	23306	0.000	ppm		29	RT34.785
15	36.183	97190	22174	0.000	ppm		32	RT36.346
16	37.782	200412	42602	0.000	ppm		34	RT37.269
17	38.446	98663	21624	0.000	ppm		35	RT38.902
18	38.918	199935	43724	0.000	ppm		35	RT38.902
19	39.749	97174	21616	0.000	ppm		36	RT39.780
20	40.864	98793	22028	0.000	ppm	V	37	RT41.073
21	42.166	95381	20922	0.000	ppm		37	RT41.073
22	43.250	95196	21133	0.000	ppm			
23	43.737	204798	40718	0.000	ppm			
24	44.901	99844	21418	0.000	ppm			
25	46.674	103055	21525	0.000	ppm			
26	46.914	98905	20725	0.000	ppm	V		
27	48.211	97556	20639	0.000	ppm			
28	49.087	95671	20337	0.000	ppm			
29	49.279	95536	20402	0.000	ppm	V		
30	49.598	208042	38954	0.000	ppm			
31	50.774	101517	21107	0.000	ppm			
32	51.507	90998	19574	0.000	ppm			
33	52.400	103825	20750	0.000	ppm	V		
34	52.751	97654	20607	0.000	ppm			
35	55.183	205645	36416	0.000	ppm			
36	56.359	101760	20139	0.000	ppm			
37	58.215	89014	17539	0.000	ppm			
Total		4660621	1108902					

Figure I.1: GC Result for Supelco 37 Component FAME Mix



METHOD: GC (Bellefonte method)

Column: SP-2560, 100 m × 0.25 mm I.D., 0.2 µm film thickness

Carrier Gas: H₂ Flow Rate: 1.65 mL/min

Inlet Temperature: 200 °C Injection Volume: 0.8 µL

Injection Mode: 20:1

Temperature Program: 100 °C (Hold 3 min) @ 3 °C/min to 200 °C (Hold 3 min) @ 3 °C/min to 240 °C (6 min)

Detector: FID Temperature: 250 °C

Elution details:

EO	RT(MIN)	ANALYTE
1	7.17	Methyl butyrate (C4:0)
2	8.75	Methyl hexanoate (C6:0)
3	11.69	Methyl octanoate (C8:0)
4	16.02	Methyl decanoate (C10:0)
5	18.50	Methyl undecanoate (C11:0)
6	21.06	Methyl dodecanoate (C12:0)
7	23.60	Methyl tridecanoate (C13:0)
8	26.11	Methyl myristate (C14:0)
9	28.03	Methyl myristoleate (C14:1)
10	28.52	Methyl pentadecanoate (C15:0)
11	30.41	Methyl cis-10 pentadecenoate (C15:1)
12	30.88	Methyl palmitate (C16:0)
13	32.39	Methyl palmitoleate (C16:1)
14	33.10	Methyl heptadecanoate (C17:0)
15	34.59	Methyl cis-10 heptadecenoate (C17:1)
16	35.28	Methyl stearate (C18:0)
17	36.16	Methyl trans-9 eladiate (C18:1)
18	36.54	Methyl cis-9 oleate (C18:1)
19	37.70	Methyl linolelaidate (C18:2)
20	38.60	Methyl linoleate (C18:2)
21	39.66	Methyl arachidate (C20:0)
22	40.24	Methyl-gamma-linolenate (C18:3)
23	41.04	Methyl cis-11-eicosenoate (C20:1)
24	41.18	Methyl linolenate (C18:3)
25	41.93	Methyl heneicosanoate (C21:0)
26	43.20	Methyl cis-11,14-eicosadienoate (C20:2)
27	44.16	Methyl behenate (C22:0)
28	44.73	Methyl cis-8,11,14-eicosatrienoate (C20:3)
29	45.44	Methyl erucate (C22:1)
30	45.60	Methyl cis-11,14,17-eicosatrienoate (C20:3)
31	45.87	Methyl tricosanoate (C23:0)
32	46.24	Methyl cis-5,8,11,14-eicosatetraenoate aka methyl arachidonate (C20:4)
33	47.42	Methyl cis-13,16-docosadienoate (C22:2)
34	48.27	Methyl lignocerate (C24:0) + Methyl cis-5,8,11,14,17-eicosapentaenoate (C20:5)
36	49.44	Methyl nervonate aka methyl cis-15-tetracosanoate (C24:1)
37	53.26	Methyl cis-4,7,10,13,16,19-docosahexaenoate (C22:6)

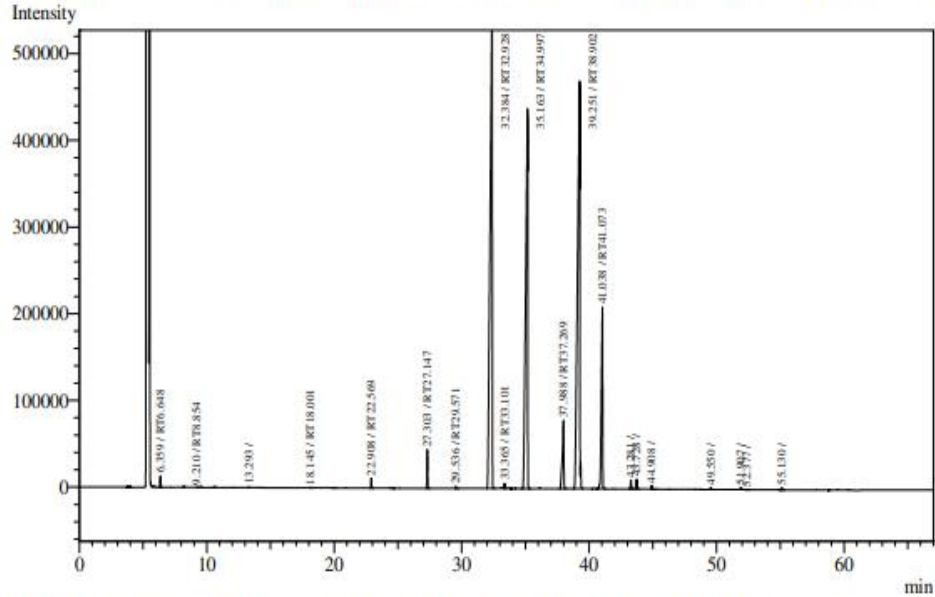
Figure I.2: Certificate of Analysis – Certified Reference Material

Table I.1: Retention Time with Respective Analyte

Peak	Analyte	Retention time (min)
1	Methyl butyrate (C4:0)	6.714
2	Methyl hexanoate (C6:0)	9.209
3	Methyl octanoate (C8:0)	13.292
4	Methyl decanoate (C10:0)	18.148
5	Methyl undecanoate (C11:0)	20.567
6	Methyl dodecanoate (C12:0)	22.916
7	Methyl tridecanoate (C13:0)	25.154
8	Methyl myristate (C14:0)	27.305
9	Methyl myristoleate (C14:1)	28.509
10	Methyl pentadecanoate (C15:0)	29.539
11	Methyl cis-10 pentadecenoate (C15:1)	30.935
12	Methyl palmitate (C16:0)	32.097
13	Methyl palmitoleate (C16:1)	33.314
14	Methyl heptadecanoate (C17:0)	34.857
15	Methyl cis-10 heptadecenoate (C17:1)	36.183
16	Methyl stearate (C18:0)	37.782
17	Methyl trans-9 eladiate (C18:1)	38.446
18	Methyl cis-9 oleate (C18:1)	38.918
19	Methyl linolelaidate (C18:2)	39.749
20	Methyl linoleate (C18:2)	40.864
21	Methyl arachidate (C20:0)	42.166
22	Methyl-gamma-linolenate (C18:3)	43.250
23	Methyl cis-11-eicosenoate (C20:1)	43.737
24	Methyl linolenate (C18:3)	44.901
25	Methyl heneicosanoate (C21:0)	46.674
26	Methyl cis-11,14-eicosadienoate (C20:2)	46.914
27	Methyl behenate (C22:0)	48.211
28	Methyl cis-8,11,14-eicosatrienoate (C20:3)	49.087
29	Methyl erucate (C22:1)	49.279
30	Methyl cis-11,14,17-eicosatrienoate (C20:3)	49.598
31	Methyl cis-11,14,17-eicosatrienoate (C20:3)	50.774
32	Methyl cis-5,8,11,14-eicosatetraenoate aka methyl arachidonate (C20:4)	51.507
33	Methyl cis-13,16-docosadienoate (C22:2)	52.400
34	Methyl lignocerate (C24:0)	52.751
35	Methyl cis-5,8,11,14,17-eicosapentaenoate (C20:5)	55.183
36	Methyl nervonate aka methyl cis-15-tetracosanoate (C24:1)	56.359
37	Methyl nervonate aka methyl cis-15-tetracosanoate (C24:1)	58.215

Analysis Date & Time : 22/9/2022 1:51:49 PM
 User Name : Admin
 Vial# : 1
 Sample Name : TYM Biodiesel Final 2.0
 Sample ID : TYM Biodiesel Final 2.0
 Sample Type : Unknown
 Injection Volume :
 ISTD Amount :

Data Name : C:\GCsolution\Data\DEV FYP(WL.P) Tang yee Mun\TYM Biodiesel Final 2.0.gcd
 Method Name : C:\GCsolution\Data\DPE FYP\GC Method\Method - STD FAME BPX70\BPX 70 STD FAME Supplier.gcm



Peak#	Ret.Time	Area	Height	Conc.	Unit	Mark	ID#	Cmpd Name
1	6.359	35734	13172	0.000	ppm		3	RT6.648
2	9.210	1076	296	0.000	ppm	V	4	RT8.854
3	13.293	2428	671	0.000				
4	18.145	2906	817	0.000	ppm		9	RT18.001
5	22.908	36635	11476	0.000	ppm		13	RT22.569
6	27.303	141082	44306	0.000	ppm		18	RT27.147
7	29.536	9473	2507	0.000	ppm		21	RT29.571
8	32.384	6500763	578623	0.000	ppm		25	RT32.928
9	33.365	24637	5937	0.000	ppm		26	RT33.101
10	35.163	4635503	437242	0.000	ppm		30	RT34.997
11	37.988	636509	78417	0.000	ppm		34	RT37.269
12	39.251	5720656	468991	0.000	ppm		35	RT38.902
13	41.038	1443219	209371	0.000	ppm		37	RT41.073
14	43.281	45210	9840	0.000				
15	43.728	52370	11374	0.000				
16	44.908	18226	3939	0.000				
17	49.550	9092	1947	0.000				
18	51.907	10438	1889	0.000		V		
19	52.377	2742	550	0.000				
20	55.130	11636	2351	0.000				
Total		19340335	1883716					

Figure I.3: GC Result for Biodiesel Produced from POME-Recovered Oil

Table I.2: Analytes in Biodiesel Produced from POME Recovered-Oil with its Respective Area

Peak	Analyte	Area
1	Methyl butyrate	35,734
2	Methyl hexanoate (C6:0)	1,076
3	Methyl octanoate (C8:0)	2,428
4	Methyl decanoate (C10:0)	2,906
5	Methyl laurate (C12:0)	36,635
6	Methyl myristate (C14:0)	141,082
7	Methyl pentadecanoate (C15:0)	9,473
8	Methyl palmitate (C16:0)	6,500,763
9	Methyl palmitoleate (C16:1)	24,637
10	Methyl heptadecanoate (C17:0)	4,635,503
11	Methyl stearate (C18:0)	636,509
12	Methyl oleate (C18:1)	5,720,656
13	Methyl linoleate (C18:2)	1,443,219
14	Methyl-gamma-linoleate (C18:3)	45,210
15	Methyl eicosanoate (C20:1)	52,370
16	Methyl linolenate (C18:3)	18,226
17	Methyl eicosatrienoate (C20:3)	9,092
18	Methyl eicosatetraenoate (C20:4)	10,438
19	Methyl docosadienoate (C22:2)	2,742
20	Methyl eicosapentaenoate (C20:5)	11,636
Total		19,340,335

Our Ref. : ITSPK/LB/5932/2022
Your Ref. : PO NO. FEGT/2022/1182

Date Received : 4th November
Date Tested : 7th – 11th November 2022
Date Issued : 11th November 2022

CERTIFICATE OF ANALYSIS

The following is a report on the analysis of one (1) sample stated to be **PALM METHYL ESTER**. The sample was tested at ITS Testing Services (M) Sdn Bhd in accordance with the test method(s) stipulated.

Representing : **UNIVERSITI TUNKU ABDUL RAHMAN**
Faculty OF Engineering And Green Technology (FEGT),
Universiti Tunku Abdul Rahman, Jalan Universiti,
Bandar Barat, 31900 Kampar, Perak.

Customer Sample Marking
Product : Biodiesel B100

Results of Analysis

<u>Test Parameter</u>	<u>Method</u>	<u>Unit</u>	<u>Results</u>
Ester content	EN 14103	% (m/m)	92.9
Oxidation stability, 110 ⁰ C (accelerated oxidation)	EN 15751	hours	29.3

ITS TESTING SERVICES (M) SDN. BHD.

C.W. NURMAUDIN
TECHNICAL MANAGER
B.Sc., LMIC
L/1308/4209/2001

The tests were performed on the samples as received. The test results relate only to the items tested.
Disclaimer: This report (including any enclosures and attachments) has been prepared for the exclusive use and benefit of the addressee(s) and solely for the purpose for which it is provided. Unless we provide express prior written consent, no part of this report should be reproduced, distributed or communicated to any third party. We do not accept any liability if this report is used for an alternative purpose from which it is intended, not do we owe any duty of care to any third party in respect of this report.

Page 1 of 1

-----END OF REPORT-----

Figure I.4: Results of Ester Content and Oxidation Stability